TECHNISCHE UNIVERSITÄT MÜNCHEN

II. Medizinische Klinik und Poliklinik

Klinikum rechts der Isar

Role of NFκB2 and MTOR in Pancreatic Ductal Adenocarcinoma

Zonera Hassan

Vollständiger Abdruck der von der Fakultät für Medizin der Technischen Universität München zur Erlangung des akademischen Grades eines

Doktors der Naturwissenschaften (Dr. rer. nat)

genehmigten Dissertation.

Vorsitzender:	Prof. Dr. Jürgen Ruland
Prüfer der Dissertation:	1. Priv.-Doz. Dr. Günter Schneider
	2. Prof. Angelika Schnieke, Ph.D.

Die Dissertation wurde am 17.01.2020 bei der Technischen Universität München eingereicht und durch die Fakultät für Medizin am 12.05.2020 angenommen.

1 List of Content

2 List of Figures

3 List of Tables

4 List of Abbreviations

µm	Micrometer
°C	Degree Celsius
4EBP1	Eukaryotic initiation factor 4E binding protein 1
4-OHT	4-hydroxytamoxifen
5-FU	5-fluorouracil
ADM	Acinar to ductal metaplasia
AFL	Atypical flat lesions
AKT	Serine and Threonine kinase
Amy1	Alpha-amylase 1
APS	Ammonium persulphate
ARD	Ankyrin repeats domain
BAFFR	BAFF receptor
BCR	B cell Receptor
bp	Base pair
CAFs	Cancer associated fibroblast
CD40	Cluster of differentiation 40
Cdkn2A	Cyclin-dependent kinase inhibitor 2A
cDNA	Complementary deoxyribonucleic acid
cIAP1	Cellular inhibitors of apoptosis 1
cIAP2	Cellular inhibitors of apoptosis 2
COSMIC	Catalogue of somatic mutations in cancer
Deptor	DEP domain containing MTOR-interacting protein
DMEM	Dulbecco's Modified Eagle's Medium
EMMA	European Mouse Mutant Archive
EtOH	Ethanol
EUCOMM	European Conditional Mouse Mutagenesis program
FCS	Fetal calf serum
Fig	Figure
Fn14	Fibroblast growth factor inducible 14

FOLFIRINOX	Folinic acid, fluorouracil, , irinotecan, oxaliplatin
FRB domain	FKBP-Rapamycin binding
FSF	Frt-Stop-Frt
GAP	GTPase-activating proteins
GAPDH	Glyceraldehyde 3-phosphate dehydrogenase
GEMM	Genetically engineered mouse model
GI_{50}	Growth inhibitory 50%
GSEA	Gene set enrichment analysis
H&E	Hematoxylin and eosin
HEAT	Huntingtin elongation factor 3 protein phosphatase 2A TOR1
HK1/2	Hexokinase 1 and 2
Hsp	Heat shock protein
IHC	Immunohistochemistry
IKK α (CHUK)	IκB Kinase α
IKK	IκB Kinases
IKKβ	IκB Kinase β
IKKγ	IκB Kinase γ
IL1βR	IL1 beta Receptor
IPMN	Intraductal papillary mucinous neoplasms
IRS	Insulin receptor substrate
kb	Kilo bases
KC	Pdx1-Cre,LSL-$Kras^{G12D}$
KRAS	V-Ki-ras2 Kirsten Rat Sarcoma viral oncogene homolog
Ldha	Lactate dehydrogenase A
LSL	Lox-Stop-Lox
LTβR	Lymphotoxin b receptor
LZ	Leucine Zipper
MCN	Mucinous cystic neoplasms
mL	Milli-liter
mLST8 subunits	Mammalian lethal with Sec13 protein 8 interaction subunit
mm	Millimeter

mM	Millimolar
mRNA	Messenger ribonucleic acid
mSin1	Stress-activated protein kinase interaction protein
mTOR	Mammalian target of rapamycin
mTORi	mTOR inhibitors
Mut	Mutated
MW	Molecular weight
NIK	NFκB-inducing kinase
NLS	Nuclear localization signals
p70S6K	p70 ribosomal S6 kinase
PAGE	Polyacrylamide gel electrophoresis
Pancrex-Vet	Mouse diet M-Z low phytoestrogen+10g/kg
PanIN	Pancreatic intraepithelial neoplasia
PBS	Phosphate buffered saline
PCR	Polymerase chain reaction
PDAC	Pancreatic ductal adenocarcinoma
PDK1	Phosphoinositide-dependent protein kinase 1
Pdx1	Pancreatic and duodenal homeobox 1
PFK	Phosphofructokinase
PfkI	phosphofructokinase 1
PI	Propidium iodide
PI3K	Phosphoinositide 3-kinase
PIP_2	Phosphatidylinositol-3,4,5-biphosphate
PIP_3	Phosphatidylinositol-3,4,5-trisphosphate
PKB	Protein kinase B
PKC	Protein kinase C
PRAS40	Proline rich AKT substrate 40 kDa
Protor ½	Protein observed with Rictor-1 & 2
PTEN	Phosphatase and tensin homolog
Ptf1a	Pancreas transcription factor subunit alpha
R26	Rosa 26

RANK	Receptor activator of nuclear factor kappa-B
Raptor	Regulatory associated protein of mTOR
RAS	Rat sarcoma viral oncogene homolog
Rb	Retinoblastoma molecule
RHD	Rel homology domain
Rictor	Rapamycin-insensitive companion of mTOR
RNA	Ribonucleic acid
RT	Room temperature
RTK	Receptor tyrosine kinases
SC	Synergy score
SD	Standard deviation
SDS	Sodium dodecyl sulphate
SGK1	Serum and glucocorticoid induced protein kinase 1
Smad4	SMAD family members
TAD	Transcriptional activation domain
TCR	T cell Receptor
TEMED	N,N,N',N'-Tetramethylethylenediamine
TLR	Toll-like Receptor
TNFR	Tumor Necrosis factor receptor
TP53	Tumor protein p53 (Homo sapiens)
TRAFs	Tumor Necrosis factor receptors associated factors
Tris	Tris(hydroxymethyl)-aminomethane
p53	Transformation related protein 53 (Mus musculus)
TSCH1/2	Tuberous sclerosis complex 1 and 2
V	Voltage
v/v	Volume per volume
w/v	Weight per volume
wt	Wild type
µl	Microliter
µM	Micromete

5 Abstract

5-year-survival rate for pancreatic ductal adenocarcinoma (PDAC) is less than 9%, due to lack of diagnostic biomarker and poor therapeutic options. Recent evidence in PDAC has shown that oncogenic Kras-driven Nfκb2 activation mediates drives tumorigenesis. However, the role of *Nfκb2* on a genetic level for the pancreatic tumorigenesis is not well understood. One of the aims of this thesis was therefore to investigate the impact of Nfκb2 signaling in PDAC tumor initiation and progression. It has been observed that Nfκb2 is essential for the $Kras^{G12D}$-driven carcinogenesis in the murine pancreas. Additionally, pre-neoplastic lesions in the corresponding mouse model showed a significant reduction in proliferation. Furthermore, a reduced expression of pro-proliferative genes in the *Nfκb2*-deficient background was detected. In contrast, *Nfκb2* is dispensable for tumor formation and progression in aggressive PDAC models, relying on the simultaneous expression of the oncogenic *Kras* and the mutated tumor suppressor *p53*. This work, therefore, demonstrates the context-dependent function of Nfκb2 and its modulation by the tumor suppressor p53.

Genetic deletion of the *Mtor* gene in the pancreas by using conventional GEMMs results in exocrine and endocrine insufficiency. Therefore, to conditionally manipulate the expression of *Mtor* at the genetic level as well as to generate a novel *Mtor* floxed cellular model, an inducible dual-recombinase system was established. Transcriptomic and metabolic analyses indicated that MTOR controls several metabolic pathways, partially through maintaining glucose uptake and growth. Despite a cytostatic growth response, a subpopulation of cancer cells survived *Mtor* inactivation giving rise to resistant clones. Importantly, blocking MTOR genetically as well as pharmacologically resulted in adaptive rewiring of oncogenic signaling with activation of canonical MEK/ERK as well as PI3K/AKT pathway. Combined inhibition of these pathways with MTOR showed synergistic effects in some of the tested PDAC models cell lines. Therefore, it provides evidence that a therapeutic strategy of optimized combination therapies is needed to combat resistance mechanisms in pancreatic cancer.

6 Zusammenfassung

Die 5-Jahres-Überlebensrate für das duktale Adenokarzinom des Pankreas (PDAC) beträgt aufgrund fehlender diagnostischer Biomarker und therapeutischer Optionen weniger als 9%. Neuere Forschungsergebnisse haben gezeigt, dass die Aktivierung von Nfκb2 durch onkogenes Kras die Karzinogenese im Pankreas antreibt. Die genaue Funktion von *Nfκb2* ist hierbei jedoch bisher nicht im Detail verstanden. Eines der Ziele war es daher, die Rolle von Nfκb2 bezüglich der Wirkung auf die Tumorinitation und -progression im Pankreas zu untersuchen. *Nfκb2* ist essenziell für die $Kras^{G12D}$-getriebene Karzinogenese im murinen Pankreas. Im *Nfκb2*-defizienten Modell konnte eine signifikant verminderte Proliferation in Vorläuferläsionen gezeigt werden. Passend hierzu zeigte sich in dem *Nfkb2*-defizienten Modell eine geringere Expression von pro-proliferativen Genen. Im Gegensatz dazu ist *Nfκb2* entbehrlich für die Tumorentstehung und -progression in aggressiven PDAC Modellen, die auf der gleichzeitigen Expression von onkogenem Kras und dem mutierten Tumorsuppressor p53 basieren. Damit zeigt diese Arbeit die Kontextabhängigkeit der Nfκb2 Funktion und die Modulation der Rolle von Nfκb2 durch den Tumorsuppressor p53.

Genetische Deletion des *Mtor* Gens im Pankreas in konventionellen genetisch veränderten Mausmodellen führte zu endokriner und exokriner Pankreasinsuffizienz. Aus diesem Grund wurde ein neuartiges, duales Rekombinationsmodell etabliert, um konditional die Expression von *Mtor* auf genetischer Ebene zu manipulieren. Metabolische und transkriptomische Analysen zeigen, dass MTOR verschiedene metabolische Signalwege kontrolliert und insbesondere die Aufnahme von Glukose und das Zellwachstum reguliert. Trotz einer zytostatischen Wirkung der Mtor Inhibition, können Pankreaskarzinomzellen an die genetische *Mtor* Deletion adaptieren. Sowohl die genetische als auch die pharmakologische Inhibition von MTOR führt zu einer Neuverschaltung Onkogene Signalwege und Aktivierung des kanonischen MEK/ERK als auch des PI3K/AKT Signalweges. Die gemeinsame Hemmung von MTOR mit diesen Signalwegen ist in mehreren zellulären Pankreaskarzinommodellen synergistisch. Damit konnten Hinweise auf neue mechanistische Kombinationsbehandlungen als therapeutische Strategien erarbeitet werden.

7 Introduction

7.1 Pancreatic Cancer

Pancreatic cancer is one of the deadliest malignancies with a 5-year-survival rate of less than 9% (Siegel et al., 2019) and currently the fourth leading cause of cancer-related death in the United States (Siegel et al., 2018). In addition, the incidence rate is still increasing and pancreatic cancer is predicted to be the second leading cancer-related mortality in the United States (Rahib et al., 2014) as well as in Germany by 2030 (Quante et al., 2016). Therefore, more efforts to prevent or treat this disease should be undertaken.

Multiple genetic syndrome as well as modifiable risk factors for development of the pancreatic cancer are described (Bhosale et al., 2018). About 5-10% of pancreatic cancer are inherited (Brand et al., 2007; Klein, 2012). Hereditary breast and ovarian cancer syndrome (Beger et al., 2004; Lucas et al., 2013), familial atypical multiple mole melanoma syndrome (FAMMM) (McWilliams et al., 2011), cystic fibrosis (Maisonneuve et al., 2007), familial pancreatic cancer history (Capurso et al., 2013), as well as hereditary pancreatitis (Becker et al., 2014; Raimondi et al., 2010) are linked with a variable increased risk of developing pancreatic cancer. Non-hereditary risk factors which include smoking (Yadav and Lowenfels, 2013), alcohol (Genkinger et al., 2009) or diet (Larsson and Wolk, 2012). In addition, obesity (Larsson et al., 2007), previous surgeries (Lin et al., 2012), different infections (Trikudanathan et al., 2011), chronic pancreatitis (Raimondi et al., 2010), age and gender (Li et al., 2009), type I (Stevens et al., 2007) and type II diabetes mellitus (Huxley et al., 2005) have also been shown to increase the risk of pancreatic cancer. However, no appropriate standard screening procedure for high risk patients is available till now.

The main reasons for the high mortality of pancreatic cancer are late diagnosis and inefficient therapeutic strategies. Surgical resection is the only potential curative option available so far. However, only 15-20% of patients are eligible for surgical resection (Adamska et al., 2017). Most patients are usually diagnosed with locally advanced or disseminated carcinomas (Siegel et al., 2017), and are therefore not suitable candidates for surgery.

For more than two decades, the nucleoside analogue gemcitabine has been the standard of care for locally advanced and metastatic pancreatic cancer (Burris et al., 1997). However, Gemcitabine provides a minimal survival benefit and a low response rates (Vincent et al., 2011). Clinical success was achieved by the introduction of combination chemotherapies. Such as combination treatment of gemcitabine and nanoparticle-albumin bound(nab)-

paclitaxel (Gem/NabP) in phase III study of metastatic pancreatic cancer patients showed a significant survival advantage of almost 2 months (Von Hoff et al., 2013) In addition, a significant survival advantage of almost 6 months has been documented by the use of the FOLFIRINOX (folinic acid, 5-Fluo-uracil (5-FU), irinotecan and oxaliplatin) regimen (Conroy et al., 2011) as compare to gemcitabine alone. Therefore, combination treatment of gemcitabine with NabP or FOLFIRNOX are currently the standard of care treatment regiments for primary and metastatic PDAC (Blomstrand et al., 2019; Chllamma et al., 2016).

Based on the success of these combination therapies, adjuvant therapies were designed, and different trials were performed for testing such combinations after resection of primary pancreatic tumors. The largest improvement has been observed more recently in a phase III study with 493 patients treated with an adjuvant modified FOLFIRINOX regimen that shows improved survival of 54.4 months as compared to 35 months with gemcitabine monotherapy (Conroy et al., 2018). However, therapeutic approaches as a whole remain unsatisfactory with a response rate of approximately ≤ 30% to the current combination therapies (Hua et al., 2018). So, there is a need to improve available therapies.

7.2 Progression model of pancreatic cancer

Among all pancreatic tumors, pancreatic ductal adenocarcinoma (PDAC) is an aggressive and predominant form of pancreatic cancer representing approximately 90% of the cases (Adamska et al., 2017). The rarer tumors types of the pancreas include neuroendocrine tumors or exocrine tumors such as acinar cell carcinoma (Khalili et al., 2006; Milan and Yeo, 2012).

Macroscopically, PDAC appears as a solid, white mass containing often a central necrotic part (Hruban and Klimstra, 2014; Hruban et al., 2007). Microscopically, according to the classical and extensively studied model, oncogenic KRAS induces trans-differentiation of acinar cells into duct like cells by a process known as acinar to ductal metaplasia (ADM). At least in mouse models, ADM precedes and give rise to pancreatic intraepithelial neoplastic lesions (PanINs) which progress to develop PDAC by accumulation of additional mutations. Moreover, ADM are known as a major characteristic of chronic pancreatitis and are often associated with PanINs in PDAC patients (Hruban et al., 2000; Kopp et al., 2012; Storz, 2017).

PanINs are present in 60% of chronic pancreatitis and 82% of invasive cancer patients, respectively. Therefore, their presence in close proximity to invasive cancer (Hisa et al.,

2007; Sipos et al., 2009), as well as in patients with strong family history of pancreatic cancer further support that model (Crnogorac-Jurcevic et al., 2013). PanINs are classified into three grades according to morphological alterations. PanIN-1A are flat lesions, while PanIN-1B are micro-papillary lesions with abundant cytoplasmic mucin. PanIN-2 exhibits additional nuclear alterations, while PanIN-3 are advanced lesions with complete disturbance of the normal epithelial architecture, including multinucleated cells, luminal necrosis, epithelial cell budding into the ductal lumen (Hruban et al., 2004) as shown in Fig. 7.1. PanIN-3 are quite similar to carcinoma, however, still with an intact basement membrane (Sausen et al., 2015). Recently, it has been observed that in addition to acinar cells, pancreatic ductal cells can also give rise to pre-neoplastic lesions which progress to PDAC (Lee et al., 2018).

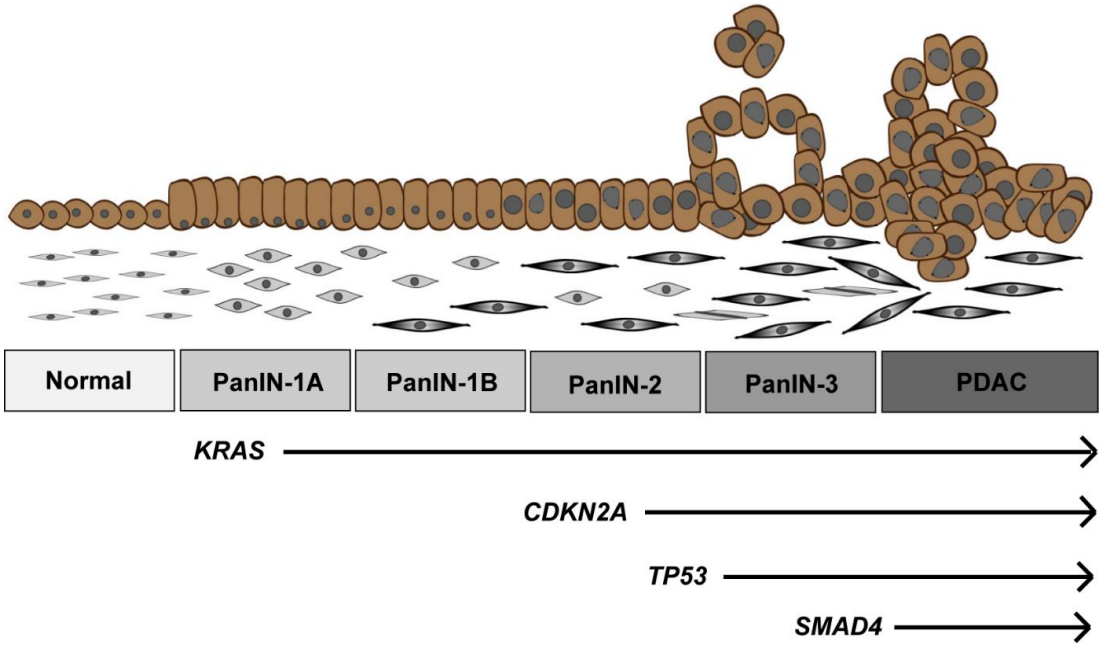

Fig. 7:1 Initiation and progression model of Pancreatic Ductal Adenocarcinoma (PDAC)

Genetically, normal cells passed through sequence of pancreatic intraepithelial lesions (PanIN-1A, -1B, -2 and -3) to develop PDAC. Morphological changes correlate with distinct molecular events. Early lesions already possess mutation of KRAS. Advance lesions accumulate inactivation of the tumor suppressors CDNK2A, TP53 or SMAD4. Adapted from (Bhosale et al., 2018).

In addition, PDAC can arise from alternative lesions such as intraductal papillary mucinous neoplasms (IPMNs) and mucinous cystic neoplasms (MCNs) (Yamaguchi et al., 2018). Furthermore, the trans-differentiation of pancreatic acinar cells to ductal cells can develop via atypical flat lesions (AFL), that may represent another type of precursor for pancreatic cancer development (Basturk et al., 2015). However, the relationship between these different PDAC precursors lesions with one another as well as their cellular origin remains to be fully explored (Hezel et al., 2006).

Simultaneously with the morphological progression of PanIN lesion, genomic changes occur (Lennerz and Stenzinger, 2015; Waddell et al., 2015), For PDAC, frequent genetic lesions include mutations in the *KRAS* oncogene or deletion of tumor suppressors such as *TP53*, *CDKN2A* and *SMAD4* (Fotopoulos et al., 2016; Sidaway, 2017) as shown in Fig. 7.1. Beyond these four major genetic events, the tumor is genetically heterogeneous, and the frequency of events drop below 10% (Bailey et al., 2016; Biankin et al., 2012).

7.3 Oncogenic KRAS

The RAS (rat sarcoma viral oncogene homolog) comprises one of the most frequently mutated oncogene in the human cancer (Waters and Der, 2018). It has four different isoforms (HRAS, NRAS, KRAS4A, and KRAS4B), encoded by three genes: *HRAS, NRAS, and KRAS* (Tsai et al., 2015). Each has similar functional domains responsible for binding and hydrolyzing GTP, while having different C-terminal membrane targeting domains (Cox et al., 2015).

RAS is one of the GTPase family member that function as a binary ON-OFF switch that cycle between an active guanosine triphosphate (GTP) and an inactive guanosine diphosphate (GDP)-bound state. The conversion from stable, inactive GDP-bound form to the active GTP-bound form is regulated by guanine nucleotide exchange factors (GEFs), while, GTPase-activating protein (GAPs) are responsible for RAS-mediated GTP hydrolysis that leads to inactivation of KRAS molecule (Cherfils and Zeghouf, 2013). GEFs and GAPs can make a variety of interactions with different extracellular stimuli such receptor tyrosine kinases (RTKs) or other cell-surface receptors that control the level of active and inactive RAS, which further regulate different signaling networks (Cox and Der 2010).

Majority of cancers exhibit missense mutations at one of the three common hot spots regions at codon 12 (89%), 13 (9%) and 61 (1%), that impairs intrinsic and GAP mediated hydrolysis (Waters and Der, 2018). Moreover, the G12D mutation is presumably the most prevalent form among three frequent codon 12 mutations in PDAC: G12C (14%), G12D (36%) and G12V (23%) mutations. In addition, G13C (7%) and Q61H (0.6%) mutations are also observed (Lu et al., 2016). These mutations result into constitutive activation of KRAS and hence persistent stimulation of downstream pathways, including canonical mitogen-activated protein kinase kinase (MEK)/extracellular signal-regulated kinase (ERK) and non-canonical phosphoinositide 3-kinase (PI3K)/the Ser/Thr kinase mechanistic target of rapamycin (MTOR) pathways or the nuclear factor kappa light chain enhancer of activated B cells (NFκB) that leads to cancer development (Jonckheere et al., 2017). Overall, oncogenic

KRAS activation is an initiating event in PDAC, as somatic mutations in KRAS are detected even in early PanINs (Kanda et al., 2012). KRAS is also required for maintenance and progression of PDAC tumorigenesis and the importance of the gene for PDAC is underscored by a mutation frequency of 95% (Choi et al., 2019; Raphael et al., 2017; Witkiewicz et al., 2015).

7.3.1 KRAS-driven mouse models for pancreatic cancer

Currently genetic engineered mouse models (GEMMs) of pancreatic cancer have been developed by the induction of the tissue-specific expression of initiating *Kras*^{G12D} oncogene with or without the deletion of relevant tumor suppressor genes. The most commonly used mouse models use a *Lox-Stop-Lox (LSL)* cassette silenced oncogenic *Kras*^{G12D} allele (Jackson et al., 2001). Excision of the LSL cassette by a Cre-recombinase under control of a pancreatic tissue-specific promoter such as the *Pdx1* promoter or the *Ptf1a* promoter leads to expression of oncogenic Kras in the murine pancreas. Hereby expression of the oncogene is driven by the endogenous promoter, avoiding artificial overexpression of the oncogene (Hingorani et al., 2003; Veite-Schmahl et al., 2017). *Pdx1* expression is initiated at embryonic day 8.5 (Gannon et al., 2000), while *Ptf1a* expression occurs later at embryonic day 9.5 (Kawaguchi et al., 2002; Nakhai et al., 2007). Expression of *Kras*^{G12D} alone in these mouse models (*Pdx1-Cre; LSL-Kras*$^{G12D/+}$ and *Ptf1a*$^{Cre/+}$*; LSL-Kras*$^{G12D/+}$) is sufficient to induce ADMs, low and high grade PanINs that gradually progress to PDAC and metastasize to lung and liver in 40% of cases (Eser et al., 2013; Hingorani et al., 2003; Schönhuber et al., 2014). However, progression to invasive cancer occurs gradually and slowly. Additional genetic events such as inactivation of tumor suppressors genes like *p53* (Hingorani et al., 2005; Morton et al., 2010), *Cdkn2a (Ink4a/arf*) (Aguirre et al., 2003), *Smad4* (Kojima et al., 2007) and *Brca2* (Skoulidis et al., 2010) are needed to accelerate PDAC development.

The *TP53* gene is altered in almost 75% of human PDAC (Fotopoulos et al., 2016), predominantly through missense mutations. To study its role in PDAC development, a *p53*^{R172H} mutation (the mouse ortholog of human *TP53*^{R175H}) was inserted into the endogenous *p53* locus, which was again silenced by a *LSL* cassette to allow tissue specific expression of the mutant (Olive et al., 2004). The *p53*-mutated mice (*Pdx1-Cre, LSL-Kras*$^{G12D/+}$*, LSL-p53*$^{R172H/+}$) display accelerated PanIN formation and PDAC development (Hingorani et al., 2005) and survive only 4 to 5 months (You et al., 2016). Due to the inactivation of *p53*, cancers are characterized by extensive chromosomal instability in this model (Gopinathan et al., 2015; Hingorani et al., 2005).

In conclusion, these studies demonstrate that pancreas-specific expression of oncogenic *Kras* in mice is sufficient to initiate ADM, PanINs and metastatic PDAC. The described models also revealed some short comings, like the impossibility to study mutli-step carcinogenesis, like genetically targeting the established cancers or to genetically manipulate different compartment of the tumor. Such shortcomings were recently overcome by the development of a dual recombination-system (Schönhuber et al., 2014).

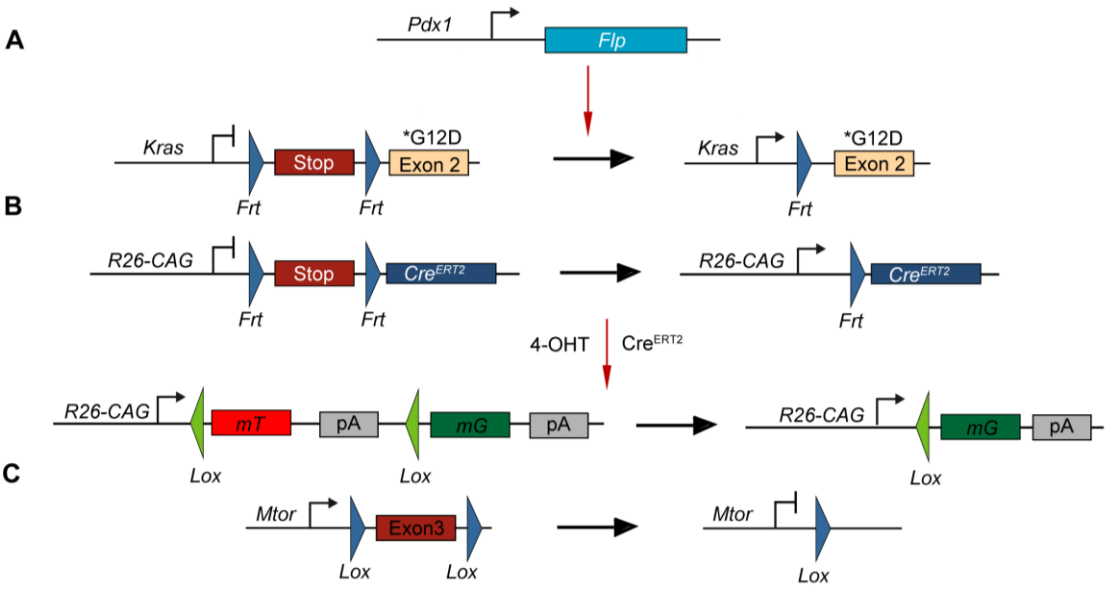

Fig. 7:2 Schematic illustration of the dual recombination system

A) Pancreas-specific *Pdx1* promoter induces *Flp* recombinase expression. B) Excision of the *FSF* cassette by *Flp*-mediated recombination leads to *Kras*^{G12D} activation and *Cre*^{ERT2} expression. C) Excision of the *LSL* cassette by the Tamoxifen (4-OHT) activated Cre^{ERT2} recombinase that results in deletion of *mTomato (mT)* and ultimately expression of *eGFP (mG)* as well as results into deletion of exon 3 of *Mtor.* Modified from (Hassan et al., 2018).

To study the multistep carcinogenesis, a dual recombination system combining the *Cre/Lox* and the *Flp/Frt* recombinase was used. In the *Flp/Frt* model, the expression of the Flp recombinase is under the control of the *Pdx1* promoter and expression of the oncogenic *Kras*^{G12D} allele (*FSF-Kras*$^{G12D/+}$) can be activated by deletion of the *Frt-Stop-Frt (FSF)* cassette. *Pdx1-Flp;FSF-Kras*$^{G12D/+}$ mice develop PanIN lesions, which progress gradually to PDAC (Schonhuber et al., 2014), similar to the established *Cre/lox*-based *Kras*^{G12D}-driven PDAC models (Hingorani et al., 2003). A tamoxifen inducible Cre^{ERT2} recombinase is expressed after *Flp* mediated recombination of a stop cassette as shown in Fig. 7.2. However, Cre^{ERT2} remains sequestered in the cytoplasm by binding to Hsp90. This inducible Cre^{ERT2} recombinase is under the control of the CAG promoter that is present in the *Rosa26* locus and is silenced by an *FSF* cassette (*FSF-R26*$^{CAG\text{-}CreERT2}$). Moreover, upon administration of tamoxifen (estrogen analogue), Cre^{ERT2} can dissociate from Hsp90 and

translocate to the nucleus where it catalyzes the recombination of *floxed* genes such as the reporter gene *R26*$^{mT/mG}$ (Schönhuber et al., 2014) or potential therapeutic targets, like the *Mtor* gene (Hassan et al., 2018). This model is illustrated in Fig. 7.2.

7.3.2 KRAS downstream effector pathways

Oncogenic KRAS is a key therapeutic target and preclinical research is focused on targeting its membrane localization as well as inhibiting the formation of the RAS-GTP complex (Scott et al., 2016). Although, the first KRAS (G12C) inhibitor AMG 510 entered into the clinical phase I/II studies based on precise selectivity and potency towards tumor cells in non-small cell lung cancer (NSCLC) (Canon et al., 2019), direct targeting of KRAS has not yet been clinically successful till now (Coxet al., 2014).

The most promising therapeutic option so far is therefore still indirect targeting of the oncogene by inhibition essential downstream effectors. The most intensively studied classical KRAS downstream targets are RAF/MEK/ERK and PI3K/AKT/MTOR (Awasthi et al., 2018; Murthy et al., 2018). In addition, many other pathways such as NFκB and JNK pathways are regulated by oncogenic KRAS (Davies et al., 2014; Karandish and Mallik, 2016; Ling et al., 2012).

7.4 NFκB

The NFκB signaling pathway is a central hub for the regulation of more than 1500 genes (Yang Yang, 2016), which are involved in the regulation of the immune response, cellular stress responses, the cell cycle, or apoptosis (Pires et al., 2018).

In mammalian cells, the NFκB family of transcription factors consist of five subunits termed RelA (p65), c-Rel, RelB, NFκB1/p105 and NFκB2/p100 (Fig. 7.3), which are defined by the presence of an approximately 300 amino acid-long conserved Rel homology domain (RHD), that is responsible for binding to DNA, dimerization and interaction with inhibitory IκB proteins (Kaltschmidt et al., 2018; Xia et al., 2018). RelA, RelB and cRel have trans-activation domains (TAD) in their C terminal regions that enable them to interact with transcriptional co-regulators and activate transcription of target genes. In normal conditions, ankyrin repeats domains (ARD) that are also known as inhibitory domains mask nuclear localization signals (NLS) and sequester NFκB in the cytoplasm. IκBα, IκBβ; IκBε and BCL3 as well as unprocessed NFκB1 and NFκB2 molecules contain ARDs (Pires et al., 2018). NFκB family members can form homo and heterodimers with each other with different

affinities and can act as both transcriptional repressor as well as activator. Among them, the p65/p50 heterodimer is the most common and stable NFκB dimer (Hayden and Ghosh, 2012).

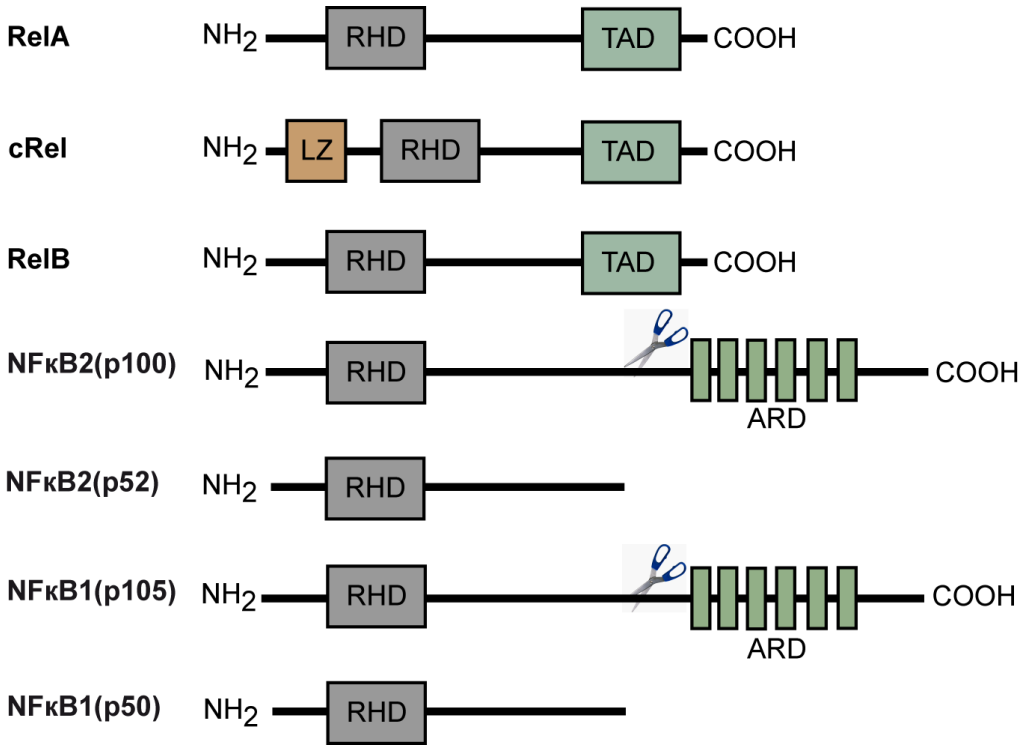

Fig. 7:3 Schematic diagram for the NFκB family members

NFκB family consist on five members such as RelA, cRel, RelB, p100 (NFκB2) giving rise to p52 and p105 (NFκB1) giving rise to p50. p50 and p52 are generated by proteasomal processing which is symbolized by scissors. RHD: Rel homology domain, TAD: Transcriptional activation domain, LZ: Leucine Zipper while ARD: Ankyrin repeats domain (modified from Hayden & Ghosh, 2012).

7.4.1 Canonical NFκB pathway

Activation of the tumor necrosis factor receptor (TNFR), IL1β receptor (IL1βR), toll like receptor (TLR), T cell receptor (TCR) and B cell receptor (BCR) by their corresponding ligands activates adaptor proteins such as tumor necrosis factor receptor associated factors (TRAFs) or receptor interacting kinases (RIPs). These adaptor proteins activate the IκB Kinases (IKK) complex which is consisting on catalytic subunits IKKα (CHUK) and IKKβ as well as the regulatory subunit IKKγ (NEMO) (Hayden and Ghosh, 2012; Taniguchi and Karin, 2018). The activated IKK complex phosphorylate the inhibitory IκB domain at conserved serine residues (DSGXXS), followed by K48-ubiquitination and 26S based proteasomal degradation of inhibitor proteins such as inhibitor of IκBα or IκBβ (Chen and Chen, 2013), which initiates the classical NFκB pathway. Consequently, different NFκB dimers like

p65/p50 and cREL/p50 can translocate to the nucleus to induce the transcription of target genes (Pires et al., 2018).

7.4.2 Non-canonical NFκB pathway

A subset of the TNF receptor superfamily such as BAFF receptor (BAFFR) (Claudio et al., 2002), cluster of differentiation 40 (CD40) (Coope et al., 2002), lymphotoxin β receptor (LTβR) (Dejardin et al., 2002), fibroblast growth factor inducible 14 (Fn14) (Saitoh et al., 2003), and receptor activator of nuclear factor kappa-B (RANK) (Novack et al., 2003) can induce the non-canonical NFκB pathway as shown in Fig. 7.4.

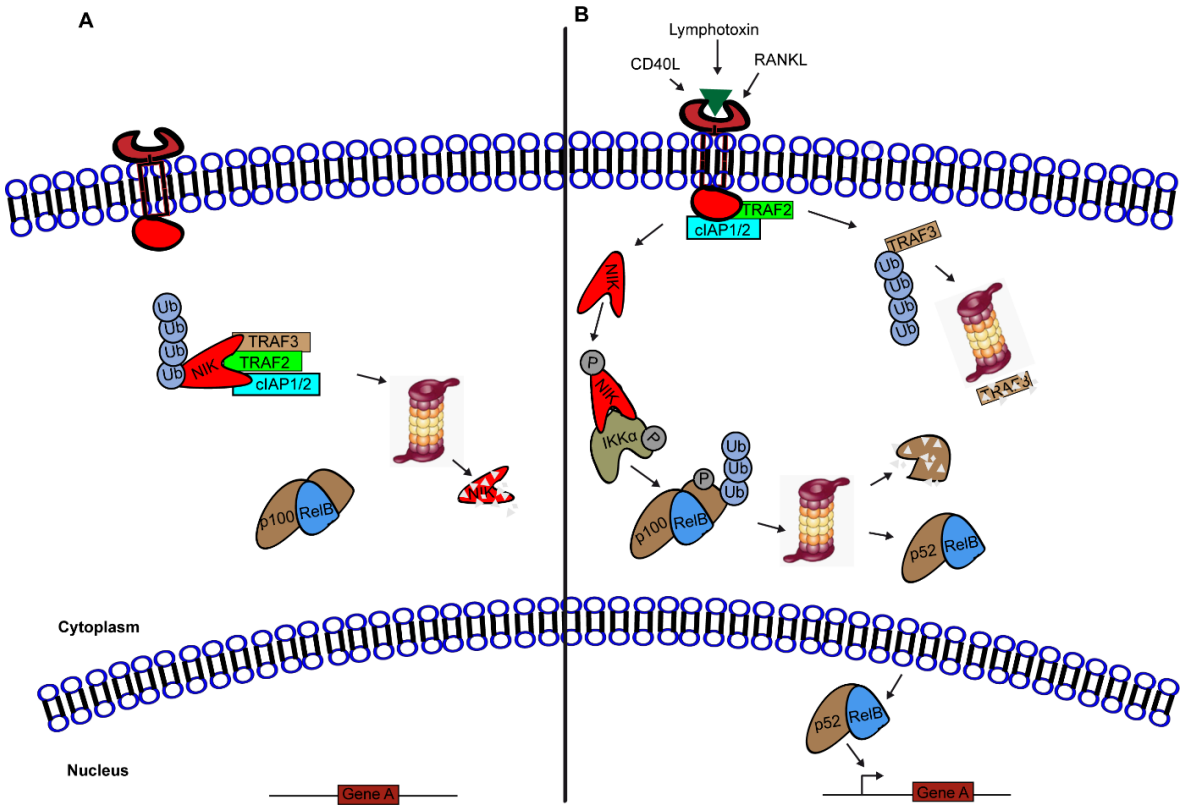

Fig. 7:4 Illustration of the non-canonical NFκB signaling pathway

A) Under unstimulated conditions, the multiprotein ubiquitination complex consisting out of TRAF2, TRAF3, cIAP1 and cIAP2 contributes to the continuous ubiquitination and consequent proteasomal degradation of NIK. B) Receptor activation occur in response to certain stimuli such as Lymphotoxin, receptor activator of nuclear factor kappa-B ligand (RANKL), cluster of differentiation 40 ligand (CD40L) that result into degradation of TRAF3 and NIK stabilization, IKKα phosphorylation and activation of p100 which is phosphorylated by IKKα becomes ubiquitination and proteasomal processes to p52. Afterwards the resulting RelB-p52 dimer translocate into the nucleus and activate transcription.

The activation of these receptor molecules leads to the degradation of the adaptor molecules such as TRAF3 and the stabilization of NFκB- inducing kinase (NIK), which phosphorylates

and activates the IKKα subunit (Maubach et al., 2019). Consequently, IKKα phosphorylates p100 at Serine 866 and 870 (Xiao et al., 2004), leading to the recruitment of the β-TrCP (SCF) ubiquitin ligase (Liang et al., 2006), the ubiquitination of p100 and the subsequent proteasomal processing of p100 to generate active p52 (Polley et al., 2016). Newly generated p52 dimerizes with RelB and translocate into the nucleus to activate transcription of specific target genes of the non-canonical NFκB pathway (Gray et al., 2014).

7.4.3 Role of NFκB in Cancer

NF-κB has been extensively studied in the past decades as an important cancer relevant pathway and potential therapeutic target. The role of NFκB in cancer was initially described in chicken lymphomas almost four decades ago (Beug et al., 1981). Both solid and hematopoietic malignancies such as gastric cancer (Yamei Shen, 2019), PDAC (Li et al., 2018; Weichert et al., 2007), glioma (Lee et al., 2013) and multiple myeloma (MM) (Keats et al., 2007; Roy et al., 2018) show dysregulation of NFκB. Moreover, constitutive activation of NF-κB in multiple cancers is linked with poor survival, like in acute myeloid leukemia (AML), breast cancer, glioblastoma and ovarian cancer (Annunziata et al., 2010; Brown and Law, 2006; Darwish et al., 2019; Rojo et al., 2016).

In addition to high expression, certain mutations are also linked with aberrant NFκB signaling in cancers. About 20% of MM patients show aberrant NFκB pathway linked mutations in *NIK, TRAF2, TRAF3, NFκB1 and NFκB2* (Annunziata et al., 2007; Keats et al., 2007; Lohr et al., 2014; Roy et al., 2018). Among them, *TRAF3* inactivation is the most frequent alteration (Keats et al., 2007). Solid tumors, however, rarely show mutations in the *NFκB* genes (DiDonato et al., 2012).

Regulation of multiple pathways like proliferation, apoptosis, metabolism, metastasis, inflammation and therapy resistance underscore the relevance of the NFκB pathway in cancer (Colombo et al., 2018; Pramanik et al., 2018; Riedlinger et al., 2018; Saxon et al., 2018). Like, NFκB controls the expression of several pro-inflammatory genes, which are important risk factors for cancer development. Elevated NFκB activity in patients with inflammatory bowel disease (IBD) leads to increased expression of pro tumorigenic cytokines TNF-α, IL-1, and IL-17,which increased the risk of developing colon cancer (Lakatos and Lakatos, 2008; Terzić et al., 2010). Likewise, activation of the non-canonical NFκB pathway in lung and breast cancer leads to increased proliferation and cell survival (Rojo et al., 2016; Saxon et al., 2018), as well as stabilize tumor initiating cells (TICs) for the development of metastasis in breast cancer (Kendellen et al., 2014; Lawrence and Baldwin, 2016).

Furthermore, non-canonical NFκB pathway driven transcriptional reactivation of TERT in glioblastoma (Li et al., 2015b), as well as upregulation of DNA editing enzymes APOBECs enhanced cancer mutagenesis (Leonard et al., 2015). Most importantly, NFκB is involved in the adaptive resistance to many standard clinical used drugs such as gemcitabine and FOLFIRONOX regime, further supporting the notion of NFκB as an important therapeutic target (Mezencev et al., 2016; Pramanik et al., 2018; Yu et al., 2018).

7.4.4 NFκB pathway in PDAC

NFκB signaling contributes to the pathobiology of PDAC development and maintenance (Prabhu et al., 2014; Storz, 2013). For example, constitutive activation of the canonical NFκB pathway via RELA marked PDAC patients with poor survival (Weichert et al., 2007). Stabilization of p65 by higher expression of IL-1α (Ling et al., 2012) or by TRIM31 marked worse prognosis in PDAC patients (Yu et al., 2018). Moreover, constitutive activation of all members of the NFκB pathway has also been detected in patient derived human PDAC cell lines (Chandler et al., 2004).

Consistent with survival data, genetic evidences in mouse models demonstrated the important role of NFκB pathway as an oncogene in tumor initiation (Liou et al., 2016; Maier et al., 2013). For example, oncogenic KRAS upregulate NFκB mediated EGFR activity, which facilitates de-differentiation of acinar cells and PanIN formation (Liou et al., 2016). In line with this observation, *Kras*^{G12D}-driven PDAC GEMMs demonstrated that constitutive activation of NFκB via NEMO/IKKγ is responsible for the enhanced expression of cytokines such as TNFα, IL1α and IL1β as well as NOTCH pathways which impact on propagation of PanIN lesions (Maier et al., 2013). In line with this finding, there are many GEMMs studies available which depict the pro-tumorigenic role of NFκB in PDAC progression. For example, it has been observed that crosstalk of NFκB via IKKβ with NOTCH signaling promote PDAC progression (Maniati et al., 2011).

In contrast, there are some NFκB family members which play dual role in pancreatic carcinogenesis, depending on certain mutational burden. Like, RelA truncation results into reduced CXCL1 production which impairs CXCR2 activity (Lesina et al., 2016). As a result, senescence associated secretory phenotype (SASP) composition is changed (Tchkonia et al., 2013), which allows cells to bypass the oncogene-induced senescence (OIS) barrier and accelerate PanINs formation (Lesina et al., 2016). While, by accumulation of genetic mutations such as *p53 or Ink4a* deletion, which enables cells to bypass senescence and OIS

barrier, NFκB support tumor progression as RelA truncation gives survival benefit (Lesina et al., 2016; Morton et al., 2010; Serrano et al., 1997).

In addition to the canonical NFκB pathway, non-canonical NFκB pathway is also constitutively active and functional in PDAC (Doppler et al., 2013; Nishina et al., 2009; Wharry et al., 2009). Moreover, high activity of RELB marked PDAC patients with bad survival (Hamidi et al., 2012).

Functionally, the non-canonical NFκB (p100/p52) activity is connected in PDAC with proliferation (Bang et al., 2013; Doppler et al., 2013; Schneider et al., 2006), as well as (RelB) with apoptosis and stress (Hamidi et al., 2012). Like, ablation of *Relb* in a *Kras*^{G12D}-driven mouse model of PDAC blocked PanINs development (Hamidi et al., 2012). Mechanistically, nutrient deprivation leads to co-activation of Nuclear Protein 1 (Nupr1) and RelB activation which protects cells from apoptosis (Hamidi et al., 2012). In addition, oncogenic KRAS dependent upregulation of glycogen synthase kinase 3α (GSK-3α) contributes to PDAC cell proliferation and growth by promoting TGFβ activated kinase 1 (TAK1)/TAK1 binding partners (TAB) complex formation, which facilitates processing of p100 and activation of p52 (Bang et al., 2013). Other study showed that non-canonical NFκB pathway activity is mediated by proteasomal degradation of TRAF2 and NIK stabilization that enhanced cell proliferation (Doppler et al., 2013). The importance of the non-canonical NFκB signaling pathways is furthermore underscored by a recent study where *Nfκb2* gene amplification was demonstrated in *Kras*^{G12D}-driven murine PDAC cell lines (Mueller et al., 2018). However, still lacks genetic studies for the non-canonical NFκB (p100/p52).

So, in order to get a clearer picture, there is a need to study in detail the function of the non-canonical NFκB pathway genetically in PDAC

7.5 MTOR

The mammalian target of rapamycin (MTOR) is an important kinase responsible for the regulation of proliferation, apoptosis, autophagy and metabolism (Paquette et al., 2018; Saxton and Sabatini, 2017).

MTOR is a 289 kDa protein with multiple domains. The N-terminus of MTOR consists of multiple huntingtin elongation factor 3 protein phosphatase 2A TOR1 (HEAT) repeats, responsible for interaction with other proteins. MTOR belongs to the phosphoinositide 3 kinase family due to the presence of the FKBP-Rapamycin binding (FRB) domain and the C-

terminal evolutionarily conserved serine/threonine kinase domain. Furthermore, due to the interaction of different binding partners, MTOR is included in two distinct large protein complexes termed MTOR complex 1 and 2 (abbreviated as MTORC1 and MTORC2) (Jhanwar-Uniyal et al., 2019).

The MTORC1 complex is mainly responsible for inducing protein synthesis and contains RAPTOR (regulatory associated protein of MTOR) (Hara et al., 2002) and PRAS40 (proline rich AKT substrate 40kDa), in addition to DEPTOR (DEP domain containing mTOR-interacting protein) and mLST8 (mammalian lethal with Sec13 protein 8 interaction). Mechanistically, MTORC1 enhances translation of mRNAs, such as ribosomal proteins, elongation factors and insulin growth factors by mediating phosphorylation of p70S6K (p70 ribosomal S6 kinase) and 4EBP1 (eukaryotic initiation factor 4E binding protein 1) (Saxton and Sabatini, 2017)

The MTORC2 complex interacts with RICTOR (Rapamycin-insensitive companion of mTOR), mSIN1 (stress-activated protein kinase interaction protein) and PROTOR 1/2 (protein observed with RICTOR 1 & 2), in addition to DEPTOR and mLST8. Mechanistically, little is known about MTORC2. There are hints that MTORC2 is involved in the regulation of cytoskeletal organization as well as AKT(S473) dependent proliferation and survival of cells (Fuhler et al., 2009; Saxton and Sabatini, 2017).

7.5.1 Activation of MTOR

Receptor tyrosine kinases (RTK) can be activated in response to growth factors like insulin that can activate phosphoinositide 3-kinase pathway (PI3K) via insulin receptor substrate (IRS) molecules (Tanti and Jager, 2009). This activation is counteracted by the tumor suppressor phosphatase and tensin homolog (PTEN) that blocks that pathway. However, activated PI3K converts phosphatidylinositol-3,4,5-biphosphate (PIP_2) into the active phosphatidylinositol-3,4,5-trisphosphate (PIP_3) form that further leads to activation of downstream molecules such as serum and glucocorticoid induced protein kinase (SGK), phosphoinositide-dependent protein kinase 1 (PDK1) and Serine and Threonine kinase (AKT) (Mayer and Arteaga, 2016). AKT is also known as protein kinase B (PKB) and exists in three isoforms called AKT1 (PKBα), AKT2 (PKBβ) and AKT3 (PKBγ). However, AKT1 is the most important and commonly expressed isoform having two important phosphorylation sites at T308 and S473 (Manning and Toker, 2017). Due to the presence of a pleckstrin homology (PH) domain at its N-terminus, AKT1 can be activated by phosphorylation at T308 by

interacting with PIP3 via PDK1 (Alessi et al., 1997), or by phosphorylation at S473 by MTORC2 complex (Moore et al., 2007) as shown in Fig. 7.5.

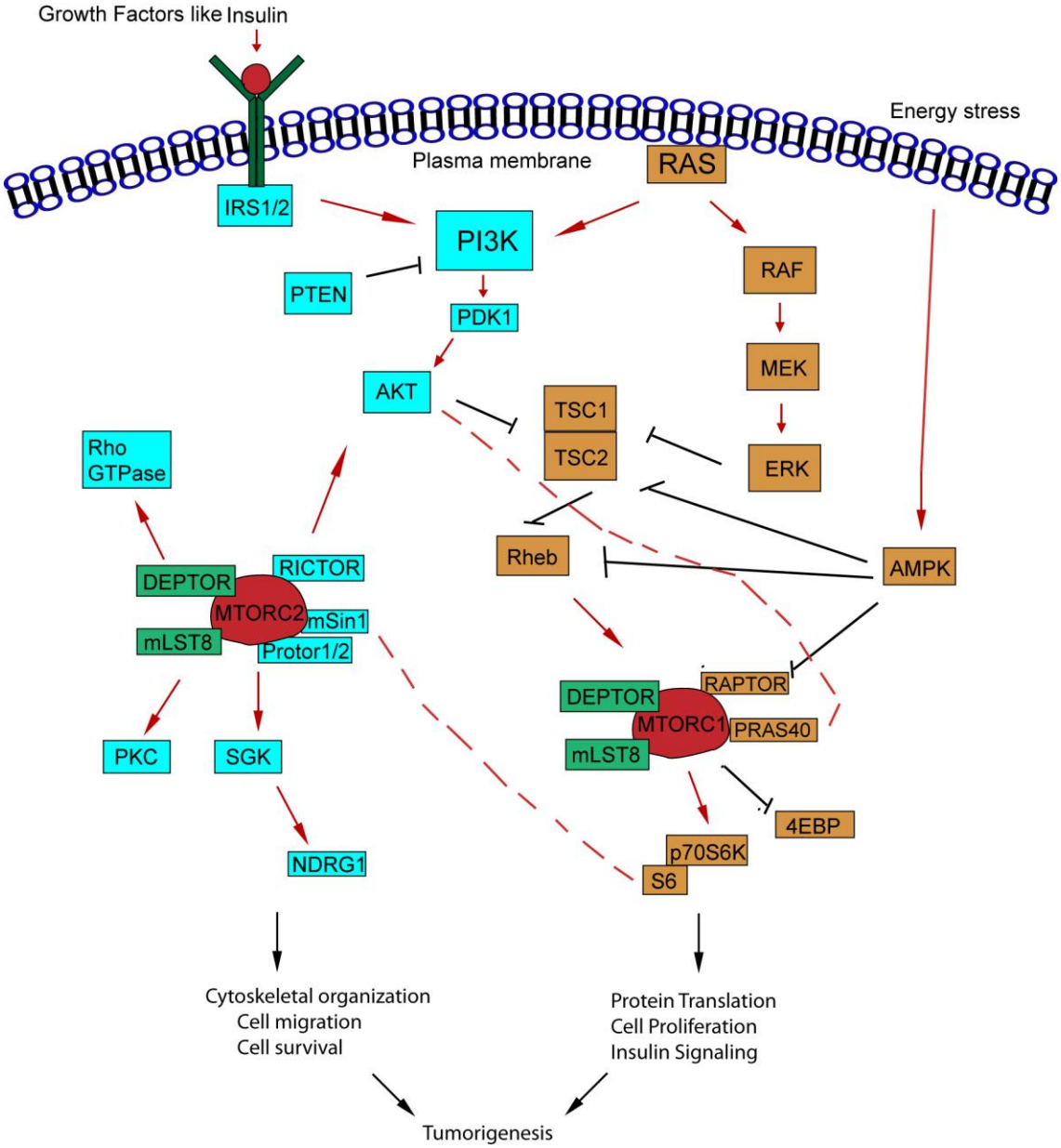

Fig. 7:5 Schematic representation of the MTORC1/2 complexes and MTORC1/2 signaling

The signaling pathways upstream and downstream of MTORC1 signaling in orange and MTORC2 signaling in blue. Positive regulations are shown by red arrows, while negative alleles are indicated by black lines. Negative feedback loops are shown by dotted red lines. Contribution of MTOR through different targets in tumor is shown by black arrows.

MTORC1 signaling is influenced by intracellular and extracellular stresses such as low food supply, hypoxia and DNA damage that activate AMPK and ultimately block MTORC1 signaling, by activating either heterotrimeric complex Tuberous sclerosis complex 1 and 2 (TSC1/2) by inhibiting RAPTOR binding (Herzig and Shaw, 2018), or by regulating the

formation of RAG and RHEB complexes (Saxton and Sabatini, 2017). Moreover, different growth factors can also enhance activity of RHEB GTPases by inhibiting TSCH1/2 to regulate MTORC1 complex (Inoki et al., 2003; Tee et al., 2003). AKT, ERK1/2 and p70S6K are some of the effector kinases that are involved in direct interaction with TSC1/TSC2 complex in order to activate MTORC1 activity (Jhanwar-Uniyal et al., 2019) as shown in Fig. 7.5. By contrast, little is known about MTORC2 regulation. However, there are hints of MTORC2 and AKT interaction that leads to regulation of many important pathways such as cell growth, metabolism and survival. Other downstream effector molecules for MTORC2 include many members of AGC kinases such as protein kinase C (PKC) or serum and SGK1 contributing to cell survival as well as cytoskeleton regulation (Linke et al., 2017).

Interestingly both complexes can influence each other by a negative feedback loop. AKT, for example can interact with PRAS40 to modulate MTORC1 activity, while S6K interaction with SIN1 can regulate MTORC2 activity (Jhanwar-Uniyal et al., 2019) as shown in Fig. 7.5. Furthermore, hyperphosphorylated retinoblastoma molecule (RB) can act as a negative regulator of the MTORC2 complex by altering the AKT signaling pathway (Zhang et al., 2016). This negative feedback loop of PI3K and MTOR signaling is very important for the pharmacological targeting of MTOR and the development of various drugs (Rozengurt et al., 2014).

7.5.2 MTOR in cancer

The MTOR kinase plays an important role in the regulation of many pathways that promote tumor initiation and progression, as it is crucial for cell proliferation, survival, autophagy and metabolism (Tian et al., 2019). Aberrant MTOR pathway activity characterized by molecular alterations (mutation, amplification, overexpression of positive regulators or loss of negative regulators at protein or RNA level) in MTOR itself or in different components of the MTOR complex as well as in upstream signaling cascade is observed in many cancers (Grabiner et al., 2014; Tian et al., 2019; Zhang et al., 2017). For example, oncogenic KRAS promotes overall MTOR signaling in lung cancer (Liang et al., 2019). RICTOR, a component of MTORC2, has been found to be amplified in breast, non-small lung cancer (NSLC) and in squamous cell lung carcinoma (SQCLC)(Balko et al., 2014; Cheng et al., 2015; Morrison Joly et al., 2016). While overexpression has been observed in glioma and breast cancer (Masri et al., 2007; Morrison Joly et al., 2016), which is linked with a worse prognosis and shortened survival (Cheng et al., 2015). Likewise, inactivation of TSC1 and TSC2, which leads to hyperactivation of MTOR pathway, has been demonstrated in urothelial carcinoma, bladder cancer, renal carcinoma and pancreatic neuroendocrine tumors (Jiao et al., 2011; Platt et al., 2009; Sjodahl et al., 2011). Moreover, loss of function mutations in PTEN promote MTOR

activity in prostate cancer, breast cancer and endometrium cancer (DeGraffenried et al., 2004; Guertin et al., 2009; Milam et al., 2007).

7.5.3 Role of MTOR in PDAC

Although PI3K mutations are only found in 5% of PDAC cases, PI3K/AKT signaling has been shown to be deregulated in almost 60% of PDAC patients (Murthy et al., 2018; Schild et al., 2009; Schlieman et al., 2003). Moreover, around 20% of human PDAC show hyperactivation of MTOR, which relates to poor survival (Kong et al., 2016; Morran et al., 2014; Utomo et al., 2014). In addition, human PDAC tissues with high RICTOR expression marked patients with poor survival (Schmidt et al., 2017).

Consistent with survival data, genetic evidence also demonstrated the importance of PI3K pathway for tumor development in the pancreas. In the classical KC mouse model, oncogenic activation of the PI3K pathway (Payne et al., 2015) or genetic deletion of *Pten* (Ying et al., 2011) have been demonstrated to be sufficient to drive ADM, PanIN and PDAC formation as well as in metastasis development. In addition, $Kras^{G12D/+}$ driven PDAC carcinogenesis is blocked or delayed by genetic deletion of *p100α* (*Pik3ca*) (Wu et al., 2014), *Pdk1* (Eser et al., 2013; Schonhuber et al., 2014), or *Rictor* (Driscoll et al., 2016).

Moreover, it has been demonstrated pharmacologically that inhibition of the PI3K pathway can block tumor growth in PDAC GEMMs as well as in patient derived orthotopic xeno-transplant models (Cao et al., 2009; Eser et al., 2013; Payne et al., 2015). Therefore, blocking MTOR signalling has become an attractive target in PDAC.

7.5.4 MTOR mediated tumor metabolism

PDAC tumors which are highly desmoplastic and hypoxic in nature, reprogram their cellular metabolism to fulfill their energy demands. In normal cells, glucose is catabolized aerobically to generate pyruvate, which fuels the tricarboxylic acid (TCA) cycle and the electron transport chain (ETC) to produce energy. However, tumor cells produce lactate by anaerobic glycolysis known as Warburg effect (Warburg, 1956). These metabolic alterations that range from increased glycolysis to changes in the activity of the oxidative phosphorylation are one of the hallmarks of cancer (Son et al., 2013; Vazquez et al., 2016). According to metabolic profiling, human PDAC tumors can be classified into glycolytic, lipogenic and slow proliferative subtypes with different clinical outcome and therapeutic responses (Collisson et al., 2011; Daemen et al., 2015).

Oncogenic KRAS fundamentally alters the metabolic pathways by upregulating many important rate limiting enzymes involved in glycolysis like increased expression of the glucose transporter GLUT1 as well as upregulation of fatty acids and nucleotide metabolism (Pinho et al., 2016; Ying et al., 2012). It is known that KRAS engages various metabolic alterations by regulating PI3K/AKT/MTOR (Csibi et al., 2013) or MAPK (Ying et al., 2012) signalling.

MTOR is a central metabolic hub that regulates cellular metabolism directly or indirectly mediating various cellular metabolic pathways (Hosein and Beg, 2018; Murthy et al., 2018). For example, the PI3K/AKT/MTOR pathway has been shown to regulate the metabolism of PDAC cells by increasing glycolysis and enhancing motility and invasiveness (Melstrom et al., 2008; Shukla et al., 2015). This PI3K/AKT/MTOR pathway dependent metabolic control is also achieved by upregulating stress driven HIF1α expression (Chaika et al., 2012; Kang et al., 2014; Kilic-Eren et al., 2013), or by enhancing AKT activation (Lee et al., 2014). In addition, MTOR also regulates an important crosstalk between Insulin/Insulin like growth factor-1 (IGF) receptors and G protein-coupled receptor (GPCR) in pancreatic cancer, which is responsible for regulating metabolism, DNA synthesis and cell proliferation (Rozengurt et al., 2010).

Collectively, these studies imply that PI3K/MTOR promotes metabolic reprograming and raise the possibility that PI3K/MTOR associated metabolic inhibition could be a therapeutic option for PDAC treatment.

7.5.5 Resistance towards MTOR inhibition

Like other targeted therapies in PDAC (Chung et al., 2017a), targeting PI3K in the clinic has not been successful so far (Javle et al., 2010). First generation MTOR inhibitors like Rapalogues (Sirolimus) and its derivatives (Temsirolimus, Everolimus, and Ridaforolimus) that bind to the intracellular rapamycin binding domain (FKBP-12) fails in the clinical trials as monotherapy, raising questions about its therapeutic significance in PDAC (Babiker et al., 2019; Javle et al., 2010). One of the reasons might be adaptive rewiring of upstream receptor tyrosine kinases such as insulin-like growth factors-1 receptor (IGF-1R) that leads to reactivation of AKT phosphorylation by MTORC2 and attenuates cellular response (Javle et al., 2010; O'Reilly et al., 2006; Pópulo et al., 2012).

In order to block the MTOR pathway completely, second generation MTORi such as AZD8055, INK-128, and AZD2014 were developed, which target both MTORC1 and MTORC2 subunits and specifically block the catalytic domain in an ATP-competitive manner.

These inhibitors have shown relatively effective results in PDAC pre-clinical trials both *in vitro* and *in vivo* (Driscoll et al., 2016; Lou et al., 2014; Rodrik-Outmezguine et al., 2011; Sun, 2013), due to downregulation of the AKT pathway (Chresta et al., 2010; Li et al., 2015a), which argues that dual MTOR inhibitors might be a therapeutic option in PDAC. However, tumor growth resumed after a certain time period due to adaptive rewiring as demonstrated by a marked increase in the activation of receptor tyrosine kinase (RTK) signaling, which induced PI3K pathway activity by reactivating AKT (T308) and subsequently AKT substrates (Rodrik-Outmezguine et al., 2011) or via non-canonical IκB-related kinase (IKBKE) mediated AKT (S473) activation in PDAC (Rajurkar et al., 2017). These above-mentioned studies underscore the need to design synthetic lethality-based combinations therapies to target MTOR efficiently (Golan et al., 2019; Hua et al., 2019; Zhou et al., 2018). As a proof of principle, synergistic effects due to cell cycle associated inhibition of adaptive rewiring mechanisms have been observed by combining MTOR (AZD8055) and AKT (MK2206) inhibitors in different cancer cell lines (Phyu and Smith, 2019). In line with that finding, it has recently been described that combined inhibition of TORC1/2 and PI3K *in vivo* inhibits the progression of pancreatic cancer (Driscoll et al., 2016). However, mechanistic effects of MTOR linked dual combination of drugs needs further clarification.

7.6 Outlook

The aim of this work was to study the role of NFκB2 and MTOR in PDAC

Hyperactivation of NFκB2 as well as its connection to proliferation is described in various cellular PDAC models. However, the precise molecular and mechanistic role of NFκB2 in the KRAS-driven carcinogenesis in the pancreas is unknown so far. Therefore, in this work, I analyzed the role of NFκB2 signaling in tumor initiation and PDAC development by genetic deletion of *Nfκb2* gene in the oncogenic $Kras^{G12D}$-driven mouse model. Furthermore, its modulation was also studied in the presence of variable aggressiveness by addition of $p53^{R172H}$ mutation.

Although data demonstrating the importance of the PI3K/AKT/MTOR kinase for PDAC development and maintenance are available, no studies addressing the role of MTOR at the genetic level. Therefore, I used a conditional *Mtor* allele to analyze the function of the MTOR in the KRAS-driven carcinogenesis. In addition, I developed a complex genetic model allowing to target MTOR in established murine PDAC models. Genetic data were substituted with pharmacological data. Furthermore, knowledge of the molecular alterations occurring after the inactivation of MTOR were used to develop new mechanistic combination therapies.

8 Materials

8.1 Technical equipment

Table 8:1 Technical Equipment

Devices	Source
96-well magnetic ring-stand	Applied Biosystems, Inc., Carlsbad, CA, USA
Analytical balance A 120 S	Sartorius AG, Göttingen
Analytical balance BP 610	Sartorius AG, Göttingen
Autoclave 2540 EL	Tuttnauer Europe B.V., Breda, The Netherlands
AxioCam HRc	Carl Zeiss AG, Oberkochen
AxioCam MRc	Carl Zeiss AG, Oberkochen
Bag sealer Folio FS 3602	Severin Elektrogeräte GmbH, Sundern
Centrifuge Rotina 46R	Andreas Hettich GmbH & Co. KG, Tuttlingen
CO_2 incubator HERAcell®	Heraeus Holding GmbH, Hanau
CO_2 incubator MCO-5AC 17AI	Sanyo Sales & Marketing Europe GmbH, Munich
Dewar carrying flask, type B	KGW-Isotherm, Karlsruhe
Electrophoresis power supply Power Pac 200	Bio-Rad Laboratories GmbH, Munich
Gel Doc™ XR+ system	Bio-Rad Laboratories GmbH, Munich
Glass ware, Schott Duran®	Schott AG, Mainz
Heated paraffin embedding module EG1150 H	Leica Microsystems GmbH, Wetzlar
HERAsafe® biological safety cabinet	Thermo Fisher Scientific, Inc., Waltham, MA, USA
Hiseq2000 platform	Illumina, San Diego, CA; USA
Hiseq2500 platform	Illumina, San Diego, CA; USA
Homogenizer SilentCrusher M with tool 6F	Heidolph Instruments GmbH & Co. KG, Schwabach
Horizontal gel electrophoresis system	Biozym Scientific GmbH, Hessisch Oldenburg
Horizontal shaker	Titertek Instruments, Inc., Huntsville, AL, USA
Laminar flow HERAsafe	Heraeus Holding GmbH, Hanau
Magnetic stirrer, Ikamag® RCT	IKA® Werke GmbH & Co. KG, Staufen
Microcentrifuge 5415 D	Eppendorf AG, Hamburg
Microcentrifuge 5417 R	Eppendorf AG, Hamburg
Multiskan RC Microplate reader	Thermo Labsystem
Microscope Axio Imager.A1	Carl Zeiss AG, Oberkochen
Microscope Axiovert 25	Carl Zeiss AG, Oberkochen
Microscope DM LB	Leica Microsystems GmbH, Wetzlar
Microtome Microm HM355S	Thermo Fisher Scientific, Inc., Waltham, MA, USA
Microwave	Siemens AG, Munich
Mini centrifuge MCF-2360	LMS Consult GmbH & Co. KG, Brigachtal
Multipette® stream	Eppendorf AG, Hamburg

Neubauer hemocytometer, improved	LO-Laboroptik GmbH, Bad Homburg
Odyssey® infrared imaging system	Licor,Biosciences Bad Homburg, Germany
Paraffin tissue floating bath Microm SB80	Thermo Fisher Scientific, Inc., Waltham, MA, USA
pH meter 521	WTW Wissenschaftlich-Technische Werkstätten GmbH, Weilheim
Pipettes Reference®, Research®	Eppendorf AG, Hamburg
Pipetus®	Hirschmann Laborgeräte GmbH & Co. KG, Eberstadt
Power supplies E844, E822, EV243	Peqlab Biotechnologie GmbH, Erlangen
Spectrophotometer NanoDrop 1000	Peqlab Biotechnologie GmbH, Erlangen
Stereomicroscope Stemi SV 11	Carl Zeiss AG, Oberkochen
Surgical instruments	Thermo Fisher Scientific, Inc., Waltham, MA, USA
Thermocycler T1	Biometra GmbH, Göttingen
Thermocycler Tpersonal	Biometra GmbH, Göttingen
Thermocycler UNO-Thermoblock	Biometra GmbH, Göttingen
Thermomixer compact	Eppendorf AG, Hamburg
Tissue processor ASP300	Leica Microsystems GmbH, Wetzlar
Vortex Genius 3	IKA® Werke GmbH & Co. KG, Staufen
Water bath 1003	GFL Gesellschaft für Labortechnik mbH, Burgwedel
Western blot system SE 260 Mighty Small II	Hoefer Inc, Hollisten, MA; USA
Glucometer	Abbott Laboratories, Wiesbaden, Germany
Aperio Image Scanner	Leica Biosystem, Nußloch, Germany
TaqMan, PE StepOnePlus™ Real time PCR System	Applied Biosystems Inc., Carland, CA; USA
UV transilluminator	Gel DocTM XR+ system.
Gamma Counter	1480 Wizard, Wallac
Gallios flow cytometer	Beckman Coulter, Krefeld, Germany
Luminescence microplate reader (FLUOstar OPTIMA.)	BMG Labtech Germany

8.2 Disposables

Table 8:2 Disposables

Disposable	**Source**
Cell culture plastics	Becton Dickinson GmbH, Franklin Lakes, NJ, USA; Greiner Bio-One GmbH, Frickenhausen; TPP Techno Plastic Products AG, Trasadingen, Switzerland
Cell scrapers	Sarstedt AG & Co., Nümbrecht
Cell strainer, 100 µm, yellow	BD Biosciences, Franklin Lakes, NJ, USA
Chromatography paper, 3 mm	GE Healthcare Europe GmbH, Munich
Falcon 15mL Conical Centrifuge Tubes	Sarstedt AG & Co., Nümbrecht
Falcon 50mL Conical Centrifuge Tubes	Sarstedt AG & Co., Nümbrecht

Combitips BioPur®	Eppendorf AG, Hamburg
Cover slips	Gerhard Menzel, Glasbearbeitungswerk GmbH & Co. KG, Braunschweig
CryoPure tubes	Sarstedt AG & Co., Nümbrecht
Disposable scalpels	Feather Safety Razor Co., Ltd., Osaka, Japan
Filtropur S 0.2	Sarstedt AG & Co., Nümbrecht
Filtropur S 0.45	Sarstedt AG & Co., Nümbrecht
Glass slides Superfrost® Plus	Gerhard Menzel, Glasbearbeitungswerk GmbH & Co. KG, Braunschweig
MicroAmp® optical 96-well reaction plate	Applied Biosystems, Inc., Carlsbad, CA, USA
Microtome blades S35 and C35	Feather Safety Razor Co., Ltd., Osaka, Japan
Pasteur pipettes	Hirschmann Laborgeräte GmbH & Co. KG, Eberstadt
PCR reaction tubes	Brand GmbH + Co. KG, Wertheim; Eppendorf AG, Hamburg
Petri dishes	Sarstedt AG & Co., Nümbrecht
Pipette tips	Sarstedt AG & Co., Nümbrecht
Reaction tubes, 0.5 ml, 1.5 ml and 2 ml	Eppendorf AG, Hamburg
Safe seal pipette tips, professional	Biozym Scientific GmbH, Hessisch Oldenburg
Safe-lock reaction tubes BioPur®	Eppendorf AG, Hamburg
Serological pipettes	Sarstedt AG & Co., Nümbrecht
Single use needles Sterican® 27 gauge	B. Braun Melsungen AG, Melsungen
Single use syringes Omnifix®	B. Braun Melsungen AG, Melsungen
Tissue embedding cassette system	Medite GmbH, Burgdorf
Silver nitrate applicator	Graham Field
Transfer membrane Immobilon-P	Millipore GmbH, Schwalbach am Taunus
Nitrocellulose membranes	Millipore GmbH, Schwalbach am Taunus

8.3 Reagents and enzymes

Table 8:3 Reagents and Enzymes

General Reagent and Enzymes	Source
1 kb DNA extension ladder	Invitrogen GmbH, Karlsruhe
1,4-Dithiothreitol (DTT)	Carl Roth GmbH + Co. KG, Karlsruhe
2-Log DNA ladder (0.1–10.0 kb)	New England Biolabs GmbH, Frankfurt am Main
2-Mercaptoethanol, 98%	Sigma-Aldrich Chemie GmbH, Munich
2-Propanol (isopropanol)	Carl Roth GmbH, Karlsruhe
Agarose	Sigma-Aldrich Chemie GmbH, Munich
Ammonium persulfate	Sigma-Aldrich Chemie GmbH, Munich
Blotting grade blocker non-fat dry milk	Bio-Rad Laboratories GmbH, Munich

Bovine serum albumin, fraction V	Sigma-Aldrich Chemie GmbH, Munich
4% formaldehyde	Carl Roth, Karlsruhe, Germany
Bromphenol blue	Sigma-Aldrich Chemie GmbH, Munich
Complete, EDTA-free, protease inhibitor cocktail Tablets	Roche Deutschland Holding GmbH, Grenzach-Wyhlen
Dimethylsulfoxide (DMSO)	Carl Roth GmbH + Co. KG, Karlsruhe
dNTP mix, 10mM each	Fermentas GmbH, St. Leon-Rot
Dodecylsulfate Na-salt in pellets (SDS)	Serva Electrophoresis GmbH, Heidelberg
Dulbecco's phosphate buffered saline, powder	Biochrom AG, Berlin
Ethanol (100%)	Merck KGaA, Darmstadt
Ethidium bromide	Sigma-Aldrich Chemie GmbH, Munich
Ethylenediaminetetraacetic acid (EDTA)	Invitrogen GmbH, Karlsruhe
Gel loading dye, blue (6x)	New England Biolabs GmbH, Frankfurt am Main
GeneRuler™ 100bp DNA ladder	Fermentas GmbH, St. Leon-Rot
Glycerol	Sigma-Aldrich Chemie GmbH, Munich
HEPES Pufferan®	Carl Roth GmbH + Co. KG, Karlsruhe
Roti® Histofix (4%)	Carl Roth GmbH + Co. KG, Karlsruhe
Hydrochloric acid (HCl)	Merck KGaA, Darmstadt
Magnesium chloride	Carl Roth GmbH + Co. KG, Karlsruhe
Methanol	Carl Roth GmbH + Co. KG, Karlsruhe
Nonidet NP-40	Roche Deutschland Holding GmbH, Grenzach-Wyhlen
Orange G	Carl Roth GmbH + Co. KG, Karlsruhe
Phosphatase inhibitor mix I	Serva Electrophoresis GmbH, Heidelberg
Precision Plus Protein™ all blue standard	Bio-Rad Laboratories GmbH, Munich
Proteinase K, recombinant, PCR grade	Roche Deutschland Holding GmbH, Grenzach-Wyhlen
QuantiFast® SYBR® green PCR master mix	Applied Biosystems/ThermoFisher)
REDTaq®ReadyMix™ PCR reaction mix	Sigma-Aldrich Chemie GmbH, Munich
RNase-free DNase set	Qiagen GmbH, Hilden
RNaseA	Fermentas GmbH, St. Leon-Rot
Rotiphorese® gel 30	Carl Roth GmbH + Co. KG, Karlsruhe
Sodium chloride (NaCl)	Merck KGaA, Darmstadt
Sodium hydroxide solution (NaOH)	Merck KGaA, Darmstadt
4-hydroxytamoxifen (≥70% Z isomer)	Sigma-Aldrich Chemie GmbH, Munich
TE buffer, pH 8.0	AppliChem GmbH, Darmstadt
TEMED	Carl Roth GmbH + Co. KG, Karlsruhe
Tris hydrochloride (TrisHCl)	J.T.Baker® Chemicals, Phillipsburg, NJ, USA
Tris Pufferan®	Carl Roth GmbH + Co. KG, Karlsruhe
Triton® X-100	Sigma-Aldrich Chemie GmbH, Munich
Tween® 20	Carl Roth GmbH + Co. KG, Karlsruhe

RLT Buffer	Qiagen GmbH, Hilden
Pancrex-vet	Ssniff Speziadiaten GmBH, Soest
MK-2206	Selleckchem (Selleckchem, Eching, Germany)
PD-325901	Sigma (Sigma, Munich, Germany)
GDC-0941	LC Laboratories (Woburn, MA, USA)
INK-128	LC Laboratories (Woburn, MA, USA)
Forene® isoflurane	Abbott GmbH & Co, Ludwigshafen, Germany
Reagent / Kits for Cell Culture	
Collagenase type 2	Worthington Biochemical Corporation, Lakewood, NJ, USA
Dulbecco's modified eagle medium (DMEM) #41966-029	Sigma by Life Technologies ™, Darmstadt
HEPES	Invitrogen GmbH, Karlsruhe
Glutamax	Invitrogen GmbH, Karlsruhe
Primocin	Invitrogen GmbH, Karlsruhe
N-acetyl-L-cysteine	Sigma-Aldrich Chemie GmbH, Munich
Animal-Free Recombinant Human EGF	Peprotech
Recombinant Human FGF-10	Peprotech
Gastrin	Sigma-Aldrich Chemie GmbH, Munich
Nicotinamide	Sigma-Aldrich Chemie GmbH, Munich
A 83-01 Supplier | CAS 909910-43-6	Tocris Bioscience
RPMI #1640 (1x) Ref 31870-025	Sigma by Life Technologies ™, Darmstadt
Dulbecco's phosphate buffered saline (PBS)	Invitrogen GmbH, Karlsruhe
Fetal calf serum (FCS)	Merck Millipore/Biochrom, Berlin, Germany
GFR Matrigel	Corning, Weisbaden, Germany
Fungizone® antimycotic	Invitrogen GmbH, Karlsruhe
G418, Geneticin®	Invitrogen GmbH, Karlsruhe
Giemsa solution	Sigma-Aldrich Chemie GmbH, Munich
CellTiter-Glo 3D Cell Viability Assay	Promega, Mannheim, Germany
(3-(4,5-Dimethylthiazol-2-yl)-2,5 diphenyltetrazolium bromide) MTT Reagent	Sigma-Aldrich Chemie GmbH, Munich
Penicillin (10000 units/ml) / Streptomycin (10000 µg/ml) solution	Invitrogen GmbH, Karlsruhe
Trypsin, 0.05% with 0.53 mM EDTA 4Na	Invitrogen GmbH, Karlsruhe
Trypsin-EDTA solution 10x	Sigma-Aldrich Chemie GmbH, Munich
Bradford reagent, 5x	Serva Electrophoresis GmbH, Heidelberg
Prestained protein ladder PageRuler™	Thermo Fisher Scientific by Life Technologies ™, Germany
Reagents for Histochemistry Analysis	
Acetic acid (glacial)	Merck KGaA, Darmstadt
Alcian blue 8GX	Sigma-Aldrich Chemie GmbH, Munich
Aluminium sulfate	Honeywell Specialty Chemicals Seelze GmbH, Seelze

Antigen unmasking solution, citric acid based	Vector Laboratories, Inc., Burlingame, CA, USA
Certistain® Nuclear fast red	Merck KGaA, Darmstadt
Eosine	Waldeck GmbH & Co KG, Münster
Goat serum G9023	Sigma-Aldrich Chemie GmbH, Munich
Hematoxylin	Merck KGaA, Darmstadt
Hydrogen peroxide 30%	Merck KGaA, Darmstadt
Pertex mounting medium	Leica Biosystems, Wetzlar, Germany
Rabbit serum R9133	Sigma-Aldrich Chemie GmbH, Munich
Roti® Histofix 4%	Carl Roth GmbH + Co. KG, Karlsruhe
Sirius Red Solution (Direct Red 80)	Sigma-Aldrich

8.4 Kits

Table 8:4 Kits

Kits for molecular biology	
Kit	**Source**
QIAshredder	Qiagen GmbH, Hilden
QuantiFast SYBR green PCR kit	Qiagen GmbH, Hilden
RNeasy mini kit (74106)	Qiagen GmbH, Hilden
Maxwell® LEV simplyRNA Purification Kit	Promega
Kits for Histochemistry Analysis	
Avidin/biotin blocking kit	Vector Laboratories, Inc., Burlingame, CA, USA
Vectastain® elite ABC kit	Vector Laboratories, Inc., Burlingame, CA, USA
DAB peroxidase substrate kit, 3,3'-diaminobenzidine	Vector Laboratories, Inc., Burlingame, CA, USA

8.5 Cell culture Media

Table 8:5 Cell culture media and their components

Medium	**Components**
Tumor cell medium (Murine & Human)	DMEM or RPMI 10% FCS 1% Penicillin/Streptomycin
Freezing medium	70% DMEM 20% FCS 10% DMSO
Tumor cell medium (Primary human PDAC)	AdDMEM/F12 suppliment with HEPES HEPES Glutamax B27 Primocin (1mg/ml) N-acetyl-L-cysteine (1 mM)

	Wnt3a-conditioned medium (50% v/v) RSPO1-conditioned medium (10% v/v) Noggin (100ng/ml) EGF (50ng/ml) Gastrin (10nM) Fibroblast Growth Factor 10 (100ng/ml) Nicotinamide (10nM) A83-01 (0.5µM)
Tumor cell medium (Human)	RPMI 10% FCS 1% Penicillin/Streptomycin

8.5.1 Cell Lines

Table 8:6 Cell lines

Cell Lines	Source
PaTu8889T	ATCC; Manassas, VA, USA
PSN1	ATCC; Manassas, VA, USA
HuPT4	DSMZ, Leibniz, Germany
IMIM-PC1	Provided by Prof.Schmid
BxPc3	ATCC; Manassas, VA, USA
HPAC	ATCC; Manassas, VA, USA
MiaPaCa2	ATCC; Manassas, VA, USA
Patu8889S	Provided by Prof. Ellenrieder
HPAF-II	ATCC; Manassas, VA, USA
Dan-G	DSMZ, Leibniz, Germany

8.5.2 Antibodies

Table 8:7 Antibodies

Primary antibodies for histological analysis	
Antibody	**Source**
CK19 (TROMAIII) (1:100)	Developmental Studies Hybridoma Bank, Iowa City
alpha-amylase (#3796) (1:2000)	Cell Signaling Technology, Inc., Danvers, MA, USA
Phospho-4E-BP1 (Thr37/46 (236B4) #2855 (1:100)	Cell Signaling Technology, Inc., Danvers, MA, USA
Insulin C27C9 (#3014S) (1:500)	Cell Signaling Technology, Inc., Danvers, MA, USA
Nfκb2 (1:250) (c-5, sc-7386) (1:100)	Santa Cruz Biotechnology, Dallas, TX, USA
Cyclin D1 (1:250) (Sp4; #RM9104-S) (1:100)	Lab vision, Fremont, CA (USA),
Ki-67 (1:50) (Sp6; # KI681C01) (1:500)	DCS Innovative Diagnostic System, Hamburg)
Secondary antibodies for histological analysis.	
Biotinylated anti-mouse IgG (H+L)	Vector Laboratories, Inc., Burlingame, CA, USA
Biotinylated anti-rabbit IgG (H+L)	Vector Laboratories, Inc., Burlingame, CA, USA
Biotinylated anti-rat IgG (H+L)	Vector Laboratories, Inc., Burlingame, CA, USA

Antibodies for Western Blot	
Cyclin D1 (1:250), sc-450 (72-13G) (1:250)	Santa Cruz Biotechnology, Inc., Dallas, TX, USA
RelB, sc-226 (C-19) (1:250)	Santa Cruz Biotechnology, Inc., Dallas, TX, USA
phospho-MEK1/2 (S217/221) (# 9154) (1:1000)	Cell Signaling Technology, Inc., Danvers, MA, USA
pan-MEK1/2 (#4694) (1:1000)	Cell Signaling Technology, Inc., Danvers, MA, USA
Hsp90 alpha/beta (F8), sc-13119 (#H1704) (1:500)	Santa Cruz Biotechnology, Inc., Dallas, TX, USA
Nfκb2 100/p52 #4882 (1:1000)	Cell Signaling Technology, Inc., Danvers, MA, USA
pan-Akt (#9272) (1:1000)	Cell Signaling Technology, Inc., Danvers, MA, USA
p44/42 MAPK (Erk1/2) (L34F12), #4696 (1:2000)	Cell Signaling Technology, Inc., Danvers, MA, USA
4EBP1 (#9452) (1:1000)	Cell Signaling Technology, Inc., Danvers, MA, USA
Phospho-Akt (Ser473), (D9e) (#4060) (1:1000)	Cell Signaling Technology, Inc., Danvers, MA, USA
phospho-AKT (T308) (c31e5e) (#2965) (1:1000)	Cell Signaling Technology, Inc., Danvers, MA, USA
Phospho-p44/42 MAPK (Erk1/2) (Thr202/Tyr204) (D13.14.4E) XP™, #4370 (1:2000)	Cell Signaling Technology, Inc., Danvers, MA, USA
Phospho-4E-BP1 (Thr37/46 (236B4) #2855 (1:1000)	Cell Signaling Technology, Inc., Danvers, MA, USA
Phospho-S6 Ribosomal Protein (Ser235/236) (D57.2.2E) XP® (#4858) (1:1000)	Cell Signaling Technology, Inc., Danvers, MA, USA
MTOR (# 2972s) (1:1000)	Cell Signaling Technology, Inc., Danvers, MA, USA
α-tubulin, T6199 (1:5000)	Sigma-Aldrich Chemie GmbH, Munich
anti-β-Actin #A5316 (1:5000)	Sigma-Aldrich Chemie GmbH, Munich
Novocastra Anti-p53 CM5 (Rabbit) (1:2000)	Leica Byosystems, UK
Caspase 3 (#9662) (1:1000)	Cell Signaling Technology, Inc., Danvers, MA, USA
Anti GAPDH (1:10000) (ACR001PT) (1:10000)	Acris GmbH, Herford, Germany
Cleaved PARP (Asp214) (#51-90000017) (1:1000)	BD Pharmingen
Secondary antibodies for Western blot	
Anti-mouse IgG (H+L) (1:10000) (DyLight® 680 Conjugate), #5470	Cell Signaling Technology, Inc., Danvers, MA, USA
Anti-mouse IgG (H+L) (1:10000) (DyLight® 800 Conjugate), #5257	Cell Signaling Technology, Inc., Danvers, MA, USA
Anti-rabbit IgG (H+L) (1:10000) (DyLight® 680 Conjugate), #5366	Cell Signaling Technology, Inc., Danvers, MA, USA
Anti-rabbit IgG (H+L) (1:10000) (DyLight® 800 Conjugate), #5151	Cell Signaling Technology, Inc., Danvers, MA, USA

8.6 Buffers

All buffers were prepared with distilled H_2O.

Table 8:8 Buffers

Buffers and solutions for molecular biology.	
Buffer	**Component**
RIPA Buffer	50 mM Tris-Hcl

	150 mM NaCl 2 mM EDTA 1% Triton X100 1% Sodium deoxycholate 0.1% SDS
Stacking gel buffer	0.5 M Tris adjusted to pH 6.8 with HCl
Separating gel buffer	1.5 M Tris adjusted to pH 8.8 with HCl
Running buffer, 10x	25Mm Tris 192Mm Glycine 0.1% SDS
Transfer buffer, pH 8.3	25 mM Tris 192 mM Glycine 20% Methanol
5% Protein loading buffer (Laemmli), pH 6.8	10% SDS 50% Glycerol 228 mM Tris hydrochloride 0.75 mM Bromophenol blue 5% 2-Mercaptoethanol
6x Loading buffer orange G	60% Glycerol 60mM EDTA 0.24% Orange G
10x Gitschier’s buffer	670 mM Tris, pH 8.8 166 mM (NH4)2SO4 67 mM MgCl2
Soriano lysis buffer	0.5% Triton® X-100 1% 2-Mercaptoethanol 1x Gitschier’s buffer 400 µg/ml Proteinase K (add prior to use)
SucRot solution (for PCR)	1.5mg/Ml Cresol red 100mM Tris; pH 9.0 30% Saccharose
Blocking Buffer	5% skim milk powder 0.1% Tween In PBS
50x Tris acetate EDTA (TAE) buffer, pH 8.5	2 M Tris 50 mM EDTA 5.71 % Acetic acid
Buffers for histological analysis	
Buffers	**Source**
Alcian blue, pH 2.5	1% Alcian blue 3% Acetic acid
Nuclear fast red	0.1% Nuclear fast red 2.5% Aluminum sulphate

8.7 Primers used for genotyping

Oligonucleotides were synthesized by Eurofins MWG GmbH (Ebersberg) and diluted in H_2O to a concentration of 10 µM.

Table 8:9 Genotyping Primers

Primers used for genotyping		
PCR name	**Primer name**	**Sequence (5´ → 3´)**
Pdx1-Flp	(pdx5utr-scUP)	AGA GAG AAA ATT GAA ACA AGT GCA GGT
	(Flpopt-scLP)	CGT TGT AAG GGA TGA TGG TGA ACT
Gabra	Gabra Forw (Ctrl)	AAC ACA CAC TGG AGG ACT GGC TAGG
	Gabra Rev (Ctrl)	CAA TGG TAG GCT CACT CTGG GAGA TGATA
FSF-Kras^{G12D}	(Kras-WT-UP1)	CAC CAG CTT CGG CTT CCT ATT
	(Kras-URP-LP1)	AGC TAA TGG CTC TCA AAG GAA TGTA
	(R26-Tva-SA-mut-LP)	GCG AAG AGT TTG TCC TCA ACC
R26-FSF-CAG	(R26-Tva-GT-UP)	AAA GTC GCT CTG AGT TGT TAT
	(R26-Tva-GT-WT-LP)	GGA GCG GGA GAA ATG GAT ATG
	(R26-td-E-mutLP)	TCA ATG GGC GGG GGT CGTT
R26-td-EG	CAG-sc-LP	GTAC TTG GCA TATG ATAC ACTT GATG TAC
	(R26-Tva-GT-UP)	AAA GTC GCT CTG AGT TGT TAT
	(R26-Tva-GT-WT-LP)	GGA GCG GGA GAA ATG GAT ATG
LSL-Kras^{G12D}	Kras-UP1-WT	CAC CAG CTT CGG CTT CCT ATT
	Kras-URP- LP1	AGC TAA TGG CTC TCA AAG GAA TGTA
	KrasG12Dmut-UP	CCA TGG CTT GAG TAA GTC TGC
R26^{CreERT2}	(Cre-ER-T2-sc-UP3)	GAA TGT GCC TGG CTA GAG ATC
	(Cre-ER-T2-sc-LP1)	GCA GAT TCA TCA TGC GGA
mtor	FRAP1_608_ Forw	CAG CCC CTT GGT TCT CTG TC
	FRAP1_608_ Rev	ACA AGG CTC ATG CCC ATT TC
Pdx1 Cre	Cre-neu-UP	CCT GGA AAA TGC TTC TGT CCG
	Cre-neu-LP	CAG GGT GTT ATA AGC AAT CCC
Ptf1a^{Cre}	Ptf1a-Cre-GT-LP-URP	CCTC GAAG GCGT CGTT GATGG ACTGCA
	Ptf1a-Cre-GT-wt-UP	CCA CGG ATC ACT CAC AAA GCGT
	Ptf1a-Cre-GT-mut-UP-neu	GCC ACC AGC CAG CTA TCAA
wildtype Nfκb2	P52 _In1 Up	GTC CTC CAC GCT GGC TGA AA
	P52_Exon2 LP	AGA TCC GGT GGA GGT CGA GAT
Nfκb2 knock-out	NeoT2	CCA CGA CGG CGT TCC TGG
	Neo Rev 2	CCC ATT CGC CAA GCT CTT CAG
LSL-p53R172H	p53R172H-WT-UP2	AGC CTT AGA CAT AAC ACA CGA ACT
	p53R172H-mut UP4	GCC ACC ATG GCT TGA GTAA
	p53R172H-URP-LP	CTT GGA GAC ATA GCC ACA CTG

8.7.1 Mycoplasma test primers

Oligonucleotides were synthesized by Eurofins MWG GmbH (Ebersberg) and diluted in H_2O to a concentration of 10 µM.

Table 8:10 Mycoplasma test primers

Primer for Mycoplasm test		
PCR name	**Primer name**	**Sequence (5´ → 3´)**
Mycoplasm test primers	5´primer 1	CGC CTG AGT AGT ACG TTC GC
	5´primer 2	CGC CTG AGT AGT ACG TAC GC
	5´primer 3	TGC CTG GGT AGT ACA TTC GC
	5´primer 4	TGC CTG AGT AGT ACA TTC GC
	5´primer 5	CGC CTG AGT AGT ATG CTC GC
	5´primer 6	CAC CTG AGT AGT ATG CTC GC
	5´primer 7	CGC CTG GGT AGT ACA TTC GC
	3´primer 1	GCG GTG TGT ACA AGA CCC GA
	3´primer 2	GCG GTG TGT ACA AAA CCC GA
	3´primer 3	GCG GTG TGT ACA AAC CCC GA

8.7.2 Recombination PCR primers

Oligonucleotides were synthesized by Eurofins MWG GmbH (Ebersberg) and diluted in H_2O to a concentration of 10 µM.

Table 8:11 Recombination PCR primers

Primer for recombination analysis		
PCR name	**Primer name**	**Sequence (5´ → 3´)**
FSF-Cre stop del	CAGS-sc-UP4	CGC CTG AGT AGT ACG TTC GC
	Cre-Stop-del-LP2	GTT CGG CTT CTG GCG TGT
FSF-Kras^{G12D} del	Kras-FSF-UP4	AGA ATA CCG CAA GGG TAG GTG TTG
	Kras-FSF-LP2	TGT AGC AGC TAA TGG CTC TCA AA
Mtor recombination	FRAP1_608_F	CAG CCC CTT GGT TCT CTG TC
	Mtor_lox_del_RV	TGA AAA GCT GGC TTTT AGT CTC AC

8.7.3 Quantitative real time PCR primers

Oligonucleotides were synthesized by Eurofins MWG GmbH (Ebersberg) and diluted in H_2O to a concentration of 10 µM.

Table 8:12 Quantitative real time PCR primers

Primers for quantitative real time PCR		
PCR name	**Primer name**	**Sequence (5´ → 3´)**
mNfκb2	*Nfκb2* forward	TGG AAC AGC CCA AAC AGC
	Nfκb2 reverse	CAC CTG GCA AAC CTC CAT
mPCNA	mPcna-TM-for1	GCA AGT GGA GAG CTT GGC A
	mPcna-TM-rev1	AGG CTC ATT CAT CTC TAT GGT TAC
mMtor	Mtor forward	TCT ACT CGC TTC TAT GAC
	Mtor reverse	TCC TCA TTG GAT CTG
mLdha	Ldha forward	CTG CTT CTC CTC GCC AGTC
	Ldha reverse	TGA GGG TTG CCA TCT TGG AC
mβ-Actin	β-Actin forward	GTC GAG TCG CGT CCA CC
	β-Actin reverse	GTC ATC CAT GGC GAA CTG GT
mPfkl	Pfkl forward	GAC CGG CAT GGA AAG CCT A
	Pfkl reverse	ACA TGA CCC AGC ACA GTC AC
mGapdh	mGapdh-FW-qPCR	GGG TTC CTA TAA ATA CGG ACTGC
	mGapdh-RV-qPCR	TAC GGC CAA ATC CGT TCA CA

8.8 Softwares

Different software used during this study are listed below in table 8.13

Table 8:13 Softwares

Software	**Source**
AxioVision 4.3	Carl Zeiss AG, Oberkochen
Excel	Microsoft Corporation, Redmont, WA, USA
GraphPad Prism 5	La Jolla, CA, USA
StepOne™ Software	Applied Biosystems, Inc., Carlsbad, CA, USA
Flowjo software	FlowJo, LLC, Ashland, OR, USA
Aperio ImageScope	(Leica Biosystem, Nußloch, Germany)

9 Methods

9.1 Mouse experiments

Animal studies were conducted in compliance with European guidelines for the care and use of laboratory animals and were approved by the Institutional Animal Care and Use Committees (IACUC) of the Technical University of Munich Technical University of Munich and Regierung von Oberbayern.

9.1.1 Mouse strains

All animals were on a mixed *C57Bl/6*; *129S6/SvEv* genetic background. For specific tissue expression of targeted mutations, the conditional *Cre/lox* (Feil et al., 1997) and *Flp/Frt* recombination system (Zhu and Sadowski, 1995) were used.

This was done by interbreeding mice carrying Cre or Flp recombinase under control of a tissue-specific promotor with mouse lines carrying mutated alleles that are flanked by a *Lox-Stop-Lox/Flp-Stop-Flp (LSL/FSF)* cassette. Due to the *Cre/Flp* activity, *Lox/Frt* sites are recognized and recombined, thus allowing expression or deletion of the gene of interest. Additionally, the *Flp-Frt;Cre^{ERT2}-Lox* system was used for time-dependent expression of mutated alleles.

Pdx1-Cre

This mouse line was kindly provided by Prof Andrew Lowy (UC San Diego Health, San Diego, USA) where pancreas specific *Pdx1* promoter controls expression of the Cre recombinase. *Pdx1* is mainly expressed in the pancreas during the embryonal development starting from the embryonic day E8.5. The *Pdx1-Cre* mouse line has no obvious phenotype (Hingorani et al., 2003).

Ptf1a^{Cre}

This knock-in mouse strain was kindly provided by Prof. Roland Schmid and Dr. Hassan Nakhai (Klinikum rechts der Isar, Technical University Munich), where a pancreas-specific *Ptf1a* promoter controls the expression of *Cre* recombinase. *Ptf1a* is specifically expressed in the pancreas during the embryonal development starting from embryo day E9.5 (Nakhai et al., 2007).

LSL-Kras^{G12D}

This knock-in mouse strain was kindly provided by Prof. Tyler Jacks (Massachusetts Institute of Technology, Cambridge, MA, USA). *LSL-Kras^{G12D}* mice carry a point mutation in codon 12 leading to an amino acid substitution of glycine by aspartate, which corresponds to the mutation frequently found in human PDAC. *Cre*-mediated deletion of the *LSL* cassette leads to the expression of the oncogenic KRAS, driven by the endogenous promoter (Hingorani et al., 2003; Jackson et al., 2001).

LSL-p53^{R172H}

This knock-in mouse strain was kindly provided by Prof. Tyler Jacks (Massachusetts Institute of Technology, Cambridge, MA, USA). *LSL-p53^{R172H}* mice carry a missense mutation in codon 172 of endogenous *p53,* leading to an amino acid substitution of arginine by histidine, which corresponds to the human *TP53^{R175H}* hot-spot mutation. LSL-cassette excision leads to dominant-negative oncogenic *p53^{R172H}* expression (de Vries et al., 2002; Muller and Vousden, 2014).

Nfκb2

This knockout mouse was generated by excising a 2.5-kb fragment spanning exon 1b to exon 9 that contains the translation start site and part of the Rel homology domain (Paxian et al., 1999; Paxian et al., 2002). *Cre*-mediated excision leads to the *Nfκb2* deletion.

Pdx1-Flp

This transgenic mouse line was generated in the laboratory of Prof. Dieter Saur (Klinikum rechts der Isar, Technical University of Munich). The codon-optimized Flp-o recombinase is expressed under the control of the *Pdx1* promotor. The *Pdx1-Flp* mouse line has no phenotype (Schonhuber et al., 2014).

FSF-Kras^{G12D}

This knock-in mouse line was generated in the laboratory of Prof. Dieter Saur (Klinikum rechts der Isar, Technical University of Munich). An oncogenic point mutation was introduced in the second exon of the *Kras* gene. The expression of the oncogene is blocked by *Frt*-flanked stop cassette *(Frt-Stop-Frt)* (Schonhuber et al., 2014).

FSF-R26$^{CAG-CreERT}$

This knock-in mouse strain was generated in the laboratory of Prof. Dieter Saur (Klinikum rechts der Isar, Technical University of Munich). This inducible *Cre^{ERT2}* recombinase is under the control of the *CAG* promoter that is knocked-in into *Rosa26* locus. Expression is silenced by an *FSF* cassette (*FSF-R26$^{CAG\text{-}CreERT2}$*). Upon *Flp* activation, *Frt* sites are recombined and Cre^{ERT2} is expressed and sequestered in the cytoplasm. Upon administration of tamoxifen (estrogen analogue), Cre^{ERT2} can dissociate from HSP90 and translocate to the nucleus where it catalyzes the recombination of *floxed* genes (Schonhuber et al., 2014).

Mtor$^{tm1a\ (EUCOMM)\ Wtsi}$

This mutant mouse strain was generated by European Conditional Mouse Mutagenesis program (EUCOMM) and obtained via European Mouse Mutant Archive (EMMA), having *Exon 3* floxed (Beirowski et al., 2014). In our system, upon tamoxifen administration, *Cre^{ERT2}* excised *Exon 3* and results into *Mtor$^{\Delta E3}$* deletion (Hassan et al., 2018).

R26$^{mT\text{-}mG}$

This double fluorescent reporter mouse line harbors td-Tomato and enhanced green fluorescent protein (EGFP) under the control of the *CAG* promoter that is present in the *Rosa26* locus. The *td-Tomato* gene is flanked by two *Lox* sites. Cre recombination can be visualized by EGFP expression (Muzumdar et al., 2007).

9.1.2 Genotyping

Around 2-3 weeks after birth, a 1 mm long tail biopsy was taken from the anesthetized mouse with a sterile scalpel. The wound was disinfected with a silver nitrate applicator. Each mouse got explicit earmarks representing a number code. DNA was extracted from the tails as described in section 9.4.1.

9.1.3 Blood Glucose measurement

Blood glucose monitoring was performed each week on a regular basis until 3 months of age with a glucometer (Abbott Laboratories, Wiesbaden, Germany) by standard procedures under normal feeding conditions

9.1.4 Mouse dissection

Instruments and general conditions were kept as sterile as possible. Mice were euthanatized with Forene® isoflurane, fixed and disinfected with 70% ethanol. The abdomen was cut open and samples were taken. Pancreatic tissue samples for RNA and protein isolation were homogenized in 1 mL RLT buffer supplemented with 10 µL of 2-mercaptoethanol or 600 µL IP buffer containing phosphatase and proteinase inhibitors using Silent-Crusher M, respectively. A small piece of tissue was removed for subsequent DNA isolation. All samples were snap-frozen and stored at -80°C until use. The weight of the pancreas, spleen and liver tissue was determined. In case of PDAC formation, tumor size and weight were determined, and a piece of the tumor tissue was taken for tumor cell line isolation (9.4.1).

9.2 Histological analysis

9.2.1 Tissue fixation and paraffin sections

For histopathological analysis, tissue was fixed overnight in 4 % Roti® Histofix (Carl Roth, Karlsruhe, Germany) washed with PBS, dehydrated by use of tissue processor ASP300 (Leica Microsystems GmbH, Wetzlar), embedded in paraffin and stored at RT until further use. Series of 1.5 µm sections were cut with a microtome (Microm HM355S).

9.2.2 Hematoxylin and eosin (H&E) staining of tissue sections

Paraffin-embedded sections were dewaxed in Roti® Histol (2 x 5 min), subsequently, rehydrated in a decreasing alcohol series for 3 min each (2 times in 99%, 2 times in 96% and 2 times in 80%), and washed with distilled water for 2 min. Afterwards sections were stained with hematoxylin for 10 to 15 seconds followed by bathing slides in running tap water for approximately 10 min. Slides were then stained in eosin for 15 seconds, washed again for 2 to 3 times in distilled water and applied for 15 seconds to an ascending ethanol series each (2 times in 80%, 2 times in 96% and 2 times in 99%) for dehydration. Afterwards slides were again incubated in Roti® Histol (2 x 5 min) and covered with pertex mounting medium (Leica Biosystems, Wetzlar, Germany).

9.2.3 Quantification and counting of ADM and PanINs lesions

For quantification of ADM and PanINs lesions, at least four animals per genotype were analyzed for each time point. Three individual H&E stained slides per pancreas (at intervals of 100 µm) were quantified. Whole sections were counted for the presence of ADM and

PanINs lesions at a 100-fold magnification. Mean number of lesions per field for each animal is shown. Quantification of ADMs and PanINs lesions was performed according to established grading for PanIN lesions in mice (Hruban et al., 2000).

9.2.4 Alcian blue staining

Paraffin-embedded sections were dewaxed and rehydrated as described in 9.2.2. Afterwards, slides were stained with 1% aqueous alcian blue solution (pH 2.5) for 5 min, washed, counterstained for 5 min with nuclear fast red, followed by dehydration, Roti® Histol incubation and mounting as described in the section 9.2.2.

9.2.4.1 Quantification of Alcian Blue stained ADM and PanINs lesions

For quantification of Alcian blue staining, pancreas sections of three animals per genotype were investigated. Three stained whole section slides (at intervals of 100 µm) were analyzed using a 100-fold magnification. Mean number of lesions (ADM and PanINs) per field for each animal is shown.

9.2.5 Picro sirius staining

Formalin-fixed paraffin-embedded tissue sections were dewaxed, rehydrated, incubated for one hour(hr) with the Sirius Red Solution (Direct Red 80, Sigma-Aldrich) and washed three times in acidified water (0.5% Acetic Acid) solution as described (Junqueira et al., 1979), followed by dehydration, Roti® Histol incubation and mounting as described in the section 9.2.2.

9.2.6 Immunohistochemistry (IHC)

For IHC, formalin-fixed, paraffin-embedded tissue sections were dewaxed, rehydrated and subsequently placed in a microwave (2 min, 800W and 9min/ 360 W) to recover antigens in citric acid-based antigen unmasking solution (Vector Laboratories, Inc., Burlingame, CA, USA). Slides were left at room temperature (RT) for at least 20 min to cool down and washed with H_2O. To block endogenous peroxidase activity slides were incubated with 3 % H_2O_2 for 10 min at RT. Subsequently to avoid unspecific antibody binding sections were blocked at RT with 5 % serum in PBST (0.1% Tween in PBS) for 1 hr after washing the slides (3 times PBS). For additional blocking the Avidin/Biotin blocking kit (Vector laboratories) was used

according to the manufacturer protocol. Primary antibodies were incubated on sections overnight in 5 % serum in PBS at 4 °C in blocking solutions in ranges 1:50 to 1:500. Primary antibodies were followed by incubation for 1 hr at RT with secondary antibodies conjugated to biotin (1:500, Vector Laboratories, Burlingame, CA). Slides were washed again with PBS. Detection was performed by using Vectastain Elite ABC kit followed by application of Peroxidase-conjugated streptavidin with 3,3′-diaminobenzidine tetrahydrochloride (DAB peroxidase substrate kit; Sigma-Aldrich) as chromogen for visualization. After counterstaining the sections with hematoxylin for 2-3 seconds, slides were dehydrated, incubated in Roti® Histol and mounted with Pertex mounting medium as described in section 9.2.2.

9.2.6.1 Quantification of Ki-67 and Ccnd1 expression in ADM and PanIN lesions

For quantification of Ki-67 and Ccnd1 expression in ADM and PanINs lesions of age matched pancreatic tissues, 3 animals per genotype were used. For Ki-67 quantification, three slides per animal were used, while for Ccnd1 one slide was analyzed. Depicted is the percentual fraction of Ki-67-/Ccnd1 positive ADM or PanINs cells to all ADM or PanINs cells.

9.2.7 Analysis of staining

High resolution images were captured by using the microscope Axio Imager.A1 with Axio Cam HRc and analyzed using AxioVision 4.8 software (Carl Zeiss, Jena, Germany). Slides were scanned with Aperio Image Scanner and images were captured by Aperio Image-Scope #12.3.0.5056 (Leica Biosystem, Nußloch, Germany). Representative images were shown in the results part.

9.3 Cell culture

Primary murine pancreatic cancer cells were established from tumor mice and were maintained in appropriate tumor cell medium (Table 8. 5) at 37 °C, 5 % CO_2 and 100 % humidity in a CO_2-incubator under sterile conditions.

9.3.1 Generation, culturing and cryopreservation of primary murine PDAC cells

Establishment of murine pancreatic cancer cell lines was performed from genetically engineered *Kras*^{G12D}-driven mouse models. During mouse dissection, a piece of the tumor was taken into sterile PBS under a biological safety cabinet and cut into small pieces with a scalpel. Tissue pieces were incubated in 5 mL cancer cell medium supplemented with 200U/mL collagenase type 2 (Worthington, Worthington Biochemical Corporation, Lakewood, NJ, USA) at 37°C for 24-48 hrs for collagen digestion. Afterwards, the cell suspension was centrifuged for 5 min at 1.200 rpm and the pellet was resolved in 5 mL cancer cell medium for further culturing in a 25-cm^2 cell culture flask. These isolated primary pancreatic tumor cell lines were regularly supplied with fresh pre-warmed media in table 8.5. Identity of the murine pancreatic cancer cell lines was verified using genotyping PCR in table 8.9. Cell lines were routinely tested for Mycoplasma contamination by a PCR-based method (Ossewaarde et al., 1996) with primers in table 8.10.

For passaging of cells, the medium was aspirated when they were around 80-90% confluent, washed with PBS and detached from the culture dish by incubation with trypsin/EDTA at 37°C for an appropriate time period. Trypsinization was stopped by addition of medium. Thereafter, the cell suspension was seeded into new flask at varying dilutions depending on the experimental conditions. Cell number was determined by a Neubauer hemacytometer.

For cryopreservation, cells were frozen in liquid nitrogen. Therefore, upon trypsinization, cells were resuspended in fresh medium and centrifuged at 1.200 rpm for 5 min. Supernatant was discarded, pellet was resuspended in ice-cold freezing medium, transferred to CryoPure tubes and immediately stored at -80 °C for 24 hr and then transferred to liquid nitrogen.

9.3.2 Tamoxifen treatment of isolated PDAC cell lines

To activate Cre^{ERT2} in cell culture experiments, PDAC cells were treated with vehicle (ethanol) or 600 nM 4-hydroxytamoxifen (4-OHT) for 8 days to activate nuclear translocation of Cre^{ERT2} and to excise *lox*-flanked sequences. Afterwards, cells were used for individual assays.

9.3.3 MTT assay

MTT assay was used to determine cell viability (Mosmann, 1983), based on colorimetric reaction in which the MTT substance is reduced to a purple formazan molecule by mitochondrial reductase. 3-(4,5-Dimethylthiazol-2-yl)-2,5-diphenyltetrazolium bromide (MTT)

was purchased from Sigma-Aldrich (5 mg/ml in PBS). For the assay, 2.000 cells were seeded in 100 µL of cell culture medium into each well of a 96 well plate in triplicates. On the next day, cells were treated with different inhibitors listed in table 8.3 for 72 hrs and cell viability was measured by addition of 10 µL of MTT dye per well followed by an incubation for 4 hrs at 37°C. The medium was removed carefully and the formazan crystals were dissolved in 200µL DMSO:EtOH (1:1). After incubation at RT on the shaker for 10 min, the optical density (OD) of the samples at a wavelength of 595 nm by the microplate reader (Thermo Lab systems Multiskan RC) was determined. OD of vehicle treated controls was arbitrarily set to 1 and the therapeutic effect is depicted as relative growth values. Analysis of at least three technical replicates in three independent experiments were performed.

9.3.4 Clonogenic assay

2.000 dispersed cells were plated in 6-well plates and cultured until vehicle treated cells (EtOH) showed evenly spread visible colonies (about 2 weeks after seeding). Cell culture medium was aspirated, and cells were fixed with ice cold methanol. Afterwards, colonies were stained with Giemsa solution (diluted 1:20 in distilled water) on an orbital shaker overnight. The next day, Giemsa solution was removed, and plates were washed with distilled water, air dried and scanned for visualization. For drug treatments, the same number of cells was plated in 24 well plates and cultured.

9.3.5 F-18-FDG uptake assay

$1x10^5$ murine PDAC cells were used for quantification of F-18-FDG uptake. Cells were seeded into 24-well plates in quadruples (vehicle treated and 4-hydroxytamoxifen treated cells). Normal cell culture medium was removed after 24 hrs, cells were washed twice with glucose-free medium and incubated in glucose-free cell culture medium containing F-18-FDG (0.185 MBq/mL). After 1, 1.5 and 2 hrs, plates were put on ice, washed twice with ice cold PBS, detached with 1M NaOH and harvested for glucose uptake measurements with a gamma counter. Glucose uptake of vehicle treated (ETOH) control cells was set as the F18-FDG standard and displayed as percent of the standard (uptake in %).

9.3.6 Cell cycle flow cytometry

For cell-cycle flow cytometry analysis, PDAC cells were treated with MTOR inhibitor (INK-128) and control for the indicated time point were detached by trypsinization and washed two

times in PBS followed by fixation in 1 ml cold 70% EtOH. After 24 hrs, EtOH was removed and cells were washed in PBS. RNA was digested by adding RNAse (Sigma) (final concentration 0.5 μg ml^{-1}) for 1 hr. Cells were stained with propidium iodide (PI) (50 μg ml^{-1}) (Sigma) and analyzed on a Gallios flow cytometer (Beckman Coulter, Krefeld, Germany). The proportion of the cells in each cell cycle phase was determined by using flow cytometer assessment of DNA content. Analysis of data were performed by using FlowJo software (FlowJo, LLC, Ashland, OR, USA). Same procedure was performed with PDAC vehicle (ETOH) as well as tamoxifen (4-OHT) treated cells.

9.3.7 Generation and 3D culturing of primary human PDAC

PDAC tissues were obtained from patients undergoing surgical resection at the department of surgery of the Technical University of Munich. Experiments, in accordance with the declaration of Helsinki, were approved by the ethical committee of the TUM and written informed consent from the patients for research use of the cancer tissue was obtained prior to the investigation of the specimens. All tissues were confirmed to be PDAC by pathological examination. Generation and expansion of primary PDAC 3D cultures was performed as described (Boj et al., 2015). In brief, tumor tissue was minced and digested with collagenase II (5 mg/ml, GIBCO) in primary human PDAC medium without growth factors at 37°C for a maximum of 6 hr. The material was further digested with Trypsin LE (GIBCO) for maximum of 15 min at 37°C, embedded in GFR (Growth Factor Reduced) Matrigel (Corning, Wiesbaden, Germany), and cultured in primary human PDAC complete medium as described in table 8.5.

9.3.8 CellTiter-Glo 3D cell viability assay

For drug treatments 1.000 cells from primary PDAC 3D cultures B20 and B25 were plated in each well of a 96 well plate in Matrigel. After 24 hrs, the cells were treated with different concentrations of each drug. The cell viability for human primary 3D models was measured 5 days after drug addition via CellTiter-Glo 3D Cell Viability Assay (Promega, Mannheim, Germany) using a luminescence microplate reader (FLUOstar OPTIMA).

9.3.9 GI_{50} calculation, Synergy Score

The growth inhibitory 50% (GI_{50}) concentration of the inhibitors was calculated with GraphPad Prism5 using a non-linear regression model (log inhibitor versus response (three

parameters). The synergy score (SC) was calculated according to SC= log 10($GI_{50control}$/$GI_{50combination}$).

9.4 Molecular techniques

9.4.1 Isolation of genomic DNA

Genomic DNA for subsequent genotyping and recombination PCR analysis was isolated from to a small piece of tissue or a cell pellet. by adding 60µL of Soriano lysis buffer depicted in table 8.8. Thereafter, Lysis was performed by incubation in a thermocycler at 55°C for 90 min. Furthermore, to inactivate proteinase K samples were incubated at 95°C for 15 min. After vortexing the sample, the DNA-containing supernatant was carefully separated from the debris by centrifugation at 14.000 rpm 4°C for 15 min, transferred into PCR tubes and stored at -20°C for further use.

9.4.2 Polymerase chain reaction

Standard genotyping or recombination PCR (Mullis et al., 1986) was performed with REDTaq ReadyMix buffer. Composition of REDTaq ReadyMix is shown in table 9.1.

Table 9:1 Composition of REDTaq ReadyMix for PCR

Solution	Volume for one reaction
ddH_2O	4.375 µL
10x buffer S	2.5 µL
30% Sucrose	2.5 µL
SucRot	2.5 µL
PeqTaq	0.125 µL
dNTP (10 µM each)	0.5 µL

The standard PCR reaction setup and conditions are shown in table 9.2. For each reaction, 1µL of isolated DNA was used and amplification was done for 40 cycles. PCR products were visualized directly performing agarose gel electrophoresis (9.4.3) or stored at 4°C until usage. Primer concentrations were optimized depending on the PCR product. If necessary, DMSO was added to improve PCR. For each allele, specific primers set mentioned in table 8.9. Wild type and mutated products were distinguished from each other according to their respective molecular sizes mentioned in table 9.3, by running PCR products on a 1.5%

agarose gel described in section 9.4.3. Annealing temperatures were adjusted according to the melting temperatures of the primers indicated in table 9.3.

Table 9:2 Reaction mix and conditions for standard PCR

Reaction Mix		**Conditions**		
12.5 µL	REDTaq ReadyMix	94°C	3 min	
0.25 - 2 µL	forward primer (10 µM)	95°C	45 s	40x
0.25 - 2 µL	reverse primer (10 µM)	55°C – 65°C	1 min	
1 µL	DNA	72°C	1 min, 30sec	
ad 25 µL	H_2O	72°C	5min	

As, murine PDAC cell were isolated from genetically engineered *Kras*^{G12D}-driven mouse models, recombination-PCRs were designed to test for Cre or Flp mediated recombination events listed in table 8.11.

Table 9:3 Annealing temperatures and PCR products of genotyping and recombination PCRs

Name of PCR	**Annealing temperature**	**PCR products (bp)**
Pdx1-Flp	55°C	620 (mut) / 300 (internal control)
FSF-Kras^{G12D}	55°C	351 (mut) / 270 (WT)
R26-FSF-CAG	62°C	450 (mut) / 650 (WT)
MTor^{lox}	58°C	169 (WT)/ 455 (lox)
R26^{CreERT2}	55°C	190 (mut)/ 300 (internal control)
R26-td-EG	62 °C	450 (mut) / 650 (WT)
Pdx1 Cre	58 °C	390 bp (mut)/290 bp (internal control)
Ptf1a^{Cre}	60°C	400 (mut) / 600 (WT)
LSL-Kras^{G12D}	55°C	170 (mut) / 270 (WT)
p52wt	60°C	287(WT)
P52del	60°C	500bp (del)
LSL-p53^{R172H}	60°C	270 (mut) / 570 (WT)
Mycoplasma	60°C	550bp
Recombination PCRs		
FSF-Cre stop del	60 °C	490 bp (rec)
FSF-Kras^{G12D} del	60 °C	196 bp (rec)
Mtor recombination	60 °C	358 bp (lox)/ 850bp (WT)/950bp (del)

mut = mutated allele; WT = wild type allele; rec = mutated allele without translational stop element after recombination

All human cell lines were authenticated by Single Nucleotide Polymorphism (SNP)-Profiling conducted by Multiplexion (Multiplexion GmbH, Heidelberg, Germany).

All cell lines used in this study were tested for Mycoplasma contamination by a PCR-based method. Mycoplasma primers are listed in table 8.10, while reaction mixture and PCR program are listed below in table 9.4.

Table 9:4 Reaction mix and conditions for mycoplasma check PCR

Reaction Mix		**Conditions**		
15 µL	REDTaq ReadyMix	95°C	15 min	
2 µL	7x primers combination forward primer (10 µM)	94°C	1 min	40x
2 µL	3x primers combination reverse primer (10 µM)	60°C	1 min	
2 µL	DNA	74°C	1 min	
ad 25 µL	H_2O	72°C	10min	

9.4.3 Agarose gel electrophoresis

To visualize PCR products as well as to test for RNA integrity, agarose gel electrophoresis was performed. 1.5 –2 % agarose gels (in 1 x TAE) containing ethidium bromide were loaded with 12.5 µL of each PCR sample in horizontal electrophoresis chambers and run for 1.5 hrs at 100 V. Separated bands were detected with the UV transilluminator Gel DocTM XR+ system.

9.5 Protein biochemistry

9.5.1 Isolation of the whole cell protein extract

To prepare whole-cell extracts (WCE), cells were washed with ice cold PBS and lysed by using RIPA buffer (50 mM HEPES, 150mM NaCl, 1 mM EDTA, 2.5 mM EGTA, 20 mM NEM, and 0.1 % Tween) with additional protease and phosphatase inhibitors as listed in table 8.3. Homogenized samples were immediately shock frozen in liquid nitrogen and stored at -80°C until further use. Prior to use, protein lysates were thawed on ice and centrifuged in a precooled centrifuge at 13.200 rpm for 20 min at 4°C. Supernatant containing protein extract was transferred to new tubes and stored at -80°C or further processed.

9.5.2 Measuring protein concentration

Protein concentration of cell lysate was measured by colorimetric reaction established by Bradford (Bradford, 1976). Therefore in 300 µl of 1x Bradford reagent, 1 µl of protein lysate was added. As a standard curve, defined dilutions of BSA were made. Measurement was performed in triplicates and OD values were measured with a Multiskan RC Microplate reader at a wavelength of 600 nm. Values were extrapolated from the standard curve. Samples were adjusted to equal concentrations with RIPA buffer and protein loading buffer (5x Laemmle) (Table 8. 8) (Laemmli, 1970), followed with boiling for 5 min at 95 °C. Samples were stored at -20 °C until further use.

9.5.3 Western blot

Proteins were separated according to Molecular Weight by using sodium dodecyl sulphate-polyacrylamide gel electrophoresis (SDS-PAGE) (Burnette, 1981). For this purpose, 7.5%, 10% and 12% SDS-polyacrylamide gels were used. Separation gel mix was poured into gel caster and covered with 1 ml of isopropanol. After polymerization, isopropanol was carefully removed and stacking gel was poured over the separating gel.

Table 9:5 SDS polyacrylamide gel preparation

Stacking gel				
Composition	**Amounts**			
H_2O	1500 µL			
Stacking gel buffer	650 µL			
Rotiphorese® gel 30	375 µL			
10% SDS	25 µL			
10% APS	12.5 µL			
TEMED	7.5 µL			
Running gel				
Composition	**7.5%**	**10%**	**12%**	**15%**
H_2O	2450	2050	1700	1250
Trenngel buffer	1300	1300	1300	1300
30% Acrylamid	1250	1650	2000	2500
10%SDS	50	50	50	50
10% APS	25	25	25	25
TEMED	7.5	7.5	7.5	7.5

After polymerization 80 to 120µg of protein per well was loaded onto the gel alongside Prestained protein ladder PageRuler^{TM} for molecular weight estimation of separated proteins. Electrophoresis was performed for 2 hrs in running buffer at 80 to 120V depending on

molecular weight of protein of interest. Composition of both gels is listed below in the table 9.5.

9.5.4 Immunoblotting

After separation by SDS-PAGE, proteins were transferred to Immobilon-FL or nitrocellulose membrane (Merck-Millipore). For the transfer, wet blot transfer was carried out for 2hrs at 350 mA or overnight at 90 mA at 4 °C (Towbin et al., 1979). Afterwards, membrane was incubated with blocking buffer (5% skim milk or 5 % BSA with 0.1% Tween®) for 1 hr at RT to avoid unspecific binding. Subsequently, the membrane was incubated overnight in primary antibody mentioned in table 8.7 with gentle shaking at 4°C. The next day, membranes were washed 3 times with PBST (0.1% Tween in PBS) and incubated with DyLight™ 680 or 800 conjugated secondary antibodies (dilution 1:10.000) for 1hr at room temperature in the dark with gentle shaking. Afterwards, membranes were washed again 3x for 5 min with PBST and imaged with the Odyssey® infrared imaging system (Licor, Bad Homburg, Germany).

9.6 RNA analysis

9.6.1 RNA Isolation and Reverse Transcription

For RNA isolation, PDAC cells and tissues were washed with PBS and lysed in RLT buffer supplemented with 2-mercaptoethanol. Lysates were collected with a scraper from petri plates (for 10 cm dish) and stored at -80°C until further processing. Total RNA isolation from cell lines was carried out with QIA-shredder columns and the RNeasy mini kit (Qiagen) according to the manufacturer´s instructions. For murine tissue total RNA was isolated by using the Maxwell®16 Total RNA Purification Kit (Promega, Mannheim, Germany), following the manufacturer`s instructions. RNA concentration was determined with the spectrophotometer Nanodrop 1000 and samples were stored at -80°C or directly used for further process. cDNA synthesis was performed using the TaqMan® reverse transcription reagents following the manufacturer´s instructions. Generally, 2 µg of RNA were used for generation of 100 µL of cDNA. Samples were stored at -80°C until further use.

9.6.2 Quantitative reverse-transcriptase PCR

To obtain suitable primers for quantitative real time PCR (qRT-PCR), primers were generated using the Primer-Blast tool from the NCBI. 100 nM of each primer listed in table

8.12 was used for Real-time PCR. Quantitative mRNA analysis was performed using real-time PCR analysis system (TaqMan, PE StepOnePlus™, Real time PCR System, Applied Biosystems Inc., Carland, CA, USA) and SYBR Green Master Mix (Thermo Fisher Scientific, Darmstadt, Germany) as fluorescent DNA binding dye.

All samples were normalized to housekeeping gene, β-actin as a reference. A melt curve analysis was always performed with every qPCR run to confirm that specific products were obtained. Data analysis was carried out with Stepone™ software (Applied Biosystem, Inc., Carland, CA, USA) according to the $2^{-\Delta\Delta Ct}$ method (Livak and Schmittgen, 2001). Equations are shown below.

ΔCt = Ct (target gene) – Ct (endogenous control) [calculated for every sample]

ΔΔCt = ΔCt (treated sample) – ΔCt (reference sample)

Relative expression = $2^{-\Delta\Delta Ct}$

PCR conditions can be found here in table 9.6. All experiments were performed in technical triplicates in at least three independent experiments.

Table 9:6 Conditions for quantitative real-time PCR

Temperature	Time	Number of cycles
50 °C	2 min	1x
95 °C	10min	1x
95 °C	15 sec	40x
60 °C	1 min	

9.6.3 RNAseq analysis, visualization, GSEA, GO-term and KEGG analysis

To compare gene signatures and underlying signaling pathways, whole transcriptome expression analysis was performed.

RNA is extremely sensitive to degradation due to the ubiquitous presence of the RNases. Before any downstream analysis, RNA integrity and quality were investigated by separating around 500 ng of RNA on a 1% agarose gel at 80V in horizontal electrophoresis chambers. In case of intact samples, two intensive bands were observed representing the 28S and 18S rRNA. The 28S rRNA band should be approximately 1.5-2.5 times as intense as the 18S

rRNA band. Further RNA quality control and sequencing were done by the genomics and proteomics (NGS) core facility of the DKFZ Heidelberg (Illumina HiSeq 2000, single-end). This Bioinformatical analysis of RNA sequencing data was performed by Dr. Matthias Wirth RNA-Seq Data for *Mtor* was deposited in the NCBI Gene Expression Omnibus database with the Accession ID: GSE98860, while for *Nfκb2* RNA-Seq Data were deposited in the European Nucleotide Archive (ENA) with the accession number: PRJEB30882. TrimGalore! (Galaxy Version 0.4.2) was used to remove adapters from FASTQ files. Resulting FASTQ files (approximately 25M reads/sample (single-end reads) were processed and further analyzed by Galaxy Project platform (Galaxy platform 0.4.2) (Afgan et al., 2016; Goecks et al., 2013). Resulting sequencing reads were mapped to the mouse reference genome (mm10) using bowtie2 (Langmead and Salzberg, 2012). Aligned reads which overlap to features in the mm10 GTF annotation file, obtained from the UCSC genome browser database (Kent et al., 2002). Differential expression of count data using htseq-count 0.6.1galaxy3 (Anders et al., 2015). was determined by DESeq2 (Love et al., 2014).

To assess altered biological pathways and processes in the vehicle treated and 4-OTH treated MTOR samples, Gene set Enrichment Analysis was performed by using GSEA tool (gene set matrix composed files: h.all.v6.0.symbols.gmt) (Subramanian et al., 2005). Statistical values like the FDR (false discovery rate) q-values, nominal p-values and FWER (family-wise error rate) are depicted in the respected figures. Gene ontology (GO) Term and KEGG analysis of genes down-regulated (log2FC≤-0.58) upon deletion of *Mtor* was conducted by using the Molecular Signature Database for Annotation, Visualization and Integrated Discovery (DAVID) (Huang da et al., 2009), while genes altered by *Nfκb2* deletion (log2FC ≥+/-1) were analyzed by using Hallmark gene sets of the Molecular Signature Database (MSigDB) with adjusted Benjamini p value <0.05. Heat maps were generated by Heatmapper (Babicki et al., 2016) or ClustVis (Metsalu and Vilo, 2015).

In addition, normalized human PDAC RNA-seq data (nature16965-s2) and class assignment (NMF_class_assignment sheet: ADEX; Squamous; Pancreatic Progenitor; Immunogenic) were obtained from Bailey and colleagues (Bailey et al., 2016). In this data set, ClustVis was used to clustered the expression of MTOR-connected glycolytic enzymes (Metsalu and Vilo, 2015). Following settings are used for analysis: centered-rows, unit variance scaling is applied to rows. Columns are clustered using Euclidean distance and McQuitty linkage method. Moreover, TCGA PDAC transcriptome data sets as well as clinical data of the TCGA PDAC dataset were accessed via the UCSC cancer genomics browser (https://genome-cancer.ucsc.edu). Survival data was extracted and assigned to the (lactose dehydrogenase

A) *LDHA* mRNA expression profile. Low *LDHA* mRNA expression was defined as expression <25th percentile; high *LDHA* mRNA expression was defined as expression >75th percentile; intermediate expression: remaining PDACs.

In addition, clinical data as well as DNA and mRNA sequencing data were obtained from The Cancer Genome Atlas (TCGA) database (24071849). Normalized mRNA data from n = 183 PDAC patients were divided into quartiles according to their *NFκB2* expression. In addition, the mutation status of *TP53* was determined from the DNA sequencing set of n = 127 patients. The available clinical data from PDAC patients were then included in the analysis to compare *NFκB2* expression in patients with different p53 status.

9.7 Statistical methods

ANOVA or two-sided Student`s t-test was used to investigate statistical significance. Kaplan-Meier survival curve were analyzed by Log-rank test. GraphPad Prism6 was used to calculate p-values and corrected according to Bonferroni for multiple testing unless otherwise indicated. P-values are indicated or marked by with a * in the figures that shows $p < 0.05$. All data were analyzed from at least three independent experiments, otherwise mentioned. Results are presented as mean and standard deviation (SD), otherwise depicted.

10 Results

10.1Role of NFκB2 in pancreatic cancer

10.1.1 Role of *Nfκb2* for PanIN progression and PDAC development in a *Kras^{G12D}*-driven mouse model

Nfκb2 amplifications were recently described in human and murine PDAC (Mueller et al., 2018). To further elaborate the role of NFκB2 in the carcinogenesis in the pancreas, a general knockout mouse line (*Nfκb2$^{-/-}$*) (Paxian et al., 1999; Paxian et al., 2002) was crossed with *Pdx1-Cre,LSL-Kras$^{G12D/+}$* and *Ptf1a$^{Cre/+}$,LSL-Kras$^{G12D/+}$* mice (Fig. 10.1A).

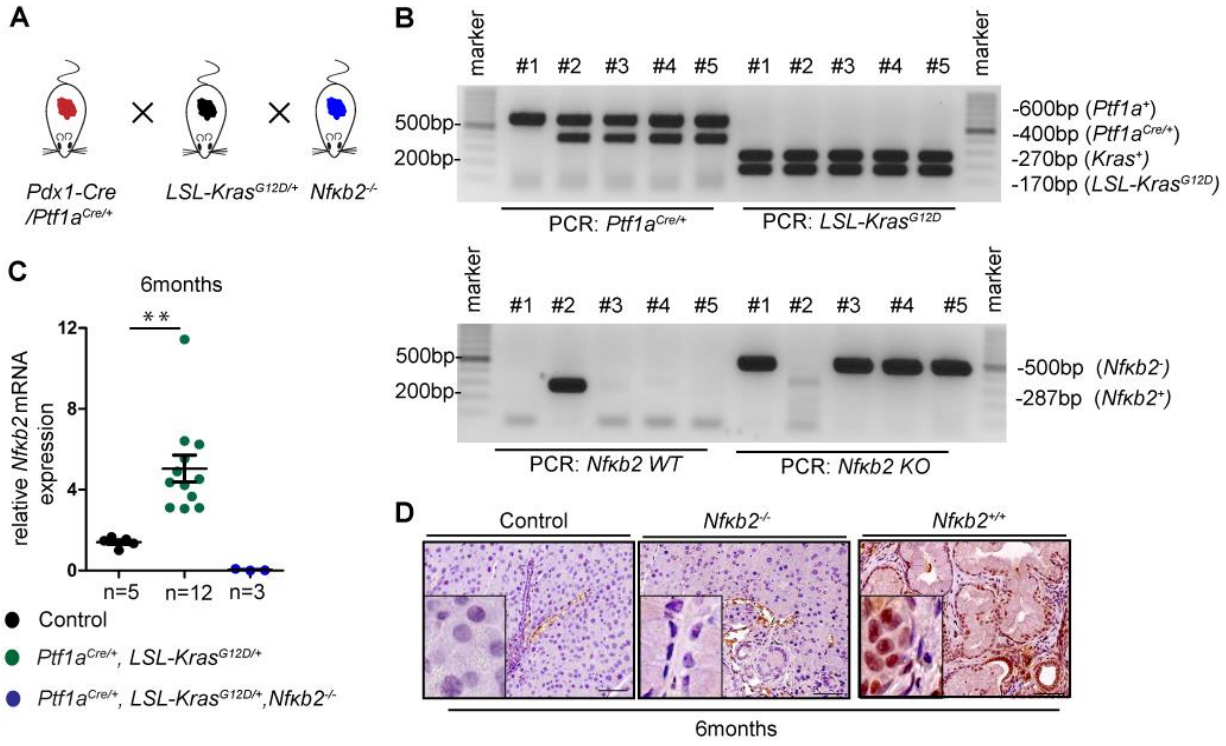

Fig. 10:1 Nfκb2 expression and genotyping

A) Scheme of mouse lines used to analyze the role of the *Nfκb2* in the carcinogenesis in the pancreas. B) Example of the genotyping PCR analysis from the tail DNA of the depicted alleles. C) Relative mRNA expression of *Nfκb2* in wild type (green dots), *Ptf1a$^{Cre/+}$,LSL-Kras$^{G12D/+}$*(black dots), and *Ptf1a$^{Cre/+}$,LSL-Kras$^{G12D/+}$,Nfκb2$^{-/-}$* (blue dots) mice at six months of age. Shown is the mean +/- SD. ** p value of a one-way ANOVA <0.01. D) Representative immunohistochemical staining of Nfκb2 in one six months old wildtype control, *Ptf1a$^{Cre/+}$,LSL-Kras$^{G12D/+}$,Nfκb2$^{+/+}$* and *Ptf1a$^{Cre/+}$,LSL-Kras$^{G12D/+}$,Nfκb2$^{-/-}$* mouse. (Scale bar: 50 μm).

Compared to wildtype pancreata, increased *Nfκb2* mRNA and protein expression was observed in the pancreata of six months old *Ptf1a*$^{Cre/+}$,*LSL-Kras*$^{G12D/+}$ mice as shown by qPCR and IHC (Fig. 10.1C & 10.1D).

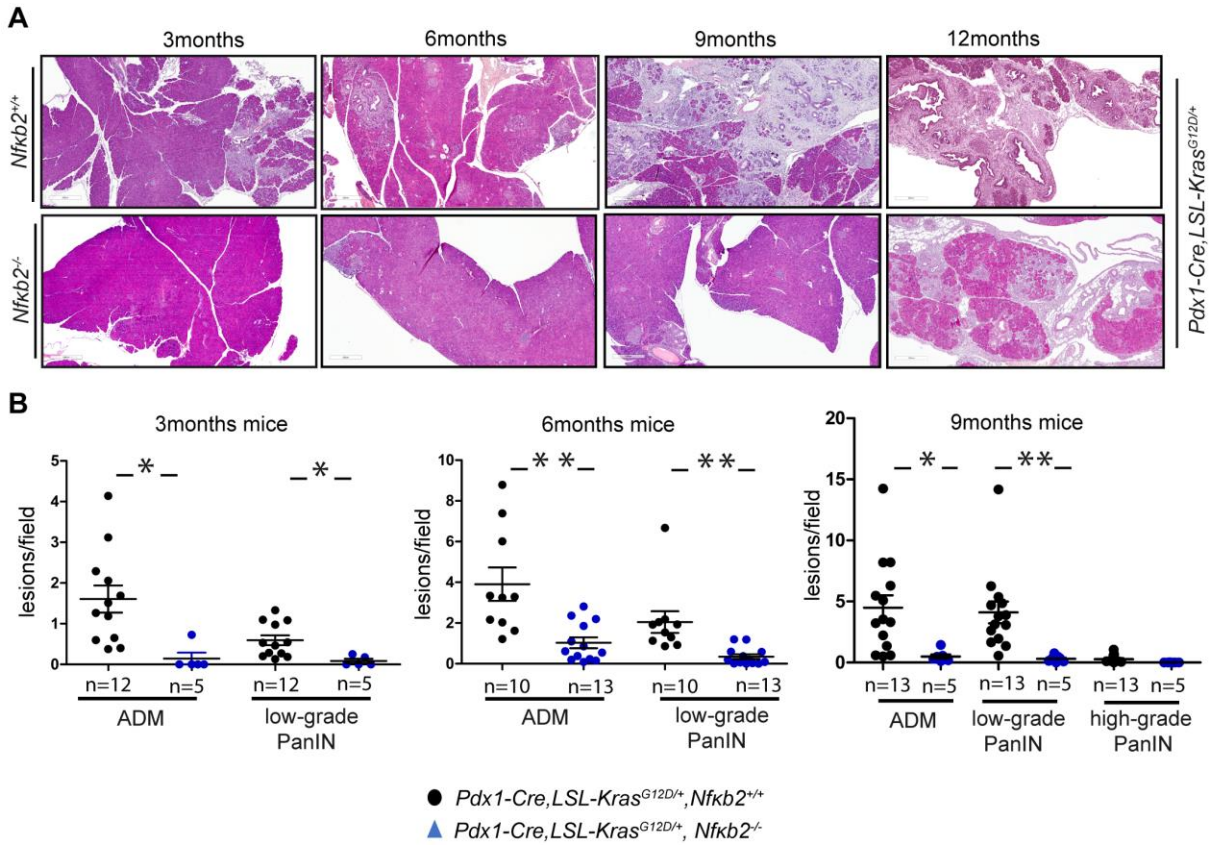

Fig. 10:2 PanIN progression is mediated by *Nfκb2* expression in *Pdx1-Cre,LSL-Kras*$^{G12D/+}$ mice

A) Representative H & E staining for sections of three, six, nine and twelve months old *Pdx1-Cre,LSL-Kras*$^{G12D/+}$,*Nfκb2*$^{+/+}$and *Pdx1-Cre,LSL-Kras*$^{G12D/+}$,*Nfκb2*$^{-/-}$ mice (Scale bar: 400 μm). B) Number of PanINs i.e. ADM, low-grade lesions (PanIN-1A and PanIN-1B), and high-grade lesions (PanIN-2/3) was counted per 200x field in three, six, nine and twelve months old *Pdx1-Cre,LSL-Kras*$^{G12D/+}$, *Nfκb2*$^{+/+}$(black dots) and *Pdx1-Cre,LSL-Kras*$^{G12D/+}$,*Nfκb2*$^{-/-}$ (blue dots) mice. Number of analysed animals is indicated. Shown is the mean +/- SD. p value of a two-tailed unpaired t-test *<0.05, **<0.01.

Hereafter, the resulting mouse models are referred to as *Pdx1-Cre,LSL-Kras*$^{G12D/+}$,*Nfκb2*$^{-/-}$ *or Ptf1a*$^{Cre/+}$,*LSL-Kras*$^{G12D/+}$,*Nfκb2*$^{-/-}$ respectively. *Nfκb2* deletion was verified by PCR from mouse tail DNA (Fig. 10.1B), followed by qPCR (Fig. 10.1C) and IHC (Fig. 10.1D).

ADM are neoplastic lesions which can subsequently develop in low and high grade PanINs and can gradually progress into PDAC (Hingorani et al., 2003). Histological analysis in this study clearly shows that development of ADM as well as PanIN lesions of all grades were

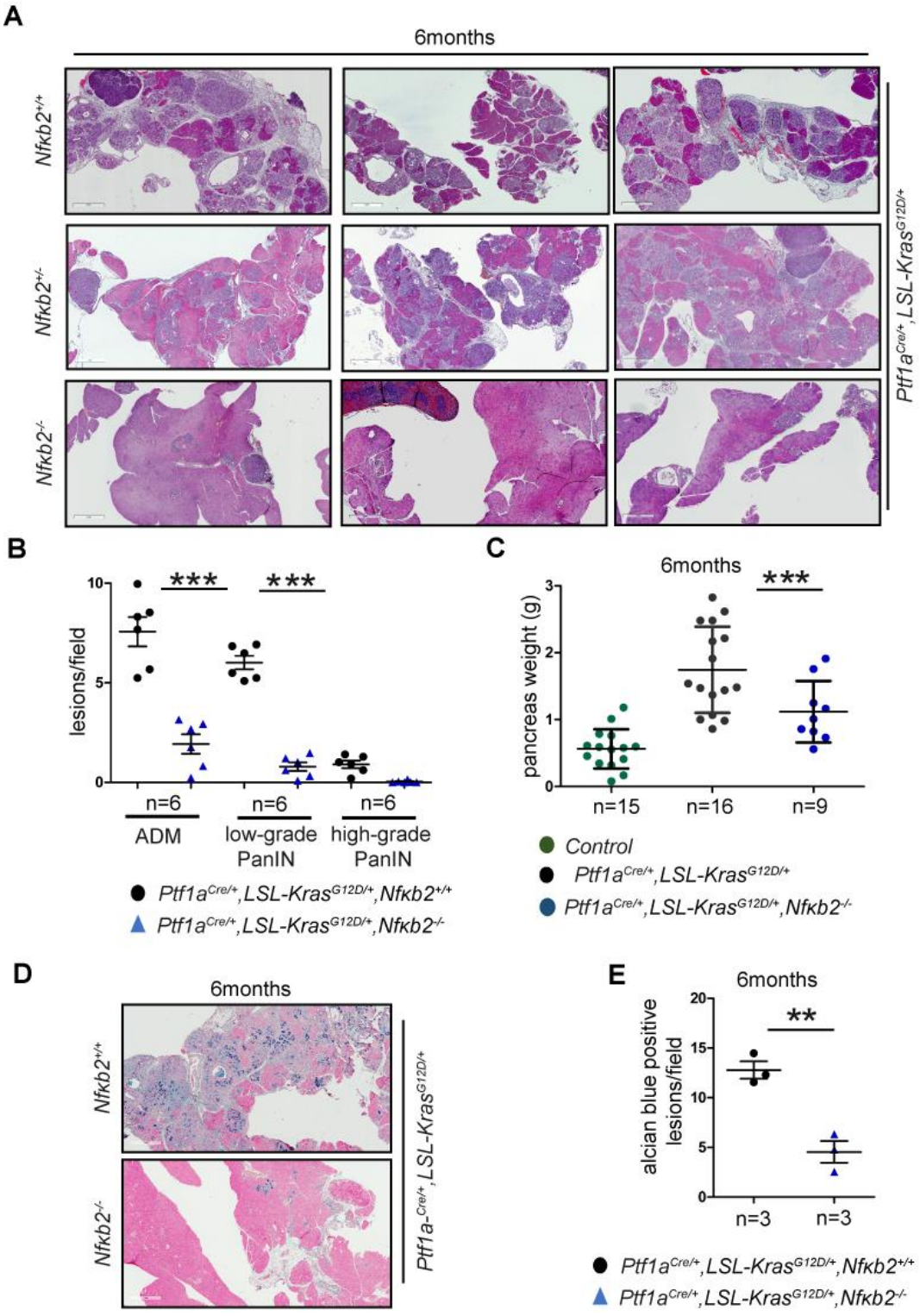

Fig. 10:3 *Nfκb2* accelerates PanIN progression in *Ptf1a$^{Cre/+}$,LSL-Kras$^{G12D/+}$*mice

A) Representative H & E staining for sections of three six months old *Ptf1a$^{Cre/+}$,LSL-Kras$^{G12D/+}$,Nfκb2$^{+/+}$; Ptf1a$^{Cre/+}$,LSL-Kras$^{G12D/+}$,Nfκb2$^{+/-}$* and *Ptf1a$^{Cre/+}$,LSL-Kras$^{G12D/+}$,Nfκb2$^{-/-}$* mice (Scale bar: 1 mm). B) Number of PanINs i.e. quantification of ADM, low-grade lesions (PanIN-1A and PanIN-1B), and high-grade lesions (PanIN-2/3) in six *Ptf1a$^{Cre/+}$,LSL-Kras$^{G12D/+}$,Nfκb2$^{+/+}$*(black

dots), and six *Ptf1a*$^{Cre/+}$,*LSL-Kras*$^{G12D/+}$,*Nfκb2*$^{-/-}$ (blue dots) mice. Number of analyzed animals is indicated. Shown is the mean +/- SD. p value of a two-tailed unpaired t-test **<0.05. C) Relative pancreas weight/body weight of six months old WT (green dots), *Ptf1a*$^{Cre/+}$,*LSL-Kras*$^{G12D/+}$ (green dots) and *Ptf1a*$^{Cre/+}$,*LSL-Kras*$^{G12D/+}$,*Nfκb2*$^{-/-}$ (blue dots) mice. Shown is the mean +/- SD. One-way ANOVA ***p<0.05. D) Alcian Blue stained pancreatic tissue of six months old *Ptf1a*$^{Cre/+}$,*LSL-Kras*$^{G12D/+}$ *Nfκb2*$^{+/+}$ mice compared to same aged *Ptf1a*$^{Cre/+}$,*LSL-Kras*$^{G12D/+}$,*Nfκb2*$^{-/-}$ mice (Scale bar: 1 mm). E) Numbers of Alcian Blue positive lesion per field of three *Ptf1a*$^{Cre/+}$,*LSL-Kras*$^{G12D/+}$, *Nfκb2*$^{+/+}$ and three *Ptf1a*$^{Cre/+}$,*LSL-Kras*$^{G12D/+}$,*Nfκb2*$^{-/-}$ mice. Shown is the mean +/- SD. p value of a two-tailed unpaired t- test **<0.01.

significantly reduced in *Pdx1-Cre,LSL-Kras*$^{G12D/+}$,*Nfκb2*$^{-/-}$ mice compared to *Pdx1-Cre,LSL-Kras*$^{G12D/+}$ mice (Fig. 8.2A).

These results are further supported by quantification of neoplastic lesions. Three, six and nine months old mice show that *Nfκb2* deletion blocks ADM development and PanIN progression in *Pdx1-Cre;LSL-Kras*$^{G12D/+}$;*Nfκb2*$^{-/-}$ mice (Fig. 10.2B).

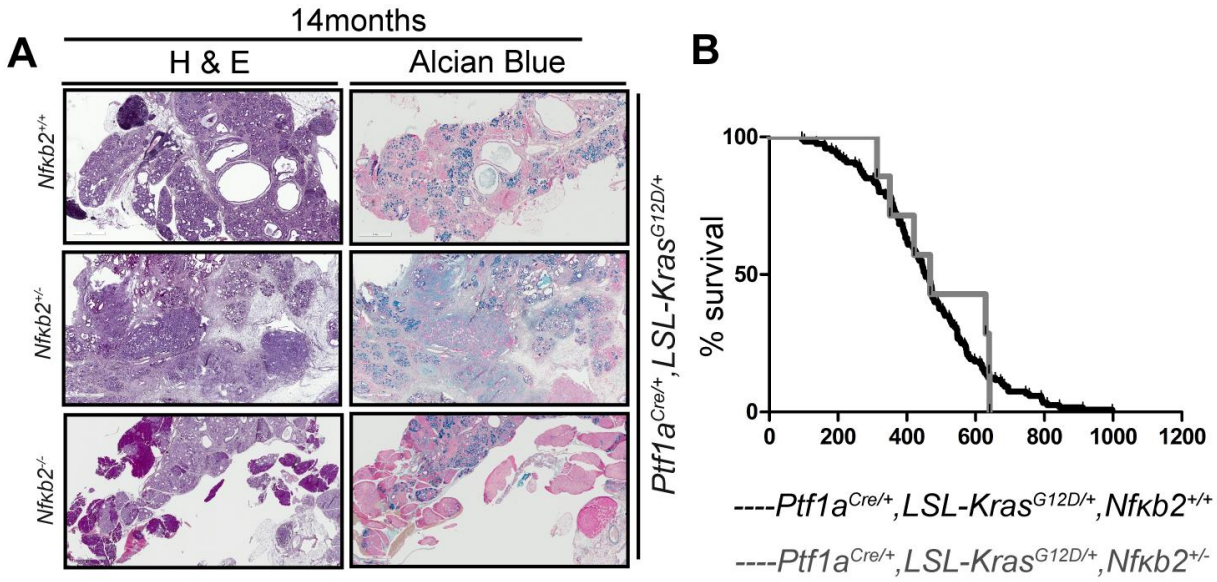

Fig. 10:4 Impaired disease progression in *Nfκb2*-deficient aged KC mice

A) Representative H & E, and alcian blue staining for sections of 14 months *Ptf1a*$^{Cre/+}$,*LSL-Kras*$^{G12D/+}$,*Nfκb2*$^{+/+}$; *Ptf1a*$^{Cre/+}$,*LSL-Kras*^{G12D} *Nfκb2*$^{+/-}$ and *Ptf1a*$^{Cre/+}$,*LSL-Kras*$^{G12D/+}$,*Nfκb2*$^{-/-}$ mice (Scale bar: 1 mM). B) Kaplan-Meier survival curve of *Ptf1a*$^{Cre/+}$,*LSL-Kras*$^{G12D/+}$,*Nfκb2*$^{+/-}$ mice having medium survival of 468 days (n=7) versus *Ptf1a*$^{Cre/+}$,*LSL-Kras*$^{G12D/+}$,*Nfκb2*$^{+/+}$ mice (n=130), with median survival of 466 days.

Consistently, histological analysis in the *Ptf1a*$^{Cre/+}$,*LSL-Kras*$^{G12D/+}$,*Nfκb2*$^{-/-}$ mouse model also shows a profound effect of *Nfκb2* deletion on ADM and PanIN development. Heterozygous *Nfκb2*$^{+/-}$ mice demonstrated normal ADM and PanIN development (Fig. 10.3A). Quantification of these neoplastic lesions in aged-matched *Ptf1a*$^{Cre/+}$,*LSL-Kras*$^{G12D/+}$,*Nfκb2*$^{+/+}$ mice versus

Ptf1a$^{Cre/+}$*,LSL-Kras*$^{G12D/+}$*,Nfκb2*$^{-/-}$ mice at six months of age also confirmed that *Nfκb2* deletion results in a significant reduction of ADM and PanIN formation (Fig.10.3B). It is well known that *Kras*^{G12D} expression in the pancreas result in growth and weight gain (Eser et al., 2013), an effect not observed in *Ptf1a*$^{Cre/+}$*,LSL-Kras*$^{G12D/+}$*,Nfκb2*$^{-/-}$ mice (Fig.10.3C).

The important contribution of *Nfκb2*$^{-/-}$ to the carcinogenesis in the pancreas is further confirmed by alcian blue staining, a marker used to identify low-grade pre-neoplastic lesion due to the high acidic mucin content. The quantification of the staining shows a clear reduction of upper mentioned lesions in age-matched pancreata of *Ptf1a*$^{Cre/+}$*,LSL-Kras*$^{G12D/+}$*,Nfκb2*$^{-/-}$ mice (Fig. 10.3D & Fig. 10.3E).

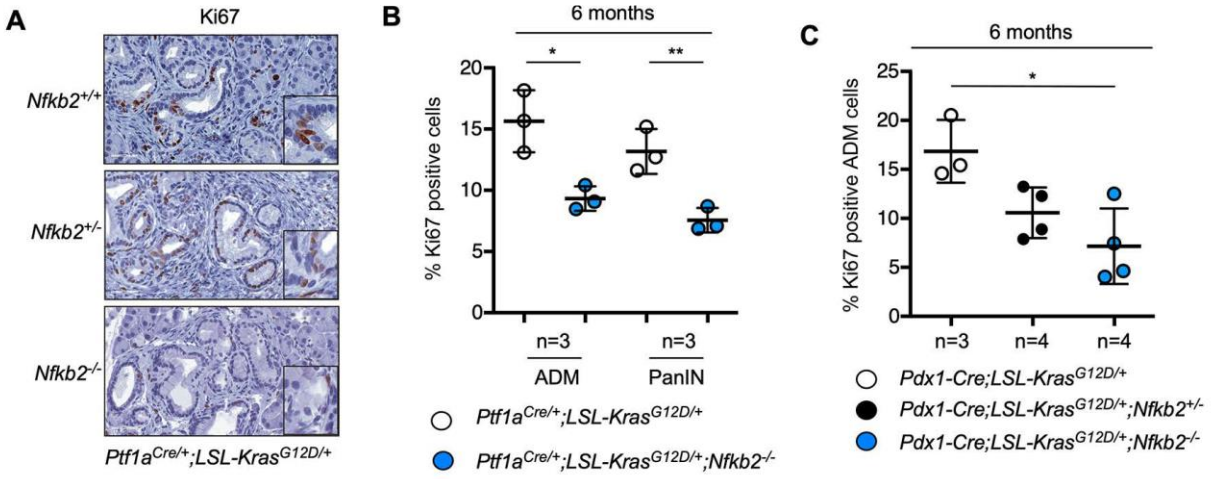

Fig. 10:5 *Nfκb2* deletion impairs proliferation *in vivo*

A) Ki67 staining of pancreatic tissue from six old month proficient *Ptf1a*$^{Cre/+}$*,LSL-Kras*$^{G12D/+}$*,Nfκb2*$^{+/+}$*:* heterozygous *Ptf1a*$^{Cre/+}$*,LSL-Kras*$^{G12D/+}$*,Nfκb2*$^{+/-}$ as well as for homozygous deleted *Ptf1a*$^{Cre/+}$*,LSL-Kras*$^{G12D/+}$*,Nfκb2*$^{-/-}$ mice. Scale bar indicates 50 μm. B) Proliferation index of neoplastic lesions of six months old *Ptf1a*$^{Cre/+}$*,LSL-Kras*$^{G12D/+}$*,Nfκb2*$^{+/+}$ mice in comparison with *Ptf1a*$^{Cre/+}$*,LSL-Kras*$^{G12D/+}$*,Nfκb2* $^{-/-}$ mice. Number of mice analyzed in each genotype is indicated. Shown is the mean +/- SD. p value of a two-tailed unpaired t-test *<0.05, **<0.01. C) Proliferation index of neoplastic lesions of six months old *Pdx1-Cre,LSL-Kras*$^{G12D/+}$, and *Pdx1-Cre,LSL-Kras*$^{G12D/+}$*,Nfκb2*$^{+/-}$ mice in comparison with *Pdx1-Cre,LSL-Kras*$^{G12D/+}$*,Nfκb2*$^{-/-}$ mice. Number of analyzed animals is indicated. Shown is the mean +/- SD. p value of a two-tailed unpaired t-test *<0. 05.

To test the role of *Nfκb2* in cancer development at later stages of the disease, aged mice were analyzed. Only PanIN lesions were detected in 14 months aged *Ptf1a*$^{Cre/+}$*,LSL-Kras*$^{G12D/+}$*,Nfκb2*$^{-/-}$ mice (Fig. 10.4A), while *Ptf1a*$^{Cre/+}$*,LSL-Kras*$^{G12D/+}$*,Nfκb2*$^{+/+}$ and *Ptf1a*$^{Cre/+}$*,LSL-Kras*$^{G12D/+}$*,Nfκb2*$^{+/-}$ mice showed invasive carcinomas (Fig. 10.4A & 10.4B). Furthermore, no PDAC-related death was detected in *Ptf1a*$^{Cre/+}$*,LSL-Kras*$^{G12D/+}$*,Nfκb2*$^{-/-}$ mice investigated between 300 and 525 days of age (data not shown). Heterozygous

Ptf1a$^{Cre/+}$*,LSL-Kras*$^{G12D/+}$*,Nfκb2*$^{+/-}$ mice, however, showed macroscopic signs of PDAC development (Fig. 10.4A), and had a median survival of 468 days (Fig. 10.4B). Which matches with the median survival (466 days) of the *Ptf1a*$^{Cre/+}$*,LSL-Kras*$^{G12D/+}$*,Nfκb2*$^{+/+}$ control cohort (Fig. 10.4B), suggesting that one *Nfκb2* allele is sufficient for PDAC development.

In summary, this data shows that *Nfκb2* is involved in ADM development and PanIN progression. In addition, these data provide evidence that also PDAC development is delayed in the investigated models.

10.1.2 *Nfκb2* contributes to *Kras*^{G12D}-induced Proliferation and Cell Cycle Control

It has been shown that con-canonical NFκB signaling is linked to proliferation and cell cycle control (Doppler et al., 2013; Saxon et al., 2018; Schumm et al., 2006). To elaborate the pro-proliferative role of *Nfκb2 in vivo*, IHC staining for the proliferation marker Ki67 was performed and the fraction of Ki67-positive ADM and PanIN cells in both mouse models was quantified. A significantly decreased Ki67 proliferation index in *Ptf1a*$^{Cre/+}$*,LSL-Kras*$^{G12D/+}$*,Nfκb2*$^{-/-}$ mice (Fig. 10.5A & 10.5B) as well as in ADM cells of *Pdx1-Cre,LSL-Kras*$^{G12D/+}$*,Nfκb2*$^{-/-}$ mice was found (Fig. 10.5C).

Moreover, qPCR for the proliferative marker gene, *Pcna* showed reduced expression in the pancreata of *Pdx1-Cre,LSL-Kras*$^{G12D/+}$*,Nfκb2*$^{-/-}$ mice (Fig. 10.6A) as compared to *Pdx1-Cre,LSL-Kras*$^{G12D/+}$ mice.

In addition, a decreased fraction of Cyclin D1 positive ADM and PanIN cells was detected by IHC in *Ptf1a*$^{Cre/+}$*,LSL-Kras*$^{G12D/+}$*,Nfκb2*$^{-/-}$ mice (Fig. 10.6B & 10.6C). Subsequently, decreased expression of Cyclin D1 was detected by western blotting of pancreatic tissue lysates (Fig. 10.6D & 10.6E), thus underscoring the important contribution of *Nfκb2* to the *LSL-Kras*^{G12D}-driven proliferation.

10.1.3 Molecular processes linked with NFκB2 signaling

To find pathways and molecular processes linked to NFκB2 signaling, RNA from one-month old mice was extracted and analyzed by RNA seq. Due to the fundamentally different disease progression in *Ptf1a*$^{Cre/+}$*,LSL-Kras*$^{G12D/+}$*,Nfκb2*$^{+/+}$ and *Ptf1a*$^{Cre/+}$*,LSL-Kras*$^{G12D/+}$*,Nfκb2*$^{-/-}$

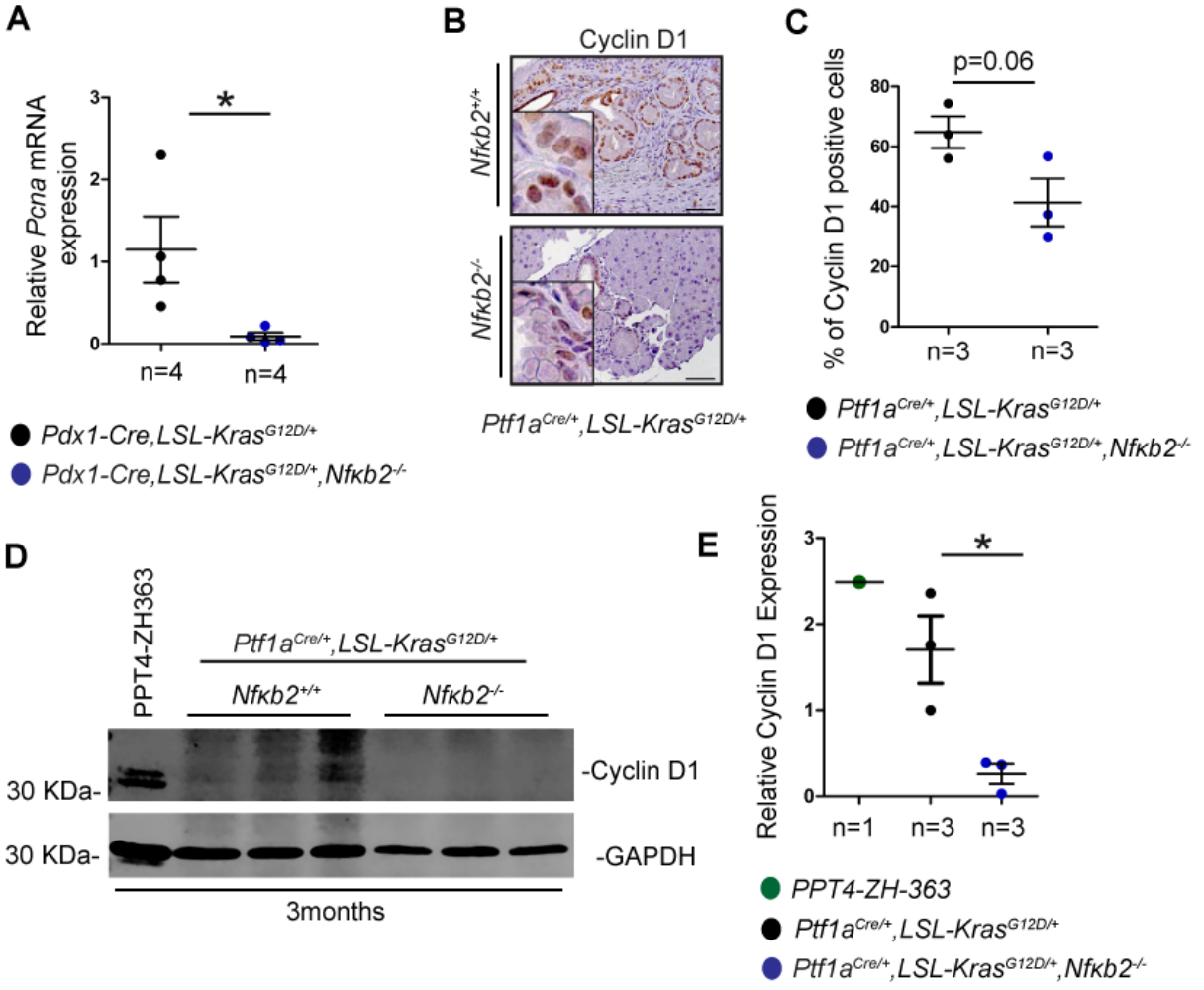

Fig. 10:6 *Nfκb2* deletion downregulate Cyclin D1 expression

A). Quantitative mRNA expression analysis of *Pcna* in *Pdx1-Cre,LSL-Kras$^{G12D/+}$*(black dots) and *Pdx1-Cre,LSL-Kras$^{G12D/+}$,Nfκb2$^{-/-}$* mice (blue dots). Number of animals analyzed at 9 months of age are indicated. Shown is the mean +/- SD. * p value of a two-tailed unpaired t-test *<0.05. mRNA expression levels were normalized to β actin. B) Immunohistochemical Cyclin D1 staining of pancreatic tissue from six months old *Ptf1a$^{Cre/+}$,LSL-Kras$^{G12D/+}$,Nfκb2$^{+/+}$* (black dots) mice in comparison to *Ptf1a$^{Cre/+}$,LSL-Kras$^{G12D/+}$,Nfκb2$^{-/-}$* mice (blue dots) (Scale bar: 50 μm). C) Quantification of Cyclin D1 positive immunohistochemical cells of neoplastic lesions of six months old *Ptf1a$^{Cre/+}$,LSL-Kras$^{G12D/+}$,Nfκb2$^{+/+}$* mice in comparison with *Ptf1a$^{Cre/+}$,LSL-Kras$^{G12D/+}$,Nfκb2$^{-/-}$* mice. Number of mice analyzed in each genotype is indicated. Shown is the mean +/- SD. *p value of a two-tailed unpaired t-test is indicated. D) Western blot analysis of Cyclin D1 expression in pancreatic tissue of three age matched (3months) *Ptf1a$^{Cre/+}$,LSL-Kras$^{G12D/+}$,Nfκb2$^{+/+}$* mice in comparison to *Ptf1a$^{Cre/+}$,LSL-Kras$^{G12D/+}$,Nfκb2$^{-/-}$* mice tissue. Murine PDAC cell lines PPT4-ZH-363 served as a control. GAPDH: loading control. E) Relative expression of Cyclin D1 for D), where the ratio of the Cyclin D1 to GAPDH was arbitrarily set to one for one of *Ptf1a$^{Cre/+}$,LSL-Kras$^{G12D/+}$,Nfκb2$^{+/+}$* mouse tissue. And murine PDAC cell line PPT4-ZH-363 served (black dot) as a positive control for *Nfκb2* expression. Shown is the relative expression. *p-value of a paired Student's t-test<0.05.

mice and to avoid a potentially biased output, an early time point of the disease was chosen for RNA seq, which was strengthen by the fact that microscopically most of the pancreatic

part of *Ptf1a*$^{Cre/+}$,*LSL-Kras*$^{G12D/+}$,*Nfκb2*$^{+/+}$ and *Ptf1a*$^{Cre/+}$,*LSL-Kras*$^{G12D/+}$,*Nfκb2*$^{-/-}$ mice at one month of age appeared to be normal with few pre-neoplastic lesions (Fig. 10.7A).

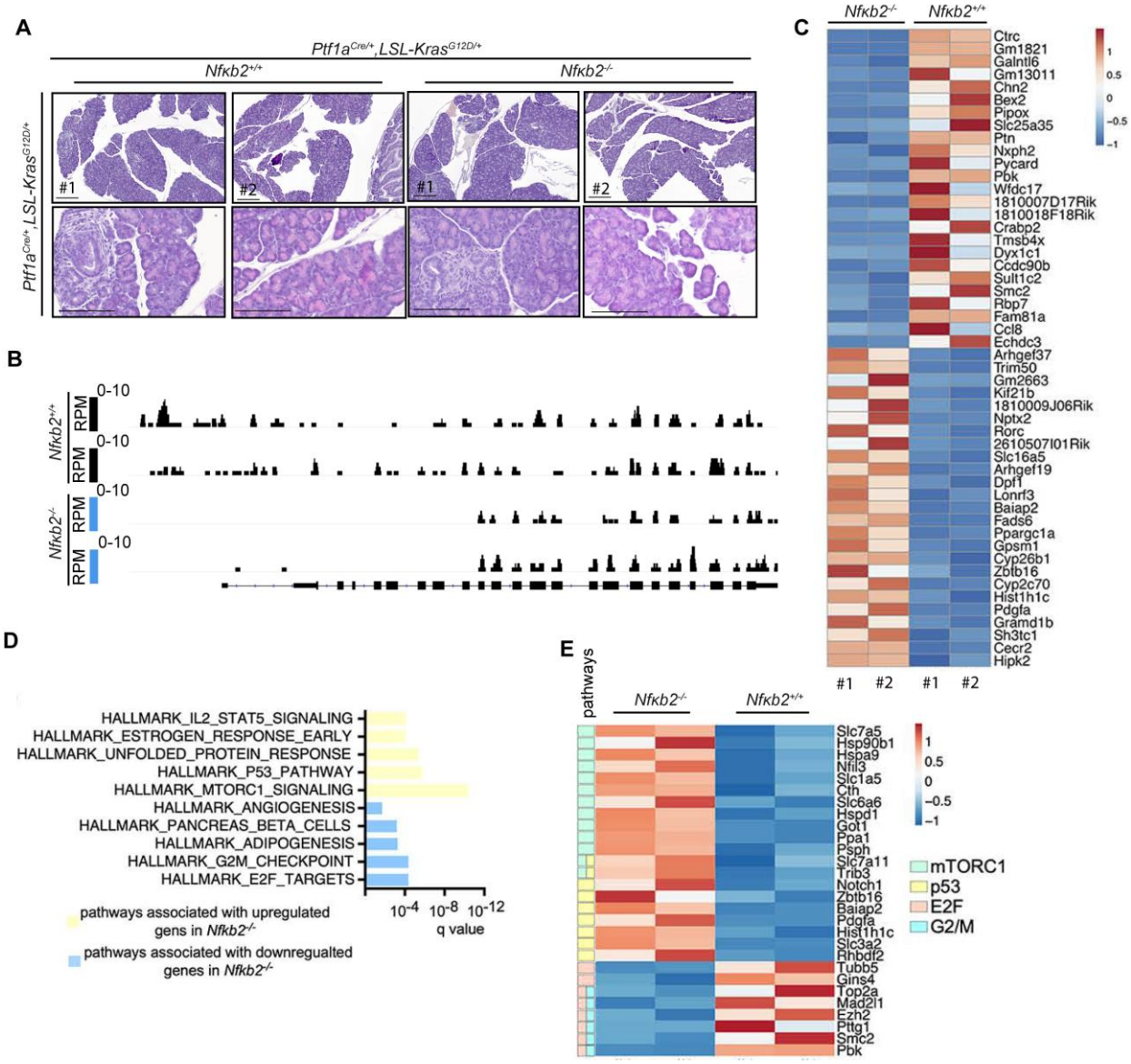

Fig. 10:7 Nfκb2-associated pathways and genes

A) Representative H & E sections of two four-weeks-old *Ptf1a*$^{Cre/+}$,*LSL-Kras*$^{G12D/+}$,*Nfκb2*$^{+/+}$ in comparison to two *Ptf1a*$^{Cre/+}$,*LSL-Kras*$^{G12D/+}$,*Nfκb2*$^{-/-}$ mice (scale bar: 60 μm and 600 μm), that were further analyzed by RNA-seq. B) RNA-Seq coverage of mRNA of tissue A) for the *Nfκb2* locus is displayed in reads per million mapped reads (RPM). No reads are detected covering the exons one to nine in the *Nfκb2*$^{-/-}$ line. C) Heatmap of the top 50 differential regulated genes for the respective phenotypes of A). D) Genes up- or down-regulated (log FC +/- 1; adj. p value < 0.05) for the respective phenotypes of A) were analyzed using the Hallmark Signatures of the Molecular Signature Database. The FDR q value is depicted. E) Heatmap of genes belonging to the top two up- or down-regulated Hallmark signatures corresponding to D) sorted by the q value. The association to the pathways is color coded.

RNA seq reconfirmed *Nfκb2* deletion in the mouse model, as specific deletion of exons 1-9 of the *Nfκb2* gene (Paxian et al., 1999) was observed (Fig. 10.7B). The top 50 differentially expressed genes between *Ptf1a*$^{Cre/+}$,*LSL-Kras*$^{G12D/+}$,*Nfκb2*$^{+/+}$ and *Ptf1a*$^{Cre/+}$,*LSL-Kras*$^{G12D/+}$,*Nfκb2*$^{-/-}$ mice are displayed (Fig. 10.7C). Analysis of differential expressed gene with the Molecular Signature Database (MSigDB; Hallmark gene sets) showed loss of signatures connected to the E2F transcription factor and the control of the G2/M phase of the

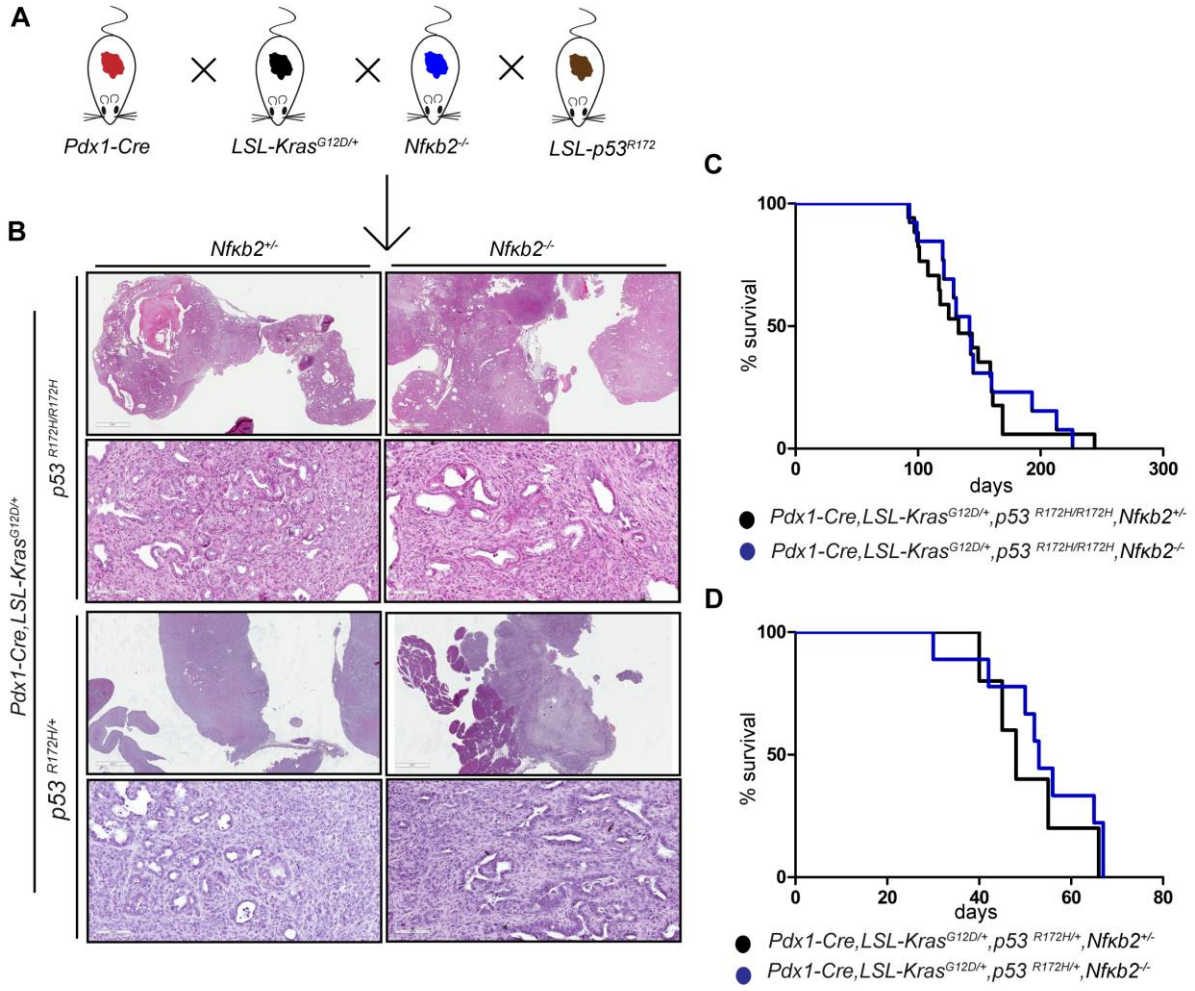

Fig. 10:8 Role of *Nfκb2* in the presence of *p53*^{R172H} for PDAC progression

A) Illustration of the mouse models used to cross the *Nfκb2* gene in the pancreas. B) Representative H&E staining of paraffin sections of *Pdx1-Cre,LSL-Kras*$^{G12D/+}$,*LSL-p53*$^{R172H/R172H}$,*Nfκb2*$^{+/-}$ mice in comparison to *Pdx1-Cre,LSL-Kras*$^{G12D/+}$,*LSL-p53*$^{R172H/R172H}$,*Nfκb2*$^{-/-}$ mice as well as *Pdx1-Cre,LSL-Kras*$^{G12D/+}$,*LSL-p53*$^{R172H/+}$,*Nfκb2*$^{+/-}$ mice in comparison to *Pdx1-Cre,LSL-Kras*$^{G12D/+}$,*LSL-p53*$^{R172H/+}$,*Nfκb2*$^{-/-}$ mice (Scale bar: 2 mm and 100 μm). C) Kaplan Meier survival curves of *Pdx1-Cre,LSL-Kras*$^{G12D/+}$,*LSL-p53*$^{R172H/R172H}$,*Nfκb2*$^{+/-}$ (n=5; median survival 48 days) in comparison to *Pdx1-Cre,LSL-Kras*$^{G12D/+}$,*LSL-p53*$^{R172H/R172H}$,*Nfκb2*$^{-/-}$(n=9; median survival 53 days) mice. D) Kaplan Meier survival curves of *Pdx1-Cre,LSL-Kras*$^{G12D/+}$,*LSL-p53*$^{R172H/+}$,*Nfκb2*$^{+/-}$ (n=17; median survival 133 days) in comparison to *Pdx1-Cre,LSL-Kras*$^{G12D/+}$,*LSL-p53*$^{R172H/+}$,*Nfκb2*$^{-/-}$ (n=13; median survival 142 days) mice.

cell cycle in the pancreas of *Ptf1a$^{Cre/+}$,LSL-Kras$^{G12D/+}$,Nfκb2$^{-/-}$* mice tissues. In addition, loss of signature specific of adipogenesis, pancreatic beta cells and angiogenesis were also detected (Fig. 10.7D). While, signatures for many pathways such as MTORC1, p53, unfolded protein response, the estrogen response, and STAT signaling are enriched in the pancreas of *Ptf1a$^{Cre/+}$,LSL-Kras$^{G12D/+}$,Nfκb2$^{-/-}$* mice tissue as compared to *Ptf1a$^{Cre/+}$,LSL-Kras$^{G12D/+}$,Nfκb2$^{+/+}$* mice tissue (Fig. 10.7D). Therefore, RNA-seq data are reconfirming the pro-proliferative role of *Nfκb2* in PDAC. To further emphasize the significance of the MSigDB results, genes linked with the top two scored hallmarks in each genotype are displayed in detail (Fig. 10.7E).

10.1.4 *Nfκb2* is dispensable in the presence of *p53^{R172H}* in PDAC GEMMs

In addition to the cell cycle signatures, *p53* signatures were upregulated in the pancreata of *Ptf1a$^{Cre/+}$,LSL-Kras$^{G12D/+}$,Nfκb2$^{-/-}$* mice compared to *Ptf1a$^{Cre/+}$,LSL-Kras$^{G12D/+}$,Nfκb2$^{+/+}$* mice (Fig. 10.7D). To elaborate this crosstalk genetically, an aggressive GEMM of PDAC, that relies on simultaneous expression of *Kras^{G12D}* and the mutated *p53^{R172H}* (Hingorani et al., 2005) (Fig. 10.8A) was used. *Pdx1-Cre,LSL-Kras$^{G12D/+}$,LSL-p53$^{R172H/R172H}$,Nfκb2$^{+/-}$* as well as *Pdx1-Cre,LSL-Kras$^{G12D/+}$,LSL-p53$^{R172H/R172H}$,Nfκb2$^{-/-}$* mice showed the same histological features and developed PDAC at the same rate with an almost equal median survival of 48 and 53 days respectively (Fig. 10.8B & 10.8C).

Surprisingly, *Pdx1-Cre,LSL-Kras$^{G12D/+}$,LSL-p53$^{R172H/+}$,Nfκb2$^{-/-}$* mice developed PDAC at the same rate and with a similar median survival as *Pdx1-Cre,LSL-Kras$^{G12D/+}$,LSL-p53$^{R172H/+}$,Nfκb2$^{+/-}$* mice (Fig. 10.8B & 10.8D). Therefore, this data argues that *Nfκb2* is dispensable for PDAC development in p53-driven PDAC In addition to this, no difference in growth between *Pdx1-Cre,LSL-Kras$^{G12D/+}$,LSL-p53$^{R172H/+}$,Nfκb2$^{-/-}$* PDAC cell lines (n=3) and *Pdx1-Cre,LSL-Kras$^{G12D/+}$,LSL- p53$^{R172H/+}$,Nfκb2$^{+/+}$* PDAC cell lines (n=3) was observed (Fig. 10.9C). Taken together, *Nfκb2* models. deletion does not block *p53^{R172H}* driven *Kras^{G12D}* PDAC formation *in vivo* nor does it impede cell proliferation *in vitro*.

To find human relevance, analysis of a clinical human PDAC data set obtained from the Cancer genome atlas database available was performed (Fig. 10.10). The expression analysis supports the cross signaling between mutated tumor suppressor TP53 and NFκB2.

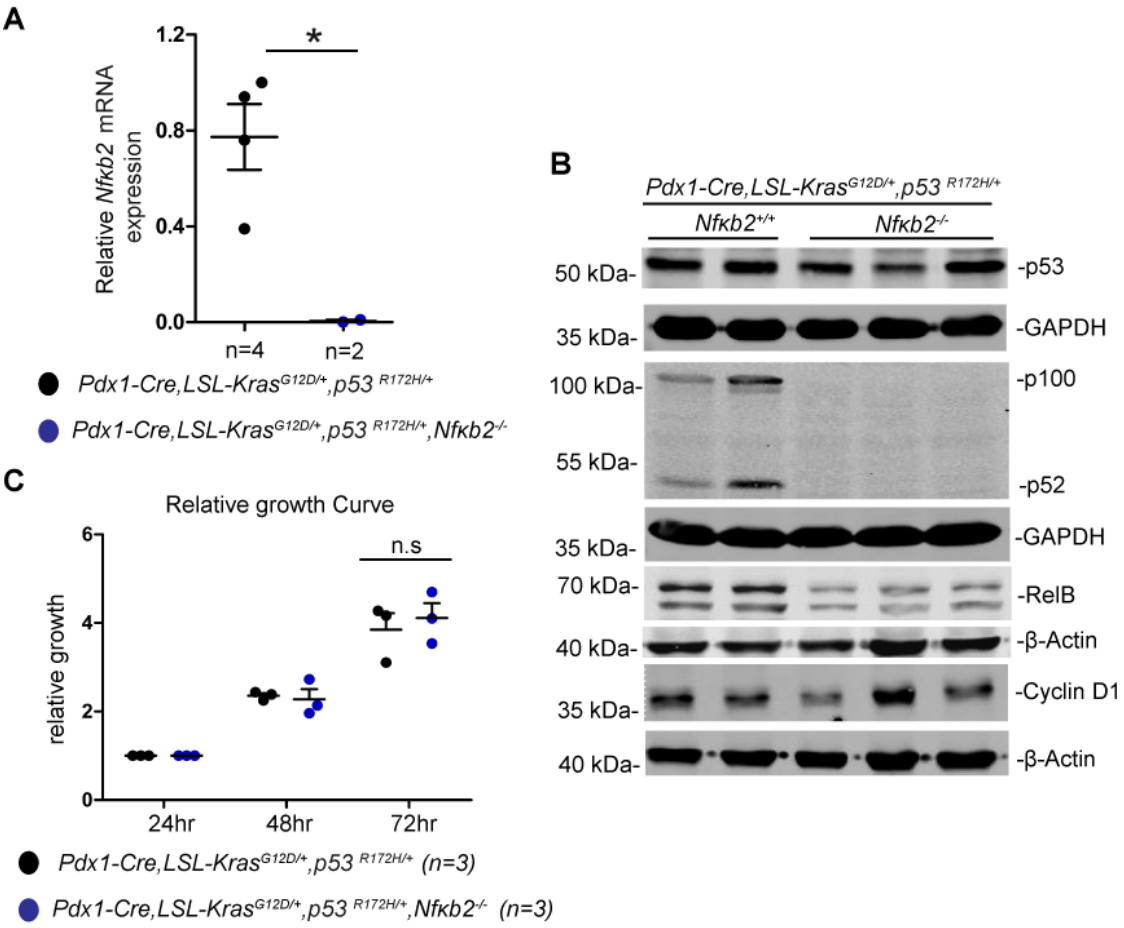

Fig. 10:9 *Nfκb2* deletion does not block growth of PDAC cells *in vitro*

A) qPCR analysis of *Nfκb2* mRNA expression in PDAC cell lines isolated from cancers of *Pdx1-Cre,LSL-Kras$^{G12D/+}$,LSL-p53$^{R172H/+}$* (n=4) mice (black dots) in comparison to PDAC cell lines from *Pdx1-Cre,LSL-Kras$^{G12D/+}$,LSL-p53$^{R172H/+}$,Nfκb2$^{-/-}$*mice (n=2) (blue dots). B) Protein expression analysis of total p100/p52, p53, RelB and Cyclin D1 by western blot in PDAC cell lines isolated from *Pdx1-Cre,LSL-Kras$^{G12D/+}$,LSL-p53$^{R172H/+}$* (n=2) mice as compare to three lines isolated from *Pdx1-Cre,LSL-Kras$^{G12D/+}$,LSL-p53$^{R172H/+}$,Nfκb2$^{-/-}$* (n=3) mice. Same extracts were blotted to different membranes and loading was controlled by β-actin or GAPDH C) Cell viability was measured after seeding equal number of PDAC cells isolated from *Pdx1-Cre,LSL-Kras$^{G12D/+}$,LSL-p53$^{R172H/+}$* (n=3) (black dots) mice as compare to cell lines isolated from *Pdx1-Cre,LSL-Kras$^{G12D/+}$,LSL-p53$^{R172H/+}$,Nfκb2$^{-/-}$* (blue dots) mice, over the time interval of 24, 48 and 72hrs The relative growth of the cells was measured and growth of the cells after 24 hrs of seeding was arbitrarily set for comparison. Three independent biological replicates were performed.

Whereas, in PDACs analysis (n=183) with known status of *TP53* (Fig. 10.10A), no effect of *NFκB2* mRNA expression to the survival of patient was detected: This was further supported by the analysis of *TP53* mutant PDAC, where no effect of *NFκB2* mRNA expression to the survival of patient was detected (Fig. 10.10B). While; high *NFκB2* expression marked patient with worse survival in PDACs with *TP53* wild type status (Fig. 10.10C).

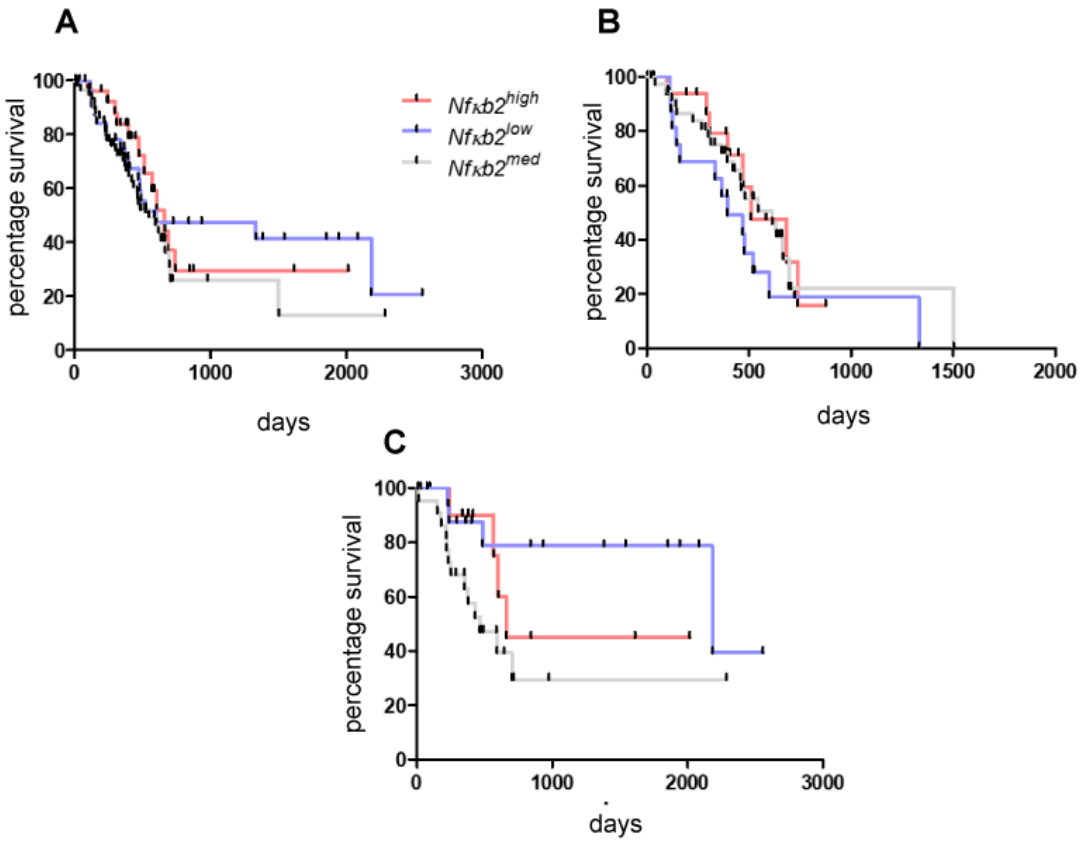

Fig. 10:10 Comparison of clinically available TCGA PDAC data set for *NFκB2* mRNA expression level

A) The mRNA expression of *NFκB2* from n = 183 PDAC patients from the TCGA dataset was separated by quartiles and trichotomized after the 1st quartile, after the 2nd-3rd. quartile and the 4th quartile. A) All patients with known *TP53* status (n = 127) were plotted in a Kaplan-Meier curve according to *NFκB2 expression*. B) Survival of *TP53* mutant (n = 72) and C) survival of *TP53* wild-type PDAC patients (n = 55).

In summary from human data, we conclude that the role of *NFκB2* is highly context dependent and influenced by the *TP53* mutational status.

10.2Role of MTOR in pancreatic cancer

10.2.1 Deletion of *Mtor* in the pancreas

To investigate the role of MTOR in the pancreatic carcinogenesis, a floxed $Mtor^{f/f}$ mouse line was crossed with the $Ptf1a^{Cre/+}$,$LSL\text{-}Kras^{G12D+/-}$ (abbreviated as KC) mouse model (Fig. 10.11A) (Hingorani et al., 2003). In that mouse model (abbreviated as $KC;Mtor^{lox/lox}$), floxed

exon 3 of *Mtor* is deleted specifically in pancreatic tissue but not in other organs such as intestine, liver or heart (Fig. 10.11B).

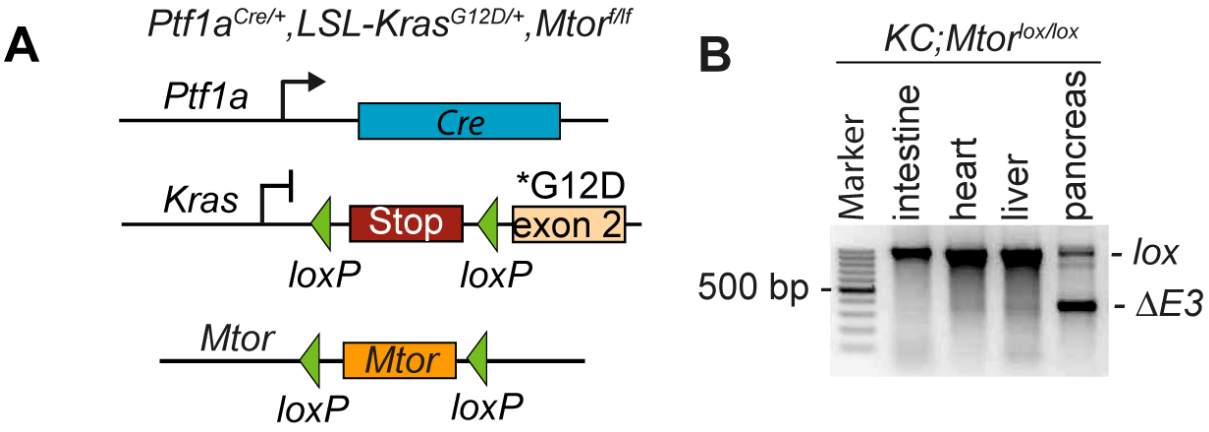

Fig. 10:11 Genetic Strategy and Validation of *Mtor* knockout in KC mouse model

A) Genetic strategy to delete *Mtor* alleles in the pancreas. B) Genotyping PCR of the indicated tissues of *KC;Mtor*$^{lox/lox}$ mice. *ΔE3*: exon three deleted *Mtor* allele; *lox*: *Mtor* exon 3 floxed allele.

The heterozygous mouse cohort *Ptf1a*$^{Cre/+}$*,LSL-Kras*$^{G12D/+}$*,Mtor*$^{lox/+}$ (abbreviated as *KC;Mtor*$^{lox/+}$) (Fig. 10.12A) showed a median survival of around 499 days that matches with the median survival of the KC mice (Diersch et al., 2013). However, homozygous *KC;Mtor*$^{lox/lox}$ mice showed a reduced survival of around 75 days (Fig. 10.12A).

Macroscopically, *KC;Mtor*$^{lox/lox}$ mice were smaller in size compared to *KC;Mtor*$^{lox/+}$ mice (Fig. 10.12B), and showed an atrophic pancreas (Fig. 10.12B). The body weight of these mice was reduced (Fig. 10.12C).

Microscopically, the acinar apparatus of *KC;Mtor*$^{lox/lox}$ mice was disorganized and showed decreased eosin staining (Fig. 10.13A). Picrosirius staining demonstrated increased collagen deposition in the pancreata of *KC;Mtor*$^{lox/lox}$ mice (Fig. 10.13B). Although acinar structures were disturbed, alpha-amylase 1 (Amy1) was still expressed to some extent (Fig. 10.13B). Islets of Langerhans were reduced in number and showed lower intensity of insulin staining (Fig. 10.13B). *KC;Mtor*$^{lox/lox}$ mice were able to gain weight (Fig. 10.13C), when the standard diet was substituted with a pancrex-vet diet containing additional pancreatic enzymes. Nevertheless, *KC;Mtor*$^{lox/lox}$ mice developed Diabetes mellitus as documented by high blood glucose levels at around 11th week of age (Fig. 10.13D).

In sum, this data shows that pancreas-specific deletion of the *Mtor* gene results in exocrine and endocrine insufficiency of the pancreas.

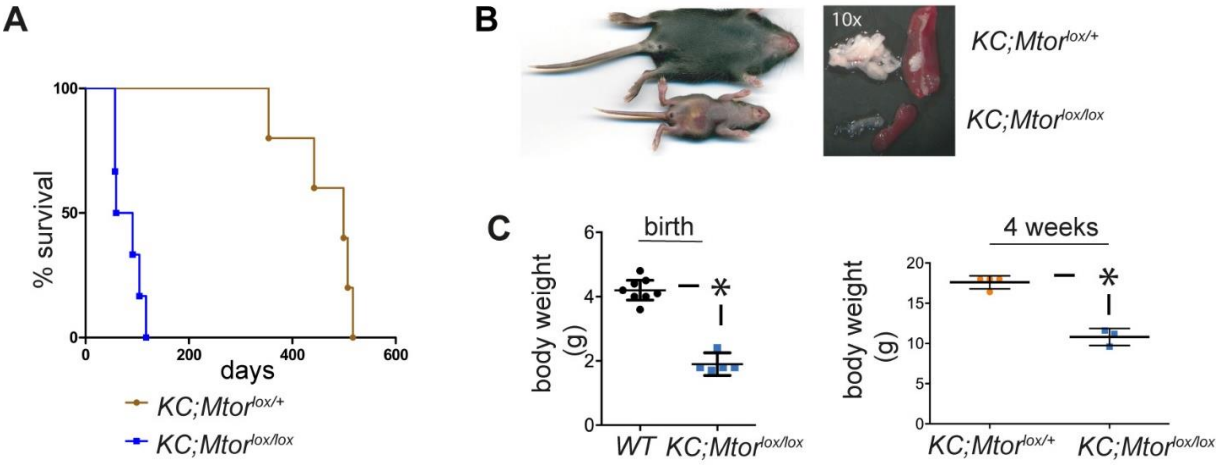

Fig. 10:12 Pancreas-specific Mtor knock-out impairs survival

A) Kaplan-Meier survival curves of *KC;Mtor$^{lox/lox}$* (n=5) and *KC;Mtor$^{lox/+}$* mice (n=5). B) Photographic documentation of appearance of 10-days-old mice as well as macroscopic picture of the pancreas of *KC;Mtor$^{lox/lox}$* and *KC;Mtor$^{lox/+}$* mice (10x magnification). C) Body weight of WT (black dots) (n=8), *KC;Mtor$^{lox/lox}$*(n=5), and *KC;Mtor$^{lox/+}$* (blue dots) (n=8) mice at birth and body weight of *KC;Mtor$^{lox/lox}$*(n=3) (blue dots), and *KC;Mtor$^{lox/+}$* (yellow dots) (n=4) mice at four weeks of age. * p value of an unpaired Student`s t-test < 0.05.

Despite the pancreas insufficiency, *KC;Mtor$^{lox/lox}$* mice developed acinar to ductal metaplasia (ADM) and low-grade pancreatic intraepithelial neoplasia (PanINs) (Fig. 10.13A), confirmed by the positive CK19 staining (Fig. 10.13B). In addition, desmoplastic changes could be also visualized (Fig. 10.13B).

To investigate whether the described phenotype is solely due to the *Mtor* deletion or due to the simultaneous expression of the oncogenic *Kras* with *Mtor* deletion, *Ptf1a^{Cre};Mtor$^{lox/lox}$* mice were analyzed. At 11 weeks of age, H&E staining revealed an atrophic pancreas embedded in adipose tissue (Fig. 10.14A). *Ptf1a^{Cre};Mtor$^{lox/lox}$* mice showed impaired weight gain even under substitution with pancreatic enzymes in the chow (Fig. 10.14B). Islets of Langerhans were present in the pancreas of the *Ptf1a^{Cre};Mtor$^{lox/lox}$* mouse (Fig. 10.14A), but blood glucose was distinctly increased (Fig. 10.14C). Therefore, it can be concluded that *Mtor* is essential to maintain the endocrine and exocrine function of the pancreas.

To demonstrate the inactivation of the Mtor signaling cascade and to exclude that the developed lesion stem from unrecombined escaper cells, IHC staining was performed.

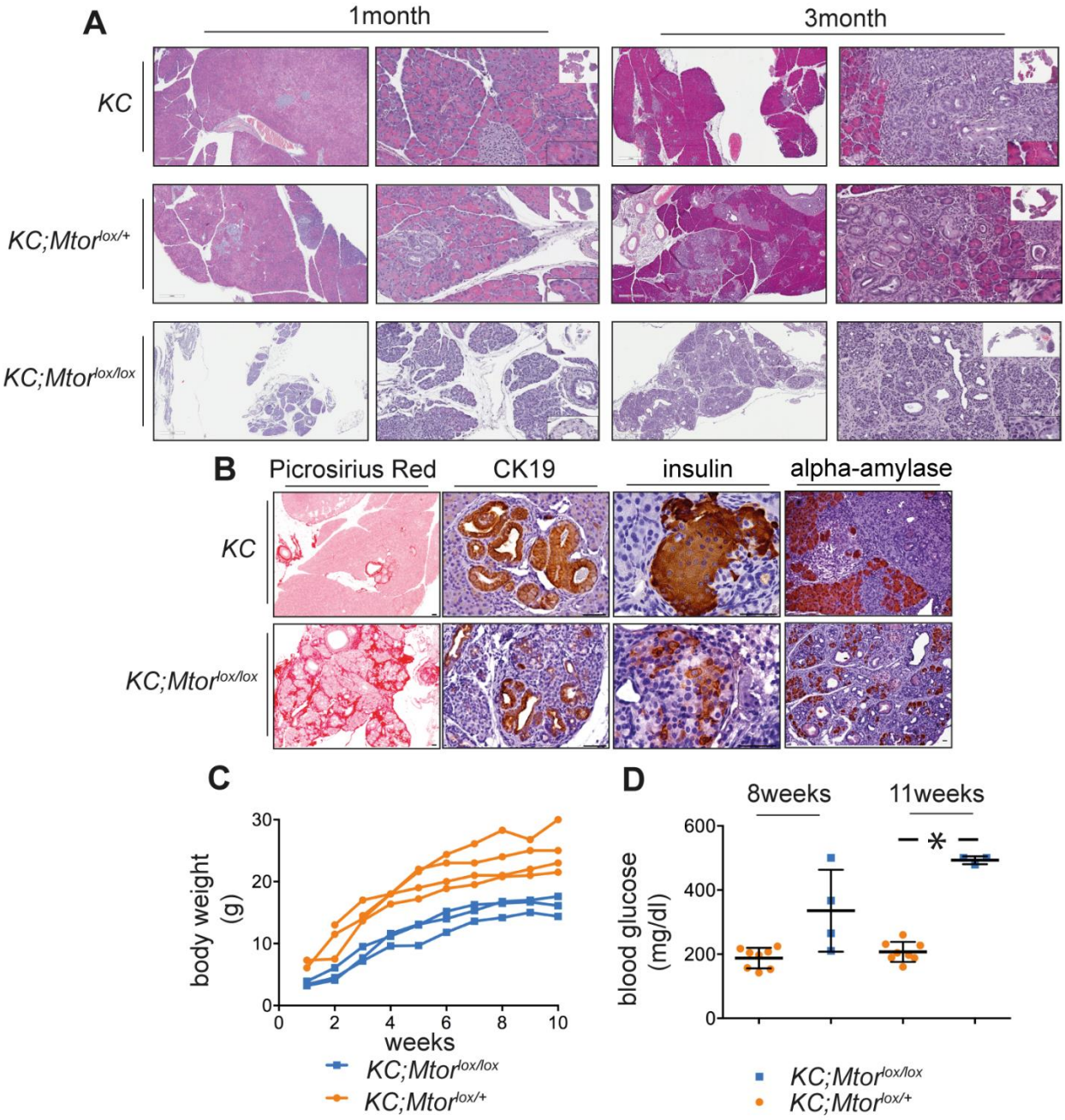

Fig. 10:13 Disturbed pancreatic architecture and homeostasis in *KC;Mtor$^{lox/lox}$* mice

A) H&E stainings of *KC, KC;Mtor$^{lox/+}$* and *KC;Mtor$^{lox/lox}$* mice at one and three months of age. Scale bare 400 µM. B) IHC of alpha-amylase, CK19 (KRT19), insulin and picrosirius red staining. Scale bare 50 µM. C) Weight gain of *KC;Mtor$^{lox/+}$* (n=4) (blue lines) and *KC;Mtor$^{lox/lox}$* mice.(n=3) (yellow lines) D) Blood glucose of *KC;Mtor$^{lox/+}$* (n=8) (blue dots) and *KC;Mtor$^{lox/lox}$* (n=3) (yellow dots) mice at eight and eleven weeks of age. * p value of an unpaired Student`s t-test < 0.05.

Staining of phospho-4E-BP1 (Thr37/46) (Fig. 10.15A) and the phospho-S6 (Ser235/236) (Fig. 10.15B) was clearly reduced in *KC;Mtor$^{lox/lox}$* mice, thus further corroborating the efficient *Mtor* deletion and its functional role in pancreatic insufficiency

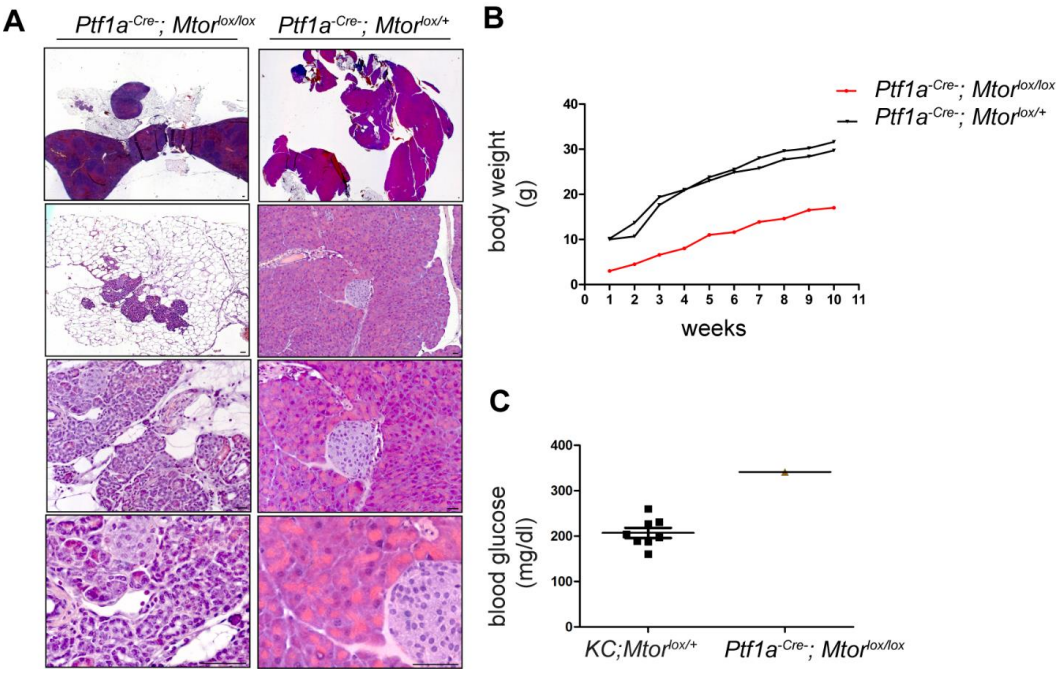

Fig. 10:14 Mtor kinase and the homeostasis of the pancreas

A) H&E staining of *Ptf1a^{Cre};Mtor$^{lox/lox}$* and *Ptf1a^{Cre};Mtor$^{lox/+}$* mice at eleven weeks of age. Scale bare 50 µM. B) Weight gain of one *Ptf1a^{Cre};Mtor$^{lox/lox}$* (black lines) and two *Ptf1a^{Cre};Mtor$^{lox/+}$* mice (red lines) C) Blood glucose of *KC;Mtor$^{lox/+}$* (n=8) (black dots) and one *Ptf1a^{Cre};Mtor$^{lox/lox}$* (n=1)(red dot) mice at eleven weeks of age.

10.2.2 Generation of an inducible model system for *Mtor* deletion

Due to the crucial role of *Mtor* in the development and homeostasis of the pancreas, generation of *Mtor*-deficient PDAC cell lines was not possible in the conventional PDAC GEMM.

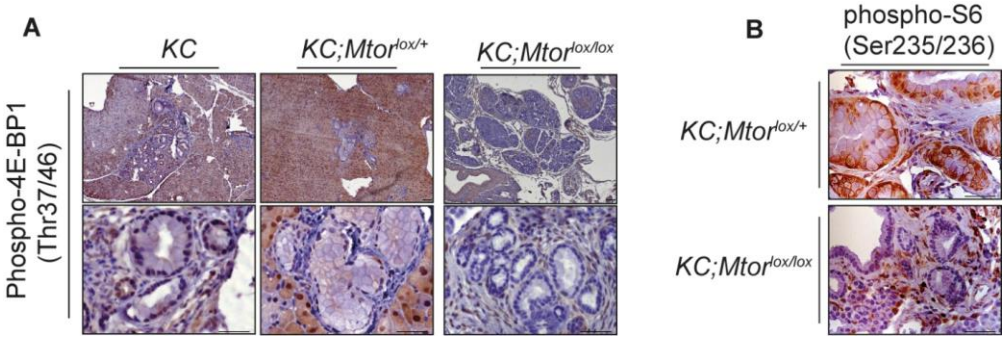

Fig. 10:15 Impaired Mtor signalling is inactivated in *KC;Mtor$^{lox/lox}$* mice

A) IHC of phospho-4E-BP1 (Thr37/46) in *KC, KC;Mtor$^{lox/+}$* and *KC;Mtor$^{lox/lox}$* mice. Scale bare 50 µM. B) IHC of phospho-S6 (Ser235/236) in *KC;Mtor$^{lox/+}$* and *KC;Mtor$^{lox/lox}$* mice. Scale bare 50 µM.

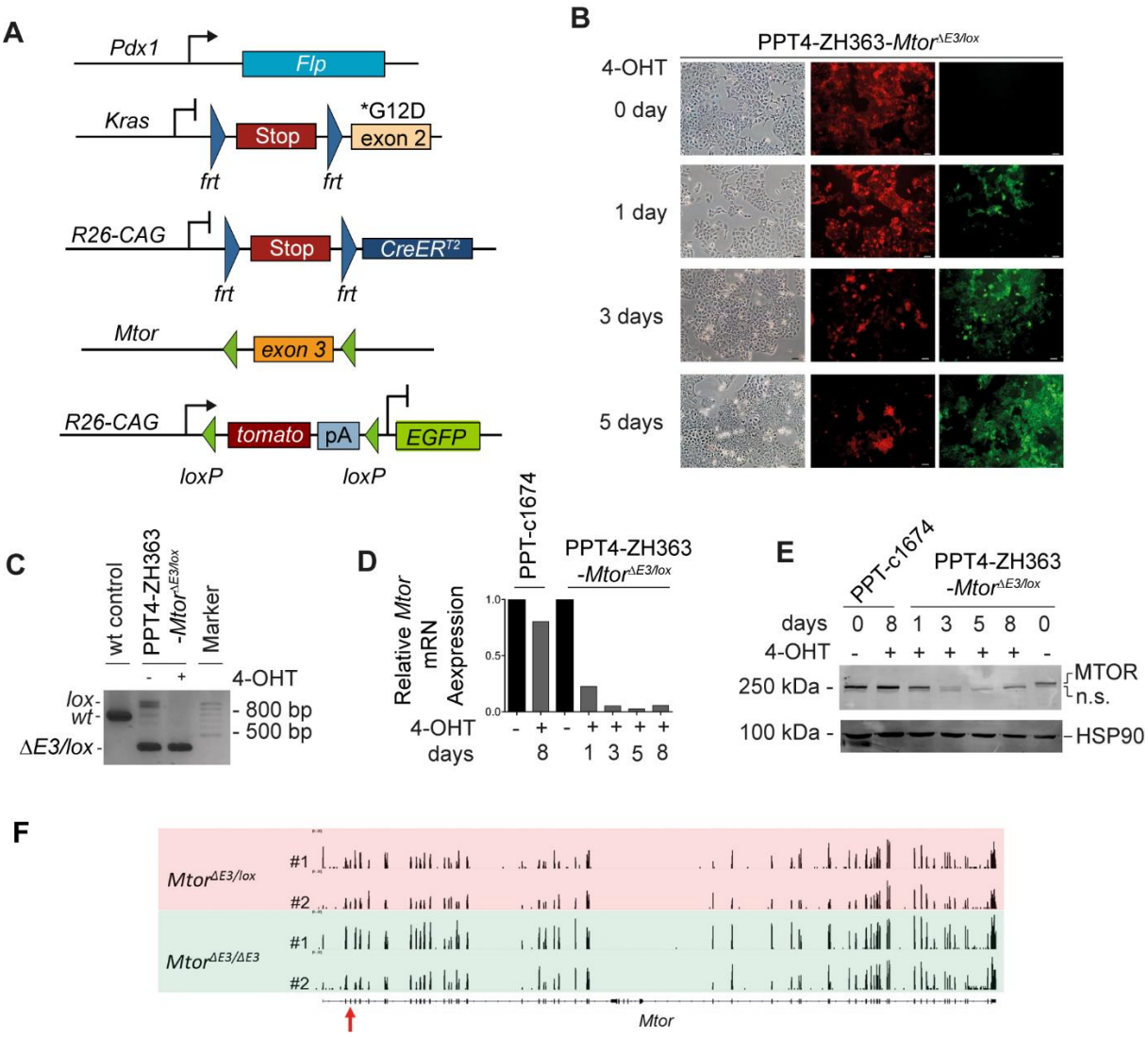

Fig. 10:16 Establishment of a genetic inducible time specific model to inactivate *Mtor*

A) Genetic strategy to delete the *Mtor* gene in *Kras*^{G12D}-driven murine PDAC cells. (B) Microscopical visualization of 4-OHT-induced recombination events with a double fluorescent floxed tdTomato-EGFP reporter line (*R26*$^{mT/mG}$). Scale bar, 10 µM. C) Genotyping PCR of the indicated PDAC cells treated with 4-OHT (600 nM, 8 days). *wt*: wild type allele; *ΔE3*: exon 3 deleted *Mtor* allele; *lox*: *Mtor* exon 3 floxed allele. D) qRT-PCR analysis of *Mtor* mRNA expression in PPT4-ZH363-*Mtor*$^{\Delta E3/lox}$ and PPT-c1674 cells after 8 days of 4-OHT treatment (n=1). Data are shown as fold change versus EtOH-treated controls. E) Immunoblot analysis of Mtor expression in PPT4-ZH363-*Mtor*$^{\Delta E3/lox}$ and PPT-c1674 cells after 8 days of 4-OHT treatment. Hsp90 served as loading control (n=2). F) RNA-Seq profiles of PPT4-ZH363-*Mtor*$^{\Delta E3/lox}$ cell line after 8 days of 4-OHT (600 nM) or vehicle treatment. The *Exon 3* of the gene is marked with an arrow. Two independent biological replicates are depicted.

To study the role of MTOR as a therapeutic target, the dual-recombinase mouse system (Schonhuber et al., 2014) was used to generate murine PDAC cell lines. This system allows the deletion of the MTOR kinase by activating Cre^{ERT2} through 4-OHT treatment (Fig. 10.16B).

To perform efficient genetic deletion and to minimize the probability of incomplete *Mtor* deletion, a murine PDAC cell line was established with already one deleted *Mtor* allele: *Pdx1-Flp;FSF-Kras*$^{G12D/+}$*,FSF-R26*$^{CAG\text{-}CreERT2}$*,Mtor*$^{\Delta E3/lox}$*,R26*$^{mT\text{-}mG}$ (abbreviated as PPT4-ZH363-*Mtor*$^{\Delta E3/lox}$ cells). The double fluorescent *floxed tdTomato-EGFP* reporter line (*R26*$^{mT/mG}$) enables monitoring of 4-OHT induced recombination by fluorescence microscopy (Fig. 10.16B). Recombination-PCR further demonstrated that *exon 3* of the *Mtor* allele was excised after 8 days of 4-OHT treatment (Fig. 10.16C). Deletion of *Mtor* was confirmed at the mRNA level by qPCR (Fig. 10.16D) and at the protein level by immunoblot (Fig. 10.16E). Consistently, RNA-Sequencing (RNA Seq) data also showed deletion of *Mtor exon 3* after 8 days of 4-OHT treatment (Fig. 10.16F).

To control for 4-OHT and Cre toxicity, a murine PDAC cell line without floxed *Mtor* alleles (*Pdx1-Flp;FSF-Kras*$^{G12D/+}$*,FSF-R26*$^{CAG\text{-}CreERT2}$), abbreviated as PPT-c1674, was used. Unlike, PPT4-ZH363-*Mtor*$^{\Delta E3/lox}$ cells, no significant reduction in MTOR kinase expression was detected after the same interval of 4-OHT treatment (Fig. 10.16D & 10.16E).

In conclusion, Hassan et al could show that generation of an inducible genetic model for *Mtor* deletion based on the dual-recombination system makes it possible to study the role of Mtor kinase as a therapeutic target (Hassan et al., 2018).

10.2.3 *Mtor* deletion inactivates downstream signaling

To find out whether the *Mtor*-downstream signaling is inactivated upon deletion of the kinase, PPT4-ZH363-*Mtor*$^{\Delta E3/lox}$ cells were treated with 4-OHT for 8 days and analyzed for phosphorylation of S6 (Ser235/236) and for phosphorylation of 4E-BP1 (Thr37/46). As expected, loss of *Mtor* impaired phosphorylation of these specific proteins (Fig. 10.17A).

Hypo-phosphorylated 4E-BP1, another marker for MTOR pathway blockage appeared in a different conformational form in 4-OHT treated ZH363-*Mtor*$^{\Delta E3/lox}$ cells, which additionally confirming *Mtor* deletion (Fig. 10.17A). Inactivation of the MTOR kinase pathway significantly impaired growth (Fig. 10.17B), while the control cell line PPT-c1647 remained unaffected by 4-OHT treatment (Fig. 10.17B). Moreover, colony formation was significantly reduced upon *Mtor* deletion in ZH363-*Mtor*$^{\Delta E3/lox}$ cells. Again, 4-OHT had no effect towards the clonogenic growth of control cells (Fig. 10.17C & Fig. 10.17D), thus demonstrating a specific *Mtor* effect.

To determine the mechanism of the impaired growth upon *Mtor* deletion, cell cycle analysis was performed by flow cytometry. 4-OHT treated PPT4-ZH363-*Mtor*$^{\Delta E3/lox}$ cells showed an

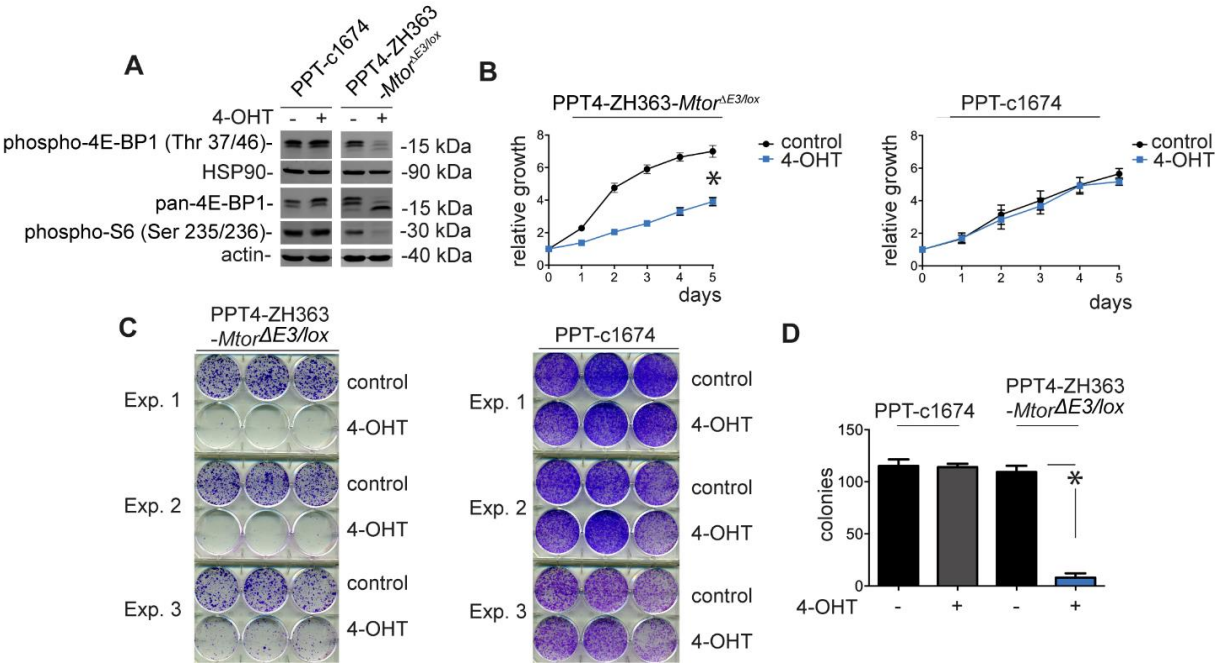

Fig. 10:17 Deletion of *Mtor* impairs cell growth in primary PDAC cells *in vitro*

A) Western blot of phospho-4E-BP1(Thr37/46), pan-4E-BP1, and phospho-S6 (Ser235/236) from vehicle or 4-OHT (600 nM) treated cells after 8 days of treatment. Same extracts were blotted to different membranes and loading was controlled by actin or HSP90 (n=3). (B) MTT assays for 8 days vehicle or 4-OHT (600 nM) treated cells. *P- value of an analysis of variance (ANOVA) test <0.05. (C) Clonogenic assays of PPT4-ZH363-*Mtor*$^{\Delta E3/lox}$ cells and the control cells treated with EtOH and 4-OHT. Three independent biological replicates are shown. D) Quantification of C). * p value of a paired Student`s t-test <0.05 is shown.

increase in the number of cells in the G1-phase of the cell cycle (Fig. 10.18A), while no overt changes in the sub-G1 fraction were observed (Fig. 10.18A), indicating that *Mtor* deletion does not induce apoptosis in PDAC cells, but rather a cytostatic response due to an G1-phase arrest. In the control cell line, cell cycle distribution was unaffected by 4-OHT treatment (Fig. 10.18B).

To compare the genetic *Mtor* inhibition with pharmacological inhibition, the dual MTORC1/TORC2 inhibitor INK-128 (Hsieh et al., 2012), that is currently tested in clinical trials, was used. Treatment of PPT4-ZH363-*Mtor*$^{\Delta E3/lox}$ cells with varying doses of INK-128 blocked phosphorylation of downstream targets such as AKT(Ser473), S6 (Ser235/236) and 4E-BP1(Thr37/46) (Fig. 10.18B).

To investigate on-target activity of INK-128, dose response curves in *Mtor*-proficient and *Mtor*-deficient cells were determined. INK-128 is more potent in *Mtor*-proficient cells (Fig. 10.18C), arguing for the on-target specificity of INK-128. Similar to the effects seen upon genetic *Mtor* deletion, G1 cell cycle arrest was also observed in INK-128 treated PPT4-

ZH363-*Mtor*$^{\Delta E3/lox}$ cells (Fig. 10.18D). Whereas the proteasomal inhibitor bortezomib increased the number of cells in the sub-G1 fraction (Fig. 10.18D), no increase was observed upon INK-128 treatment. In addition, Bortezomib and the chemotherapeutic drug Camptothecin induced cleavage of Caspase-3 and PARP (Fig. 10.18E), an effect not observed after treatment with INK-128.

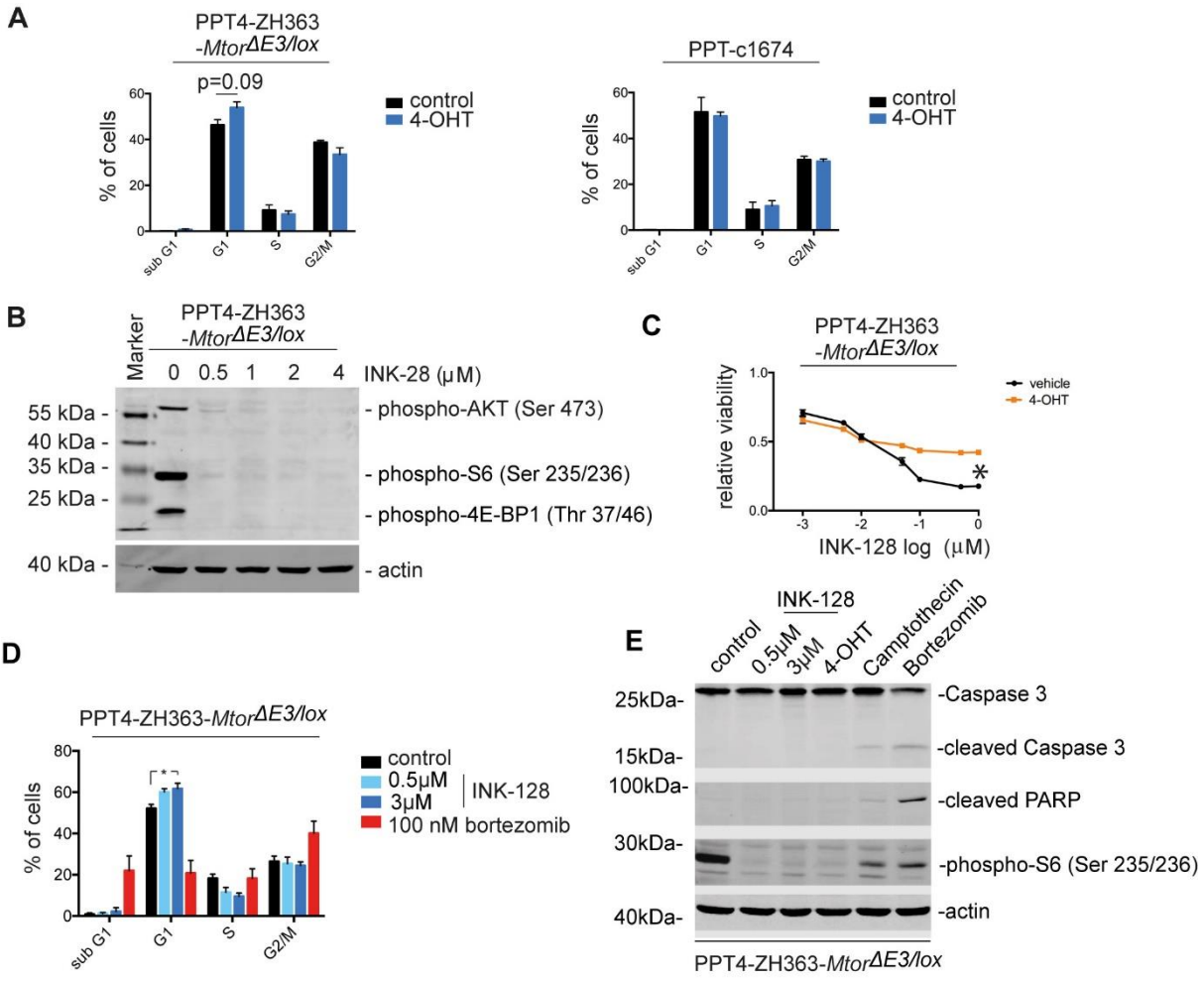

Fig. 10:18 MTOR kinase inhibition induces an G1-phase arrest

A) Cell cycle flow cytometry analysis was done with propidium iodide (PI) stained vehicle or 4-OHT (600 nM, 8 days) treated PPT4-ZH363-*Mtor*$^{\Delta E3/lox}$ and PPT-c1674 cell lines. The p value of the student t-test is indicated. B) Western blot of phospho-4E-BP1 (Thre37/46), phospho-AKT (Ser473) and phospho-S6 (Ser235/236) of PPT4-ZH363-*Mtor*$^{\Delta E3/lox}$ cells treated with vehicle or increasing doses of INK-128 for 24 hrs as indicated. Actin was used as loading control. C) MTT assay of vehicle or 4-OHT (600 nM) treated PPT4-ZH363-*Mtor*$^{\Delta E3/lox}$ cells with INK-128 treatment for 72 hrs as indicated. Viability of vehicle treated controls was arbitrarily set to 1. * p value of ANOVA < 0.05. D) Cell cycle flow cytometry analysis was done with PI stained PPT4-ZH363-*Mtor*$^{\Delta E3/lox}$ cells treated for 24 hrs with 2 different concentrations of INK-128. * p value of an ANOVA test <0.05 (n=3). E) Western blot of caspase 3, cleaved PARP, and phospho-S6 (Ser235/236) for 24hrs treated PPT4-ZH363-*Mtor*$^{\Delta E3/lox}$ cells either with vehicle, Ink-128, Camptothecin (20 μM) and Bortezomib (100 nM) or 4-OHT (600 nM) for 8 days. Actin: loading control. Same lysates were blotted to different membranes (n=3).

In conclusion, Hassan et al could show that genetic as well as pharmacologic inhibition of MTOR kinase results in a cytostatic cellular response (Hassan et al., 2018).

10.2.4 Importance of MTOR associated metabolic pathway in PDAC cells

To identify molecular pathways and processes connected to MTOR in PDAC, global RNA expression changes upon genetic deletion of *mtor* were analyzed by RNA Seq.

Obtained reads were mapped to the mouse genome and analyzed by gene set enrichment analysis (GSEA), gene ontology (GO) and KEGG pathway analysis. One of the top downregulated hallmark gene signatures in PPT4-ZH363-*Mtor*$^{\Delta E3/lox}$ cells upon 4-OHT treatment was the MTORC1 signature itself, again validating the *Mtor* deletion (Fig. 10.19A). In addition to MTOR pathway, metabolic pathways such as cholesterol biosynthesis, amino acid metabolism and glycolysis were among the top regulated signatures (Fig. 10.19A & 10.19B).

Moreover, a more in-depth analysis of the glycolytic pathway genes revealed that expression of important rate limiting glycolytic enzymes such as phosphofructokinase (*PfkI*), lactate dehydrogenase (*Ldha)* and glucose 6 phosphatase (*G6pd2*) was downregulated after *Mtor* deletion in PPT4-ZH363-*Mtor*$^{\Delta E3/lox}$ cells (Fig. 10.19C).

This connection of Mtor expression with glycolysis was additionally verified by qRT-PCR. Again, *Mtor* deletion results in a significant downregulation of glycolytic enzymes such as *Ldha*, as well as *PfkI* expression (Fig. 10.20A).

To validate the effect of *Mtor* deletion on glucose metabolism, a glucose uptake assay was performed. Glucose uptake was significantly decreased upon *Mtor* deletion in PPT4-ZH363-*Mtor*$^{\Delta E3/lox}$ cells (Fig. 10.20B), while PPT-c1674 cells showed no difference in glucose uptake which implies that the observed effect is specifically due to *Mtor* deletion (Fig. 10.20B).

To determine whether the connection of the MTOR pathway with glycolytic enzymes can also be found in human PDAC, a publicly available human PDAC mRNA expression data set was accessed (Bailey et al., 2016).

Based on cluster analysis of glycolytic enzyme expression, 12.5% of PDAC showed higher expression of the MTOR-connected glycolytic enzymes (Fig. 10.21A). This glycolytic

subgroup not only showed upregulation of glycolytic signatures but also enrichment of MTORC1, hypoxia and epithelial to mesenchymal transition signatures (Fig. 10.21B), underscoring the strong connection of the MTOR pathway to glycolysis also in the context of human PDAC. The clinical relevance of the MTOR-linked glycolytic enzymes in PDAC is further emphasized by an analysis of the TCGA PDAC data set, which showed that high expression of LDHA is connected to worse PDAC patient survival (Fig. 10.21C).

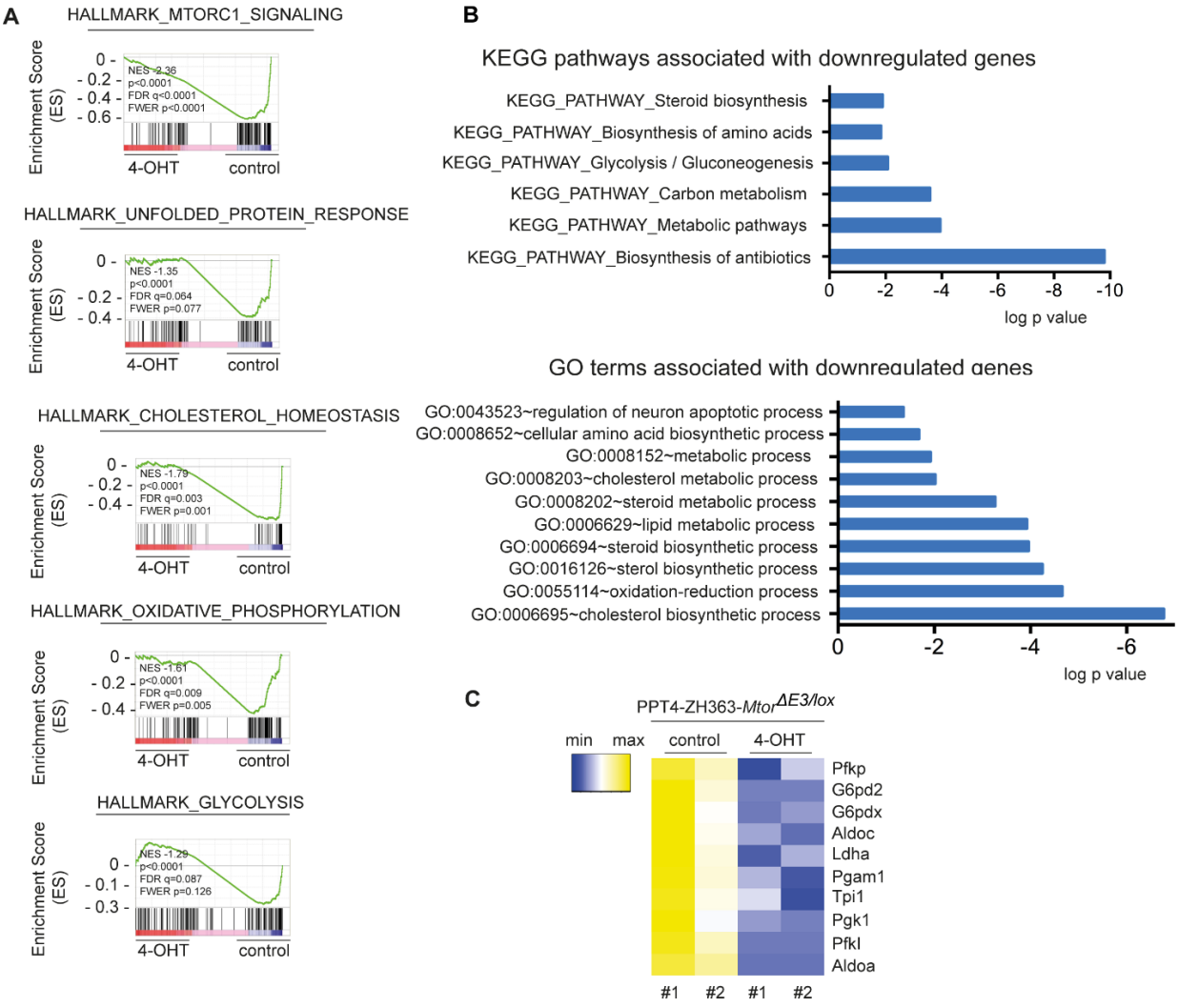

Fig. 10:19 *Mtor* controls metabolic pathways

A) RNA Seq was performed with 8 days vehicle or 4-OHT (600 nM) treated PPT4-ZH363-*Mtor*$^{\Delta E3/lox}$ and analyzed by GSEA (n=2). The normalized enrichment score (NES), nominal p value, FDR q value and FWER p values are indicated. B) GO-term and KEGG pathway analysis was performed with down-regulated genes (log2FC≤-0.58) upon *Mtor* deletion 4-OHT (600 nM, 8 days). Terms and pathways with a Benjamini corrected p-value <0.05 are depicted. C) Heat map of glycolytic enzymes expression generated from RNA Seq data of 8 days vehicle or 4-OHT (600 nM) treated PPT4-ZH363-*Mtor*$^{\Delta E3/lox}$ cells.

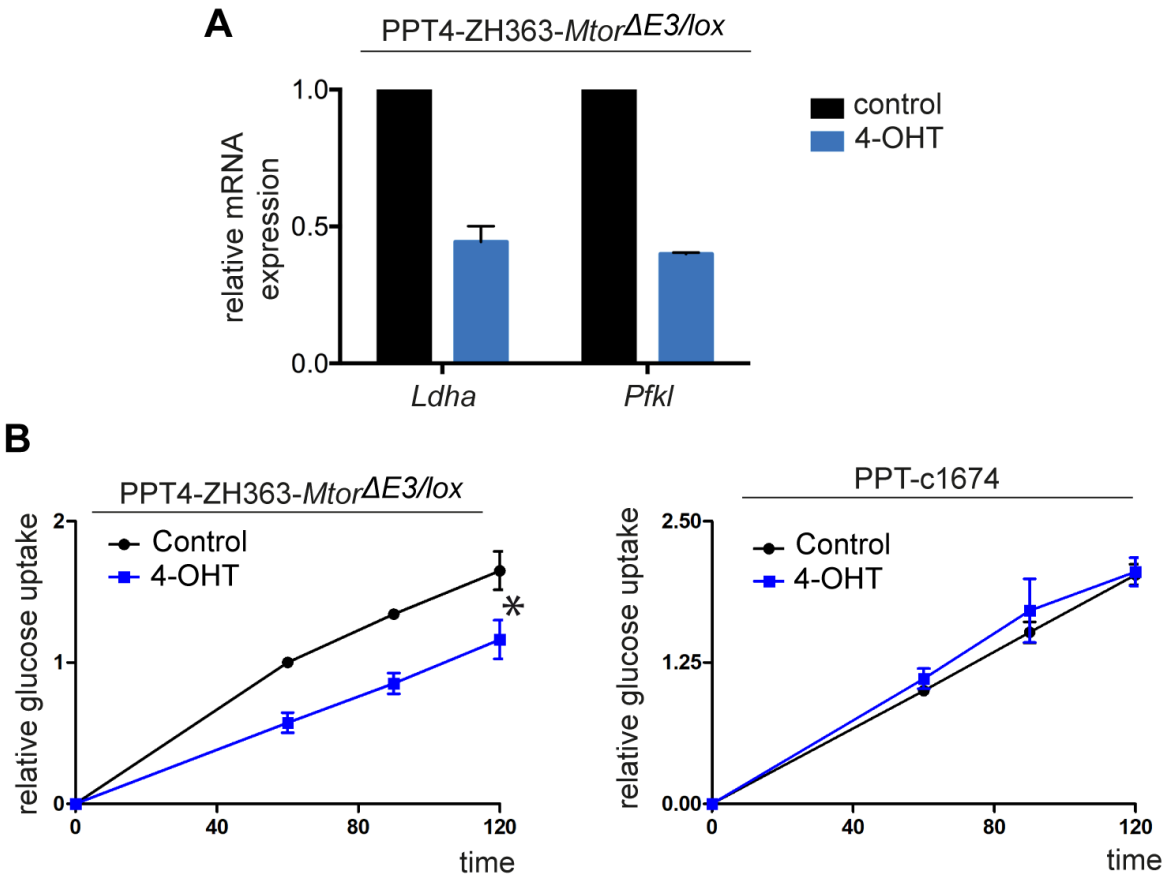

Fig. 10:20 *Mtor* controls expression of glycolytic enzymes and glucose uptake

A) mRNA expression of *Ldha* and *Pfkl* was determined by qPCR using *β-actin* mRNA expression as reference for vehicle or 4-OHT (600 nM) treated PPT4-ZH363-*Mtor*$^{\Delta E3/lox}$ or control PPT-c1674 cells over the period of 8 days (n=2). B) ZH363-*Mtor*$^{\Delta E3/lox}$ or control PPT-c1674 cell lines treated with vehicle or 4-OHT (600 nM) over 8 days before were analyzed for glucose uptake over 60, 90 and 120 min by F-18-FDG uptake assay. * p value of analysis of variance (ANOVA) test <0.05 (n=4).

10.2.5 Adaptive re-wiring of signaling pathways upon *Mtor* deletion

In order to identify adaptive rewiring processes that might compensate *Mtor* deletion and lead to a cytostatic response, the important driver pathways in PDAC such as PI3K and ERK pathways were analyzed (Fig. 10.22A).

An increased phosphorylation of AKT (Thr308 and Ser473) as well as an increased phosphorylation of ERK (Thr202/Tyr204) was observed upon *Mtor* deletion. While vehicle and 4-OHT treated PPT-c1674 control cells showed no significant difference in AKT (Thr308 and Ser473) and ERK (Thr202/Tyr204) phosphorylation (Fig. 10.22A & 10.22B). In addition,

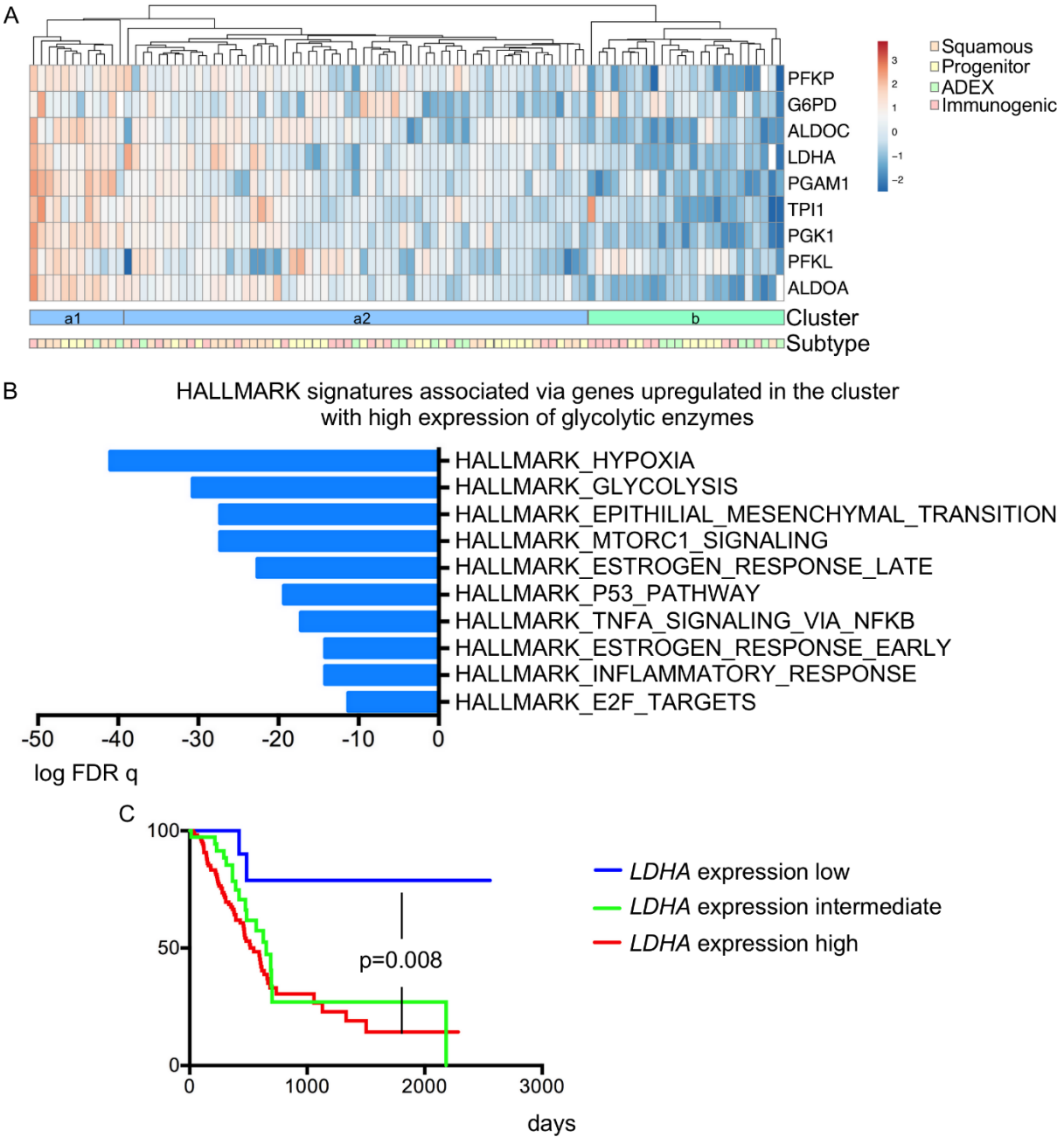

Fig. 10:21 Relevance of MTOR-connected glycolytic enzymes in human PDAC

A) Clustering of human PDAC mRNA expression data based on the expression pattern of the MTOR-connected glycolytic enzymes (n=96) (Bailey et al., 2016). Two main clusters (a & b) were obtained and cluster a was subdivided into a1 and a2. Subtypes are depicted in a color code according to the classification of Bailey and colleagues. B) Upregulated genes in the a1 cluster (a1 cluster versus rest) (log2FC≥0.58) were analyzed using the MSigDB to compute the overlap of upregulated genes with hallmark gene sets. Top ten hallmark signatures which are ranked according to FDR are depicted. C) TCGA PDAC survival data was assigned to the expression of *LDHA* (<25th percentile: low expression, >75th percentile: high expression, remaining: intermediate expression). Survival curves of PDAC with low and high *LDHA* expression were analyzed by a log-rank test and the p value is indicated.

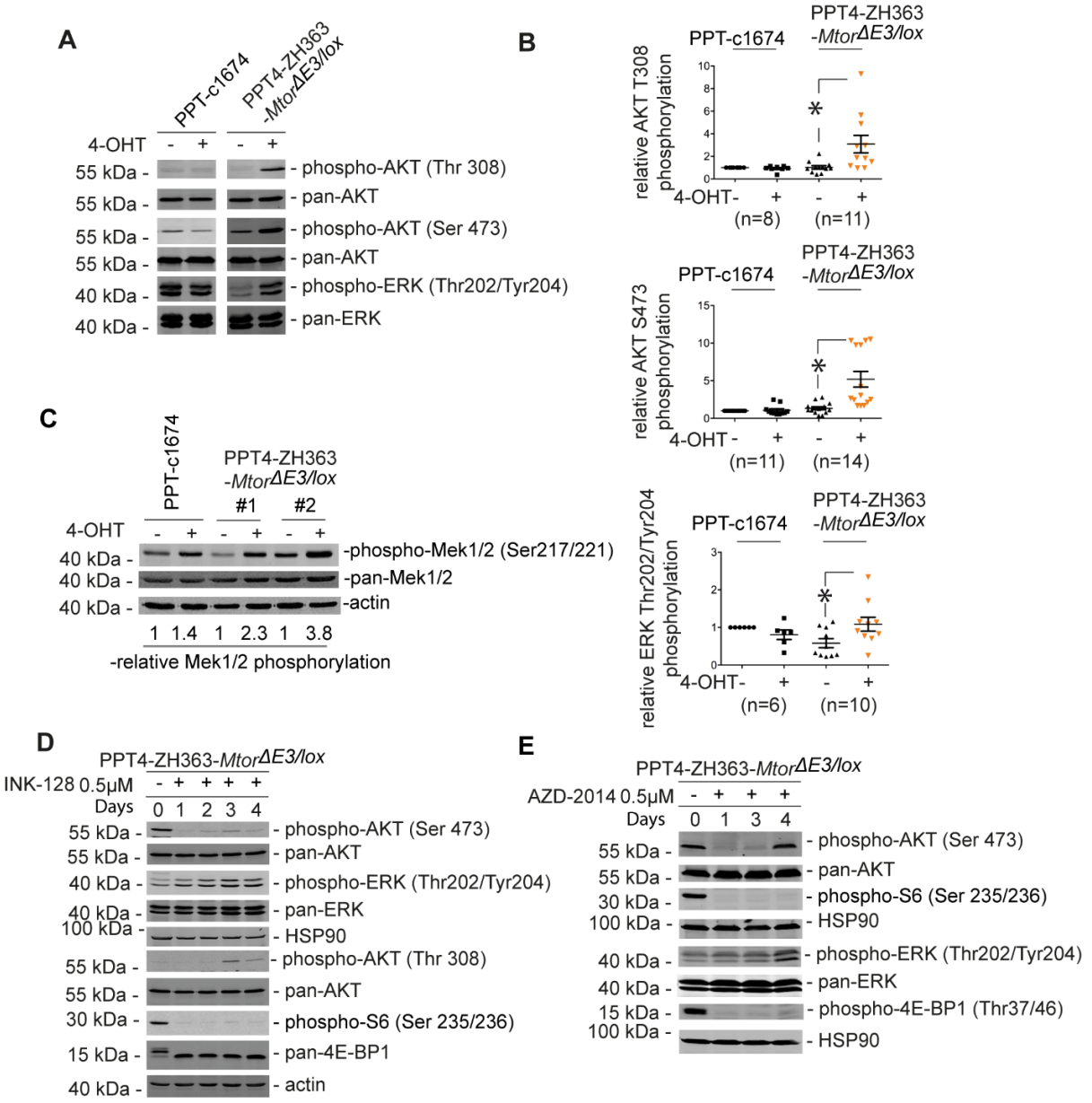

Fig. 10:22 Adaptive re-wiring upon *Mtor* deletion in murine PDAC cells

A) Western blot for phospho-AKT (Thr308 & Ser473) and phosphor-ERK (Thr202/Tyr204) of PPT4-ZH363-*Mtor*$^{\Delta E3/lox}$ cells after 8 days of vehicle and 4-OHT treatment. Equal loading was controlled by blotting pan-AKT or pan-ERK on different membranes. B) Quantification of independent replicates for (A). The ration of phosphorylated to total-protein in the vehicle-treated control PPT-c1674 cell line was arbitrarily set to 1. The number of replicates is depicted. * p-value of a paired Student`s t-test < 0.05. C) Western blot for phosphor Mek1/2 (Ser217/221) and pan-MEK1/2 for PPT4-ZH363-*Mtor*$^{\Delta E3/lox}$ cells and control PPT-c1674 cell line after 8 days of vehicle or 4-OHT treatment. Equal loading was controlled by blotting of MEK1/2 on different membranes. β-Actin was also used as loading control (n=3). The ration of phosphorylated to total-protein in the vehicle-treated control PPT-c1674 cell line was arbitrarily set to 1 and the relative MEK1/2 phosphorylation is depicted. D & E) Western blot of independent biological replicates for PPT4-ZH363-*Mtor*$^{\Delta E3/lox}$ cells after 4-days of INK-128 (0.5μM) and AZD-2014 (0.5μM) treatment were performed. Equal loading was controlled by blotting pan-AKT or pan-ERK on different membranes. HSP90 and actin were used as loading control (n=4). For D) and E) cells were treated with fresh inhibitors or vehicle control each day.

phosphorylation of MEK1/2 (Ser217/221) was also increased upon *Mtor* deletion in PPT4-ZH363-*Mtor*$^{\Delta E3/lox}$ cells (Fig. 10.22C).

To recapitulate the results obtained in the genetic model at the pharmacological level, the TOR inhibitor INK-128 was used. Cells were treated for a period of 4 days with a low dosage of INK-128 (0.5µM). MTOR inhibition was verified by analyzing downstream targets such as 4E-BP1 and S6 (Ser235/236) by immunoblot (Fig. 10.22D). Consistent with previously published data (Driscoll et al., 2016), phosphorylation of S6 (Ser235/236) and AKT (Thr308 & Ser473) was decreased after 24hrs (Fig. 10.22D). However, after three to four days, slightly increased AKT phosphorylation (Thr308 and Ser473) was observed in comparison to the 24hrs time point (Fig. 10.22D). Interestingly, the increase in phosphorylated ERK (Thr202/Tyr204) occurred much quicker and earlier, compared to the upregulation in phosphorylation in AKT (Thr308 & Ser473) level over the time course of INK-128 treatment (Fig. 10.22D).

To further validate these findings, another dual MTORi (AZD-2014) was used (Conway et al., 2018; Pike et al., 2013). Consistent with the results obtained with INK-128, after 24 hrs of AZD-2014 (0.5µM) treatment, phosphorylation of S6(Ser235/236), 4E-BP1(Thr37/46), and AKT (Ser473) was decreased (Fig. 10.22E). Phosphorylation of AKT (Ser473) and ERK (Thr202/Tyr204) was again increased after three to four days of treatment (Fig. 10.22E). Over the whole-time course of treatment, Mtor signaling was blocked as shown by the downregulation of phospho-4E-BP1(Thr37/46) and phospho-S6(Ser235/236) expression (Fig. 10.22E), demonstrating potent Mtor kinase inhibition in PPT4-ZH363-*Mtor*$^{\Delta E3/lox}$ cells by AZD-2014 inhibitor.

To identify the critical molecular processes that might be responsible for the observed adaptive rewiring, combinatorial treatment was performed by using various inhibitors of PI3K (GDC-0941), AKT (MK-2206) and MEK (PD-325901) in addition to INK-128 in vehicle and 4-OHT treated PPT4-ZH363-*Mtor*$^{\Delta E3/lox}$ cells. However, there was neither influence of the MEK inhibitor towards phosphorylation of AKT (Ser473) in *Mtor*-proficient nor in *Mtor*-deleted cells, although ERK (Thr202/Tyr204) phosphorylation was completely absent (Fig. 10.23A).

Similarly, no influence on ERK (Thr202/Tyr204) phosphorylation by different PI3K and AKT inhibitors was observed regardless of the MTOR status of the cells. Although downstream targets of PI3K such as phosphorylation of AKT (Ser473) and S6 (Ser235/236) were still blocked to different extents (Fig. 10.23A). Therefore, it can be concluded that the adaptive signaling rewiring upon *Mtor* deletion occurs upstream of MEK and AKT pathway.

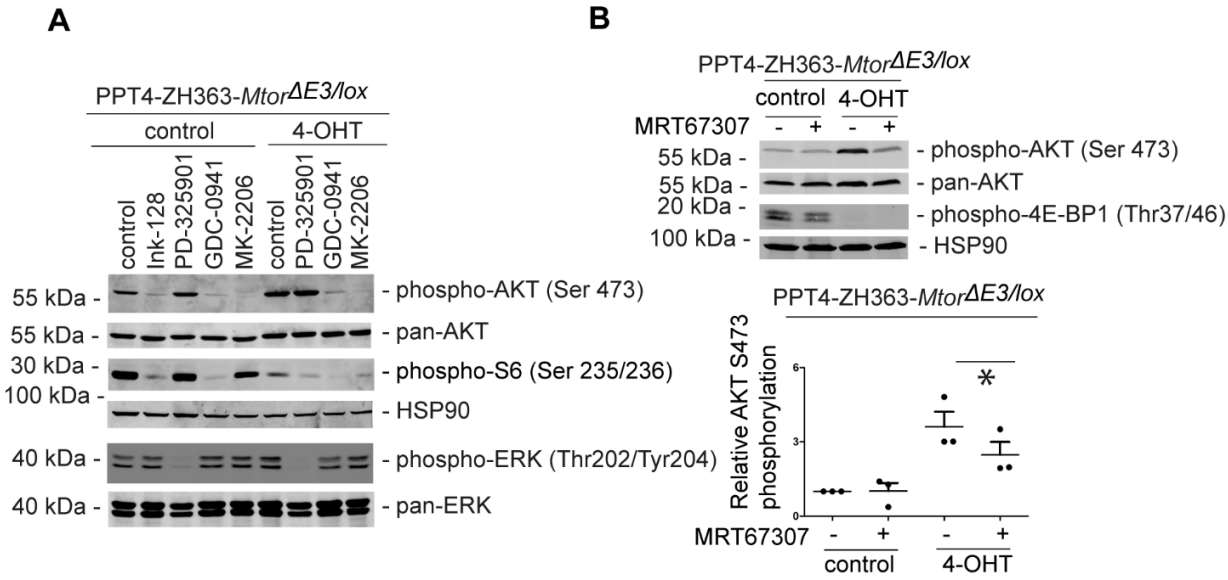

Fig. 10:23 MRT67307 blocks AKT phosphorylation upon *Mtor* deletion

A) Western blot of phospho-AKT (Ser473) and pan-AKT, phospho-S6 (Ser235/Ser236), phospho-ERK (Thr202/Tyr204) and pan-ERK. PPT4-ZH363-*Mtor*$^{\Delta E3/lox}$ cells were treated over 8 days with vehicle control or 4-OHT, followed by 6 hrs treatment with INK-128 (2 µM), PD-325901 (2 µM), GDC-0941 (4 µM), or MK-2206 (4 µM) (n=2). B) Western blot of phospho-AKT (Ser473), pan-AKT and phospho-4EB-P1 (Thr37/46) in Vehicle-control and 4-OHT (8 days) treated PPT4-ZH363-*Mtor*$^{\Delta E3/lox}$ cells for 24 hrs with MRT67307 (4µM). HSP90 expression was used as loading control. Quantification of B). The ratio of the phosphorylated to the total protein in untreated control cells was arbitrarily set to one. * p-value of a paired Student`s t-test < 0.05 (n=3).

It has been previously described that the non-canonical IκB-related kinase IKBKE phosphorylates AKT (Ser473) upon dual MTOR inhibition in PDAC (Rajurkar et al., 2017) and in other cancers (Leonardi et al., 2019). To test the contribution of IKBKE kinase to this adaptive rewiring mechanism in 4-OHT treated PPT4-ZH363-*Mtor*$^{\Delta E3/lox}$ cells, IKBKE specific inhibitor MRT67307 was used (Zhu et al., 2014). Interestingly, MRT67307 inhibitor was able to partially block the rewiring by downregulation of phospho-AKT (Ser473) in 4-OHT treated PPT4-ZH363-*Mtor*$^{\Delta E3/lox}$ cells (Fig. 10.23B), while in vehicle treated PPT4-ZH363-*Mtor*$^{\Delta E3/lox}$ cells, the level of phospho-AKT (Ser473) was unchanged (Fig. 10.23B). Therefore, this data hints to a possible role of IKBKE in the regulation of adaptive rewiring upon MTOR inhibition.

In conclusion, Hassan et al could show that the genetic deletion of *Mtor* as well as pharmacological inhibition of MTOR leads to an upregulation of AKT and ERK signaling (Hassan et al., 2018). The IKBKE pathway might be one of the candidates that play a role in the adaptive rewiring mechanism upon *Mtor* deletion.

10.2.6 Generation of MTOR-Kinase independent clones

To study MTOR kinase adaptive rewiring mechanism in more detail, PPT4-ZH363-*Mtor*$^{\Delta E3/lox}$ cells were treated with 4-OHT for 8 days and single cells were seeded in 96-well plates to generate monoclonal cell populations. Out of 150 clones generated from the PPT4-ZH363-*Mtor*$^{\Delta E3/lox}$ cell line, 36 clones were randomly chosen and analyzed for activity of the PI3K/MTOR signaling pathway (Fig. 10.24).

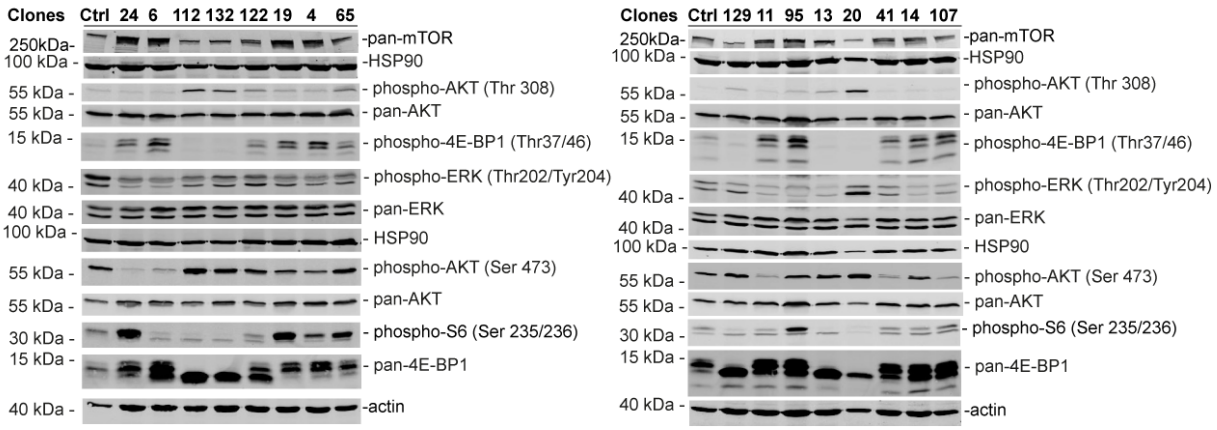

Fig. 10:24 Generation of Mtor-deficient clones

Western blot of pan-mTOR, phospho-AKT (Thr308 & Ser473), pan-AKT, phospho-S6 (Ser235/Ser236), pan-4E-BP1, phospho-4-E-BP1 (Thre37/46), phospho-ERK (Thr202/Tyr204) and pan-ERK from clones which were selected after 4.OHT treatment of PPT4-ZH363-*Mtor*$^{\Delta E3/lox}$ cells. HSP90 and β-actin were used as loading control. Same lysates were blotted to different membranes.

By this approach, it was possible to generate five Mtor-deficient clones (approximately 14% of the analyzed clones), while the other clones had functional MTOR signaling pathway (Fig. 10.24).

The Mtor-deficient clones showed robust downregulation of phospho-S6 (Ser235/Ser236) and phospho-4E-BP1 (Thr37/46), while phospho-ERK (Thr202/Tyr204) and phospho-AKT (Thr308 and Ser473) were upregulated (Fig. 10.24).

In conclusion, although *Mtor* deletion impedes cell proliferation, PDAC cells can escape from Mtor dependency and grow in an Mtor-deficient manner, possibly by adaptive rewiring of ERK and AKT signaling pathways.

10.2.7 Development of dual MTOR inhibitor-based combination therapies

To design MTOR inhibitor-based combination therapies, inhibitors of PI3K (GDC-0941), AKT (MK-2206) and MEK (PD-325901) were tested in conjunction with the MTOR-inhibitor (INK-128) in a panel (n=10) of human PDAC cell lines (Fig. 10.25A & Fig. 10.26B) as well as in four of murine cell lines including PPT4-ZH363-*Mtor*$^{\Delta E3/lox}$ (Fig. 10.25B & Fig. 10.26B).

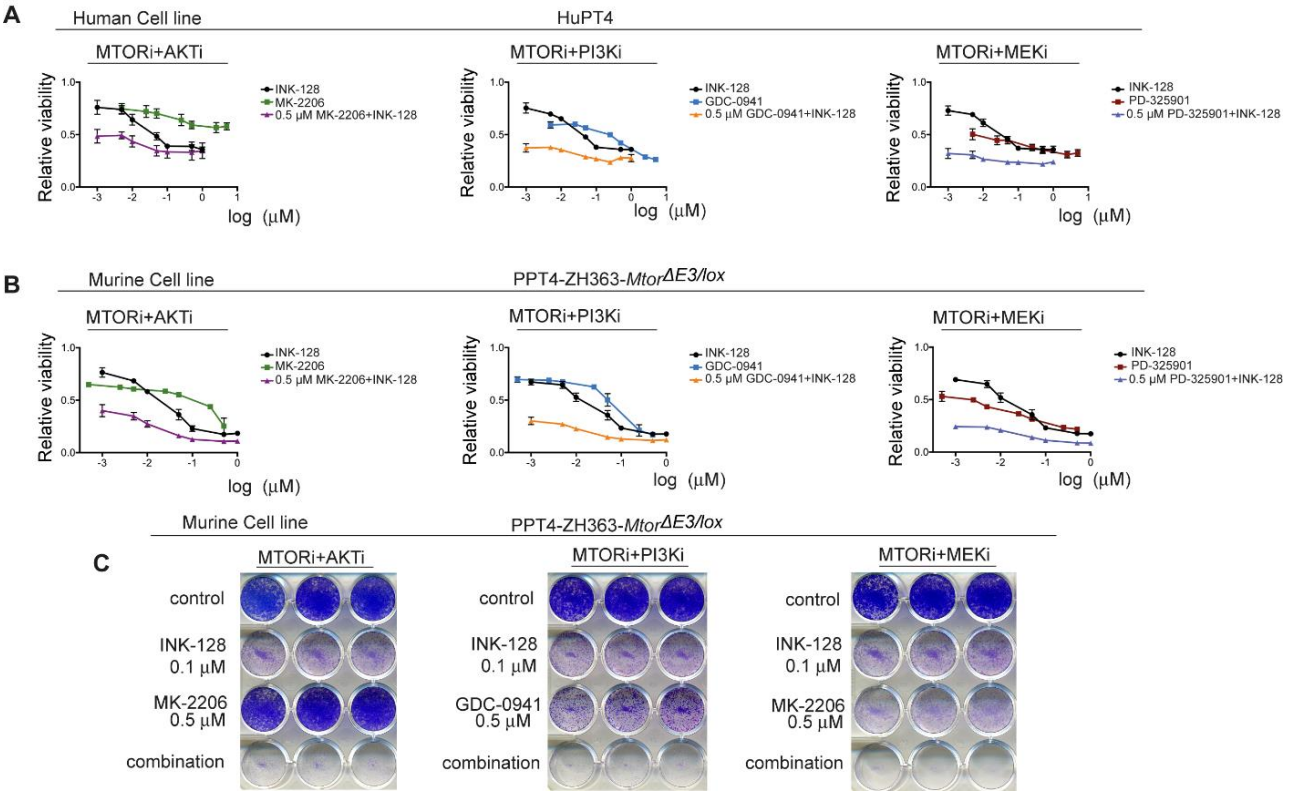

Fig. 10:25 Dual MTOR inhibitor-INK-128 in combination therapies

A) Cell viability was measured in human cell lines (PSN1 cells is shown) by MTT after 72 hrs of treatment with INK-128, MK-2206, GDC-0941, PD-325901 alone or in combination as indicated. Viability of vehicle-treated control cells was arbitrarily set to 1 (n=3). B) Cell viability of murine cells such as (PPT4-ZH363-*Mtor*$^{\Delta E3/lox}$ cell line is shown) was measured by MTT after 72 hrs of treatment with INK-128, MK-2206, GDC-0941, PD-325901 alone or in combination as indicated. Viability of vehicle-treated control cells was arbitrarily set to 1 (n=3). C) PPT4-ZH363-*Mtor*$^{\Delta E3/lox}$ cells were seeded and treated with INK-128, MK-2206, GDC-0941, and PD-325901 alone or in combination. One week later, the formed colonies in 12 well plates were stained with Giemsa solution. One representative experiment out of three independent biological replicates is shown (n=3).

The dose response of INK-128 alone as well as in the combination with the above-mentioned inhibitors was measured. All human and murine cells lines showed sensitivity to the dual MTORi INK-128 over a wide dose range, although to different extents. Moreover, the efficacy of INK-128 was increased by the combination therapy with the different inhibitors (Fig.

10.25B & Fig. 10.26B). These results were further validated by long-term clonogenic growth assays, which also demonstrated that the efficiency of INK-128 was increased by the different combinations (Fig. 10.25C).

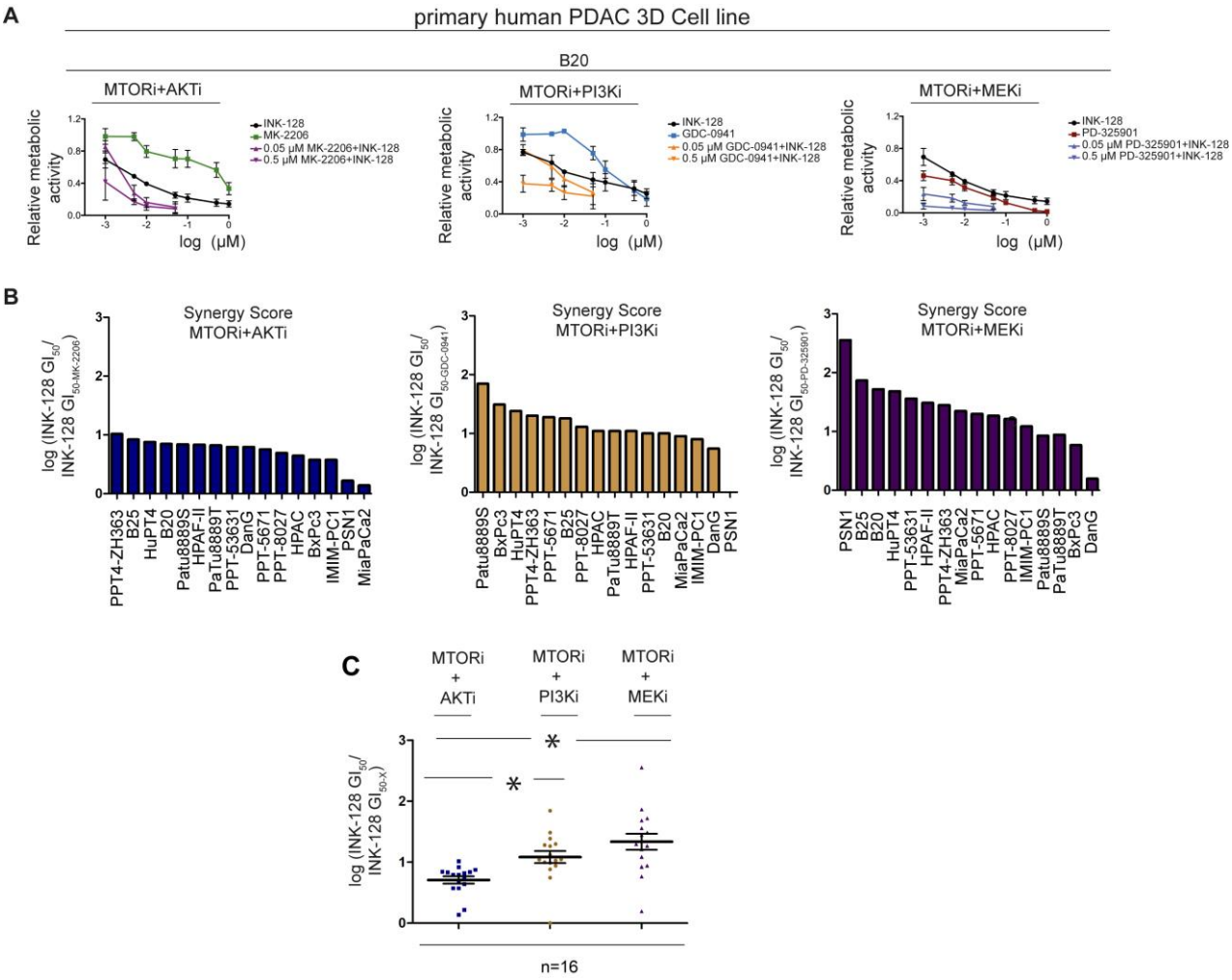

Fig. 10:26 Correlation of synergy scores in PDAC cell lines

A) Primary human PDAC 3D cultures (B20 is shown) were treated with INK-128, MK-2206, GDC-0941, PD-325901 or in combinations with the respective inhibitors as indicated. After five days of treatment, viability was measured by Cell Titer-Glo assay to determine the dose response. Metabolic activity of untreated cells was arbitrarily set to 1. B) Synergy score was calculated in 10 human, 4 murine PDAC cell lines as well as in 2 primary human PDAC 3D cultures for the combination treatment of the mTORi (INK-128) with the AKTi (MK-2206), PI3Ki (GDC-0941) and MEKi (PD-325901). C) Comparison of the synergy scores of above PDAC cell lines mentioned in B). * p of ANOVA test <0.05.

To test whether the observed combinatorial benefits also hold true in a more clinically relevant setting, a primary human PDAC 3D organoid culture model system was employed, which mimics important aspects of the *in vivo* disease situation and serves as a useful technology to investigate therapeutic approaches (Baker et al., 2016).

Consistently, isolated human primary PDAC 3D cell lines B20 and B25 showed sensitivity to INK-128 inhibitor to a similar extent as 2D human and mouse cell lines. Additionally, the sensitivity was significantly increased by combined treatment with AKT, PI3K, or MEK inhibitors (Fig. 10.26A & Fig. 10.26B). To quantify the results obtained from these combinations across species and models, the synergy scores for all tested cell lines and combinations were calculated (Fig. 10.26B). As distinct heterogeneity in the synergy score was observed (Fig. 10.26C). The synergy score for the combinations of MTOR with the MEKi was highest (mean score 1.34) (Fig. 10.26C), followed by the combination of the MTORi with the PI3Ki (mean score 1.09) (Fig. 10.26C). The combination of the MTORi with the AKTi (mean score 0.71) showed the lowest mean synergy score (Fig. 10.26C).

11 Discussion

11.1Role of NFκB2 in PDAC

Due to involvement of NFκB pathway in the variety of pathways such as proliferation, apoptosis, metabolism, metastasis, inflammation and therapy resistance, NFκB is a cancer relevant pathway (Colombo et al., 2018; Pires et al., 2018; Riedlinger et al., 2018; Xia et al., 2014; Yu et al., 2018). With respect to pancreatic cancer, both canonical and non-canonical NFκB pathway are constitutively active (Chandler et al., 2004; Nishina et al., 2009; Wharry et al., 2009; Xia et al., 2014) and linked with poor PDAC survival (Weichert et al., 2007). For example, constitutive activation of NIK which is an important mediator of non-canonical NFκB pathway has been observed in human PDAC cells, that leads to processing and nuclear localization of p52/RelB (Wharry et al., 2009). Furthermore, high activity of RelB marked PDAC patients with poor survival (Hamidi et al., 2012).

Consistent with survival data, genetic evidences in mouse models demonstrated that the NFκB pathway is important for *Kras*^{G12D}-driven transformation of pancreatic cells and drives initiation and progression of PDAC, as well as metastasis formation (Pramanik et al., 2018). For example, *NEMO/IKKγ* deletion in *Kras*^{G12D}-driven PDAC mouse model blocked the propagation of PanIN lesions, by depleting cytokines expression, such as TNFα, IL1α and IL1β as well as by downregulating the MAPK kinase and NOTCH signaling pathway (Maier et al., 2013). Moreover, crosstalk of IKKβ with NOTCH signaling is known to promote PDAC progression (Maniati et al., 2011). However, the role of *Nfκb2 (p100/p52)* in *Kras*^{G12D}-driven PDAC in genetic mouse model is unclear so far.

In order to elucidate the role of *Nfκb2 (p100/p52)* in PDAC genetically, an *Nfκb2*-deficient mouse line was studied (Paxian et al., 1999; Paxian et al., 2002). It has been observed that *Nfκb2*-deficient mice are fertile and developed into adulthood without any obvious macroscopic phenotypic abnormalities. While, it has already been also described that whole-body *Nfκb2*-null mice showed abnormalities in the development of lymphoid organs and B cells (Caamaño et al., 1998). Homozygous deletion of *Nfκb2* in KC mouse model (*Pdx1-Cre,LSL-Kras*$^{G12D/+}$*,Nfκb2*$^{-/-}$ and *Ptf1a*$^{Cre/+}$*,LSL-Kras*$^{G12D/+}$*,Nfκb2*$^{-/-}$), impairs PanIN formation and progression, irrespective of the pancreas-specific Cre recombinase. While mice with heterozygous deleted *Nfκb2* (*Pdx1-Cre,LSL-Kras*$^{G12D/+}$*,Nfκb2*$^{+/-}$ and *Ptf1a*$^{Cre/+}$*,LSL-*

Kras$^{G12D/+}$,*Nfκb2*$^{+/-}$) had a comparable survival time as KC control mice. This is consistent with published work, which shows that inhibition of the non-canonical NFκB pathway in the *Kras*^{G12D} lineage through inactivation of RelB significantly impaired PanIN progression (Hamidi et al., 2012). These observations are further strengthen by recently published work that identifies *Nfκb2* amplifications to be relevant in *Kras*$^{G12D/+}$-driven murine PDAC tumorigenesis (Mueller et al., 2018), supporting the pro-oncogenic function of NFκB2 in PDAC.

Taken together, the present work clearly demonstrates at the genetic level that *Nfκb2* is needed for *Kras*^{G12D}-driven carcinogenesis in the murine pancreas. However, the exact role of each NFκB family member is highly context dependent and both tumor promoting as well as tumor suppressive functions of individual members have been described. For example, inhibition of the NFκB family member *RelA* enhanced PanIN progression and tumor development by inhibiting OIS via the CXCL1/CXCR2 axis (Lesina et al., 2016). This effect is further supported by a study where *RelA* deleted MEFs were able to bypass senescence by increased genomic instability and defective DNA repair mechanisms (Wang et al., 2009). In contrast, by the presence of further genetic mutations such as *p53 or Ink4a* deletion, this tumor suppressor function of *RelA* is switched into an oncogenic mode that promote tumor progression by enhancing proliferation (Lesina et al., 2016; Serrano et al., 1997).

The association of non-canonical NFκB signaling with proliferation and cell cycle in the context of pancreatic cancer has already been shown (Bang et al., 2013; Doppler et al., 2013; Schneider et al., 2006). TRAF3, TRAF2 and cIAP1/2 complex plays a decisive role for NIK activity, as proteasomal degradation of TRAF2 and binding of TRAF3 results into stabilization of NIK molecule in PDAC. This stabilization leads to enhance activation of non-canonical NFκB pathway which induce cell proliferation and anchorage-independent growth (Doppler et al., 2013; Nishina et al., 2009). In line with this, *in vivo* data in the present work demonstrates that NFκB2 signaling is important for the proliferative capacity of *Kras*^{G12D}-driven tumor initiation. The reduced number of Ki67-positive cells in *Nfκb2* deleted ADM and PanIN lesions suggest a decrease in cell proliferation. This proliferative advantage might be the outcome of activation of the glycogen synthase kinase 3α (GSK-3α) pathway. GSK-3α promotes TGFβ activated kinase 1 (TAK1) stabilization and TAK1 binding partners (TAB) interaction and subsequently, TAK/TAB complex formation facilitates processing of p100 and activation of p52. This process takes place independently of glycogen synthase kinase 3β

(GSK-3β) activation (Bang et al., 2013). However, this upstream target interaction needs attention in further studies.

Furthermore, this proliferative defect might at least in part be due to cell cycle regulation, as mRNA level for *Ccnd1a* and other cell cycle regulators were downregulated in *Nfκb2* deleted tissue. This is in line with a growing number of evidence, which shows that *Nfκb2* can function as a regulator of cell proliferation and survival by enhancing the expression of various cyclins including cyclin D1 and cyclin D2 (Ijichi, 2011; Rocha et al., 2003; Taniguchi and Karin, 2018). The exact pathway has to be explored in future studies. Another known connection of *Nfκb2* with the cell cycle is through *Skp2* regulation, and has been described already by our group before (Schneider et al., 2006). However no significant changes were observed in the expression level of *Skp2* between *Nfκb2*-proficient versus *Nfκb2*-deficient cells in the RNA-sequencing or at the translational level. This leads to the conclusion that *Nfκb2* deletion somehow bypassed Skp2 interaction and this discrepancy needs further clarification.

Interestingly, a significant reduction in RelB expression is also observed in *Nfκb2* deleted pancreas tissue and cell lines as compared to *Nfκb2*-proficient models, indicating that RelB might be unstable in the absence of *Nfκb2* and no longer available for its function. This fits with the observation that both subunits, p100 as well as p52 mediate RelB stabilization and play an important role in non-canonical NFκB signaling (Fusco et al., 2008). Experiments conducted using floxed *RelB* in pancreatic carcinogenesis showed a cell-intrinsic function of RelB for cell survival upon stress through the transcriptional regulation of IER3 expression (Hamidi et al., 2012). It might therefore be possible that the observed proliferative and cell cycle defects became much more pronounced in the *Nfκb2* deleted models due to the decreased RelB expression.

In PDAC, the interaction of epithelial cells with the microenvironment such as B cells (Pylayeva-Gupta et al., 2016) and CAFs (Sun et al., 2018) is important for tumor initiation as well as progression (Zhang et al., 2018). NFκB is described to be one of the important regulators in the stromal compartment that can influence tumor growth (Pramanik et al., 2018) by regulating proliferation and cell cycle (Bang et al., 2013; Doppler et al., 2013; Nishina et al., 2009). Therefore, the possible contribution of the non-epithelial compartment to the observed phenotype cannot be excluded in the current study, since a complete *Nfκb2* knock-out was analyzed. Therefore, to elaborate the molecular function of NFκB2 in the

pancreatic epithelial compartment more precisely, these findings need to be validated by the use of conditional *Nfκb2* mouse line (De Silva et al., 2016) or advanced pancreatic cancer mouse models (Schonhuber et al., 2014).

NFκB signalling is involved in a crosstalk with numerous signalling pathways, which adds further layers to its complex regulation. One of the most prominent cross-talks of NFκB is with p53 signalling pathway (Schneider and Kramer, 2011). Tumor protein p53 (Trp 53, commonly known as p53) is a transcription factor, initially identified as an oncogene (DeLeo et al., 1979) and later on classified as a tumor suppressor (Finlay et al., 1989). It has an N-terminal transactivation domain and C-terminal DNA binding domain flanked by some intrinsically disordered regions (Freed-Pastor and Prives, 2012). Cellular stresses such as DNA damage (Kastan et al., 1991) or oncogene expression, such as upregulation of Mdm2 expression by NFκB activation, in particular by enhanced RelA expression (Tergaonkar et al., 2002), result in post-translational modification of p53, stabilization and activation (Toufektchan and Toledo, 2018). This activated form of wild-type *p53* (*p53*^{wt}) is responsible for controlling a plethora of signaling pathways including cell cycle, senescence, apoptosis and DNA damage. This mechanism controls G1 cell cycle arrest by regulating binding of p21 to Cyclin E/CDK2 and Cyclin D/CDK4 complexes (el-Deiry et al., 1993; Harper et al., 1993) and G2/M checkpoint arrest by association with Mir34a (Martin-Caballero et al., 2001; Tarasov et al., 2007). It can also control genomic stability (Toufektchan and Toledo, 2018) by regulating DNA damage response by Gadd45a upregulation (Zhan, 2005) and by phosphorylating ATM, ATR or by stabilization of CHK1 and CHK2 molecules (Bieging et al., 2014). In certain cell types under mild stress conditions, activated p53 can modulate senescence through continuous expression of NFκB2 (Iannetti et al., 2014) or regulation of p21 and phospho-Rb (Chien et al., 2011). Under chronic stress conditions, stabilized p53-mediated apoptosis is a way for elimination of harmful cells by regulation of pro-apoptotic proteins such as PUMA, NOXA or anti-apoptotic proteins such as BCL2 and MCL1 (Chen, 2016). Moreover, it also has some “non-canonical” functions such as modulation of cellular plasticity, autophagy and metabolism. Due to these diverse anti-carcinogenic properties, it is the first line of defense against accumulation of mutations and commonly known as “the guardian of the genome” (Engeland, 2018; Kastenhuber and Lowe, 2017; Lane, 1992).

Consistently with published data, higher expression of *p53* was noted by GSEA analysis in *Nfκb2*-deficient mouse model potentially explaining the impairment in cell cycle and reduced proliferation. Moreover, in human TCGA data analyzed in this study, the same trend is

observed, where patients having lower expression of *NFκB2* showed longer survival with normal expression of *TP53* status. More than half of the human cancers have genetic or structural aberrations in p53 protein, although mutational burden varies between different tumor types (Kastenhuber and Lowe, 2017). In human PDAC; *TP53* is mutated approximately in 75% of cases and unlike other tumor suppressor genes, it is generally mutated by missense mutations (also known as hot spot mutations) (Vijayakumaran et al., 2015). Common missense mutations occurring in DNA binding domains are $p53^{R172H}$ (Mus musculus) / $TP53^{R175H}$ (Homo sapiens) (Hingorani et al., 2005; Polireddy et al., 2019) or $p53^{R270H}$ (Mus musculus) / $TP53^{R273H}$ (Homo sapiens) (Schofield et al., 2018). Consequently, these mutations result in a loss of tumor suppressive capabilities and a gain of some novel oncogenic properties (Kim and Lozano, 2018; Perri et al., 2016). Several molecular mechanisms have been suggested for these gain-of-functions (GOF) properties such as cellular transformation by HSP70 stabilization (Polireddy et al., 2019) or increased expression of NFκB targets genes (Schneider and Kramer, 2011). This GOF property of $p53^{mut}$ can lead to an altered chemotherapeutic response in cancer, especially in PDAC (Fiorini et al., 2015) and promote PDAC initiation, development and invasion (Schofield et al., 2018). Based on the above-mentioned observations, *Nfκb2*-deficient GEMMs were crossed with $p53^{R172H}$ mice. However, *Nfκb2* was dispensable for PanINs and PDAC formation in heterozygous as well as homozygous $p53^{R172H}$ mutated $Kras^{G12D/+}$-driven PDAC mouse models. Moreover, *Nfκb2*-deficient PDAC cells showed the same growth as *Nfκb2*-proficient cells. Inactivation of *p53* thus allows for escape from the *Nfκb2* dependency in pancreatic carcinogenesis, which further confirms the context dependency of the NFκB2 pathway. In breast cancer, Snail has been shown to be important for tumor initiation and progression in a *p53* wild type, but not in a *p53* mutant context (Ni et al., 2016). Even in PDAC, the escape from signaling dependency upon *p53* inactivation has been observed before for various signaling factors and pathways such as ZEB1 (Krebs et al., 2017), EGFR signaling (Ardito et al., 2012; Navas et al., 2012) and RelA signaling. RelA, for example, impairs tumor growth by upregulation of OIC formation. However, when the senescence failsafe is disabled by inactivation of *p53*, RelA switches to a tumor-promoting function (Lesina et al., 2016). This shows that NFκB is a double-edged sword and that both the timing of its induction as well as the genetic background determined its context specific functions (Nakshatri, 2019).

Interestingly, analysis of a TCGA data set of human PDAC patients showed a modest survival benefit for patients with low *NFκB2* expression, when the status of *TP53* is not taken into account. However, when stratified according to *TP53* status, patients with low *NFκB2*

expression show a significant survival benefit in presence of WT *TP53*, while negligible with mutant *TP53*. One possible reason of the dispensable effect described here might be differences in the activation and interaction of cofactors with *Nfκb* and *p53* in a stimulus-dependent or cell-type specific manner (Becker et al., 2014; Hayden and Ghosh, 2012). The complex cross talk and competitive relation between *Nfκb* and *p53* for binding to a limited pool of cofactors such as CBP (CREB-binding protein) or p300 (Dhar et al., 2010) to decide between apoptotic or survival programs is well documented and might partially explain the strongly different phenotypes in the mouse models depending on the *p53* background. Which cofactors are involved in the interaction between *Nfκb2* and *p53* and under which conditions this occurs must be further clarified in future, in order to understand their exact regulation.

Collectively, this work provides the first genetic evidence for the functional involvement of NFκB2 signaling in PDAC initiation and PDAC cell proliferation. However, it also highlights the context and mutational function of *Nfκb2*. Considering this, more work is needed to characterize the molecular role of NFκB2 signaling in PDAC development and cell proliferation. In the future, a conditional *Nfκb2* knockout will provide us the opportunity to study tumor cell-autonomous signaling, in order to rule out stromal effects.

11.2Role of MTOR in PDAC

The important role of MTOR in the regulation of tissue homeostasis is well known, as MTOR integrates signals to mediate cell growth and cell cycle. In addition, embryonic MTOR signaling is known to regulate organogenesis, epithelial to mesenchymal differentiation as well as tissue differentiation (Hwang et al., 2008). Moreover, *Mtor* deletion results in severe developmental defects that cause embryonic lethality in mouse models (Murakami et al., 2004). The data shown in this thesis strongly support these findings, proposing an essential role of MTOR in the development of the exocrine and endocrine compartment of the pancreas by limiting the production of essential pancreatic digestive enzymes leading to reduced growth. The exocrine insufficiency was rescued to some extent by the provision of pancrex-vet, a special food containing pancreatic enzymes like lipase, which lead to a significant weight gain of the mice. Also in the *KC;Mtor*$^{lox/lox}$ mice, pre-mature death within eight weeks after birth due to endocrine and exocrine pancreatic insufficiency was observed. Heterozygous *Mtor* deleted mice developed normally with no signs of abnormal growth (Hassan et al., 2018). The connection of MTOR with pathways related to pancreatic development has already been shown in a mouse model, where deletion of *Mtor* in

progenitor cells caused an atrophic pancreas that led to hyperglycemia (Elghazi et al., 2017). However, in the classical *Cre/lox*-based mouse model models, activation or deletion of genes occurs at the same time due to the single Cre-recombination step, which makes it quite challenging to genetically validate the role of genes such as *Mtor* that have a critical function during organogenesis in established PDAC.

Genomic analyses of PDAC revealed complex mutational patterns and various subtypes that are believed to be important reason for therapeutic resistance and the heterogeneous drug responses (Bailey et al., 2016; Orth et al., 2019; Waddell et al., 2015). Like other targeted therapies in PDAC, inhibiting PI3K-signaling in the clinic has not been successful so far. Combined inhibition of MEK/ERK and PI3K/AKT pathways performed worse than standard chemotherapy in a group of unstratified PDAC patients (Chung et al., 2017a). This highlights the urgent need to develop stratification concepts and novel therapeutic combination strategies.

To investigate the potential role of MTOR as a therapeutic target in PDAC, a dual-recombinase mouse system combining the established *Cre/lox* with the *Flp/frt* recombination system was used (Schonhuber et al., 2014). That model allows to delete *Mtor* genetically in a time dependent manner by addition of 4-OHT that leads to impaired cell growth and colony formation. Genetic as well as pharmacological inhibition of the MTOR pathway blocked the progression of cells from G_1 to S phase of the cell cycle and resulted in G_1 phase arrest (Hassan et al., 2018). In line with these findings, MTOR is known to be a central regulator of cell growth and proliferation (Kim and Guan, 2019) by regulating G_1/S cell cycle transition in cancer (Gao et al., 2004). Interestingly, no markers of apoptosis were detected by flow cytometry or western blot, indicating that *Mtor* deletion results in cytostatic state instead of cell death. This cytostatic effect after MTOR deletion/inhibition may explain why PI3K/MTOR inhibitors are able to block tumor formation, but rarely cause tumor regression (Eser et al., 2013).

In normal conditions, even in the presence of enough oxygen, aerobic glycolysis is the main source of energy for PDAC cells, which is known as Warburg effect. In pancreatic tumor cells, activation of oncogenic KRAS leads to enhanced DNA and RNA biosynthesis by using glycolysis and the oxidative phosphorylation machinery as energy source through increased expression of glycolytic enzymes such as hexokinase 1 and 2 (HK1/2), phosphofructokinase (PFK) and lactate dehydrogenase (LDH) (Cameron et al., 2018; Ying et al., 2012). Interestingly, in agreement with the data described above, RNA sequencing in this study

revealed that *Mtor* deletion impaired metabolic pathways by downregulating glycolysis, oxidative phosphorylation and cholesterol metabolism. In line with that observation, an MTOR-linked aggressive subgroup of human PDAC also showed higher expression of glycolytic enzymes. Moreover, downregulation of glycolytic enzymes such as *Ldha* and *Pfk1* was observed after *Mtor* deletion (Hassan et al., 2018). LDH play an important role in the metabolic switch as shown in breast cancer cells, which ultimately makes tumor cells resistant to chemotherapy (Manerba et al., 2018). Moreover, high mRNA expression of LDH is found to be linked with poor survival in a TCGA PDAC extracted data set (https://genome-cancer.ucsc.edu), highlighting the clinical relevance. Altogether, these data suggest that MTOR is linked with glucose metabolism by regulating many important metabolic enzymes.

Moreover, PDAC cells use alternative pathways such as oxidative phosphorylation, glutamine metabolism and gluconeogenesis as energy sources. This biosynthetic machinery is also associated and tightly regulated by MTOR signaling (Son et al., 2013; Tee, 2018). Furthermore, PDAC cells also utilize available glucose by shuttling it to pentose phosphate pathway for nucleotide biogenesis (Ying et al., 2012), so one possibility for impaired growth of *Mtor* deleted cells is reduced availability of nucleotides due to impaired glucose metabolism. Therefore, an important point for future studies that should be addressed in more detail is whether and how metabolic pathways are important in promoting PDAC growth and how this relates to MTOR expression. Metabolomic and proteomic analysis will be helpful in the future.

Treatment with the first generation MTOR inhibitor (MTORi) Rapamycin, which is known to regulate S6 function, reduced pancreatic tumor growth in the KC mouse model, while no survival difference was observed in KPC mice (Eser et al., 2013; Morran et al., 2014). In another preclinical study, MTOR inhibition by Rapamycin showed a slight survival advantage in xenografts which showed mutation in PI3K/MTOR pathway (Garrido-Laguna et al., 2010). In most of the cases, the tumors relapsed and continued to grow after MTOR inhibition by first generation drugs. This limited effectiveness has been attributed to the extensive crosstalk of the MTOR pathway with other pathways, such as AKT (Pópulo et al., 2012) and ERK (Rozengurt et al., 2014), which attenuates therapeutic efficacy (Iriana et al., 2016). Second generation MTORi, which target both MTORC1 and MTORC2 complexes, not only suppressed growth and survival in human PDAC cells (Lou et al., 2014), but also showed mild survival benefits in PDAC GEMMs (Driscoll et al., 2016) by blocking the negative feedback activation of AKT that has limited the clinical efficacy of first generation MTORi in PDAC (Sun, 2013). This demonstrates the clinical potential of MTORC1/MTORC2 dual

inhibitors. However, considering the high cost for clinical trials as well as the extensive crosstalk associated with the MTOR pathway, a greater understanding of the molecular mechanisms responsible for the regulation of MTORC1 and MTORC2 as well as the feedback mechanisms that lead to adaptive resistance in pancreatic cancer is needed. One of the main challenges in the MTOR field is to identify the critical feedback loops that are induced as cellular escape mechanisms after treatment and how to cope with them. It has been previously described that PI3K/MTOR inhibition results in a compensatory MEK/ERK pathway activation (Soares et al., 2015). Moreover, the use of the dual MTORC1/2 inhibitor Torin-1 resulted in increased of phospho-AKT (Ser473) as a secondary resistance mechanism in PDAC (Rajurkar et al., 2017). In contrast, reduced tumor growth due to blockage of phospho-AKT (Ser473) signaling was observed in MTORi (ADZ2014) treated mice as compared to vehicle treated mice (Driscoll et al., 2016). Such discrepant results might be due to different drug dosage ranges, variations in threshold values for different techniques, as well as different time point analysis used in *in vivo* and *in vitro* studies.

Acute *Mtor* deletion in 4-OHT treated $Mtor^{\Delta E3/lox}$ PDAC cells showed a striking growth-inhibitory response. In agreement with the published data, however, a small fraction of *Mtor* deleted cells was able to give rise to colonies through feedback activation of AKT (Thr308 and Ser473) as well as marked enhancement in the MEK/ERK pathway in comparison to control clones. The same trend was observed after acute genetic deletion of *Mtor* in these cells as in a large panel of murine and human PDAC cell lines after pharmacological inhibition of MTOR in a time and concentration dependent manner (Hassan et al., 2018). In the future, detailed analysis of the *Mtor*-deficient clones should be performed by different techniques such as whole-exome sequencing, transcriptomics and phospho-proteomics. This might help in understanding the compensatory signaling pathways that ensure the persistent activation of AKT and ERK pathway and enable PDAC cells to survive and proliferate even in the absence of MTOR.

Pathway rewiring via RTK upon targeted therapies has been shown, for example for resistance to the BRAF inhibitor vemurafenib in melanoma (Wilson et al., 2012) or acquired MEK inhibitor resistance in KRAS-mutant lung and pancreatic cancers (Lu et al., 2019). Activation of RTKs has also been observed as adaptive response upon inhibition of MTOR. For example, various RTKs such as EGFR, VEGFR2 and IGFR1 are activated by treatment with dual TORC1/TORC2 inhibitors in endothelial cells (Zeng et al., 2019; Zhuang et al., 2013). Reactivation of EGFR after MTORi (AZD8055) has also been demonstrated in PDAC cells (Wei et al., 2015). Besides RTK activation, members of the NFκB family such as IKKβ

(Reid et al., 2016) or non-canonical IκB-related kinase (IKBKE or IKKϵ), a downstream effector of tumor necrosis factor (TNF), have been described as regulators of the AKT, independent of the PI3K/MTOR pathway in PDAC (Rajurkar et al., 2017) and in breast cancer (Guo et al., 2011). Treatment with the IKBKE inhibitor MRT67307 (Clark et al., 2011) in this study, could partially block the rewired increased phospho-AKT (Ser437) upon *Mtor* deletion (Hassan et al., 2018), thus pointing to a possible role of IKKϵ in the adaptive rewiring of signaling networks in the case of genetic ablation of *Mtor*.

To address the adaptive rewiring upon MTOR inhibition, inhibitors targeting the upregulated pathways such as MEKi (PD-325901), the PI3Ki (GDC-0941) or the AKTi (MK-2206) were tested in *Mtor* deleted cells as well as in multiple human and murine cell lines in combination with dual TORC1/TORC2 inhibitor treatment in both 2D or 3D culture conditions. Both MEKi and the PI3Ki showed synergistic effect in the combined treatment with INK-128. However, in comparison, the combination treatment of INK-128 and the MEKi (PD-325901) showed the highest mean synergy score (Hassan et al., 2018). These results are supported by an important study, which demonstrates that pancreatic cancer cells undergo BIM/MCL1 associated apoptosis after combined treatment with MTORi (PF5212384) and a MEKi (PD235901) (Burmi et al., 2019). Furthermore, findings from preclinical and clinical studies in many other tumor entities such as angiosarcoma diseases (Chadwick et al., 2018) and neurofibromatosis type 2 (NF-2) mutated tumors also underscore the effectiveness of MTOR/MEK combination therapies (Li et al., 2019). Interestingly, some cell lines showed an around 350-fold increased sensitivity in the combined treatment compared to individual MTORi or MEKi treatment, while others showed little to no synergism, thus underscoring the great heterogeneity in PDAC and the need to identify the traits that render the cells sensitive and accordingly develop suitable stratification strategies.

The combined inhibition of MTOR and the PI3K pathway also showed a synergistic response in this study (Hassan et al., 2018), which is consistent with recently published findings that the combination treatment of AZD2014 (MTORC1/MTORC2) with AZD8186 (PI3Ki) showed meaningful response in a mouse model of PDAC (Driscoll et al., 2016). Additionally, studies in lung cancer also showed significant synergism between PI3K and MTOR inhibitors (Shukuya et al., 2019). The possible explanation for this synergistic effect might be inhibition of PI3K-linked AKT activation upon MTOR deletion (Shukuya et al., 2019).

Combination treatments of MTORi with AKTi were the least effective of the tested combinations, although slight synergistic effects were still observed (Hassan et al., 2018).

This contrasts with studies in cholangiocarcinoma that showed quite good synergistic effects after combined treatment of MTORi (Rad001) and AKTi (MK-2206) (Ewald et al., 2013). These discrepant results might be explained, however, by the different time points analyzed or differences between the tumor entities. Moreover, detailed future studies are needed both *in vitro* and *in vivo* that combine broad range RTK inhibitors with MTORi to interfere with the likely upstream processes that activate the MEK/ERK and PI3K/AKT signaling pathways upon MTOR inhibition. However, the toxicity associated with combinatorial treatment regimens, which is still one of the major concerns in the clinic (Kordes et al., 2013), has to be taken into consideration. How the toxic effects of such combination treatments can be controlled by, for example, alternative dosing and scheduling regimens needs to be addressed in future studies in order to make combinatorial treatments safe for the clinic.

The comparison of synergy scores across different species and different models for combination treatments of MEKi, PI3Ki or AKTi with MTORi points to a noticeable heterogeneity of the cellular response between different cell lines, models as well as for individual inhibitors. AKT phosphorylation in *Mtor*-deleted cells was sensitive to PI3Ki. In a similar manner, ERK phosphorylation was sensitive to MEKi. However, inhibiting one pathway had no effect on the signaling of the other pathway in that study (Hassan et al., 2018). This might partly explain the heterogenous response of the above-mentioned inhibitors upon a complete block of MTOR pathway. Perhaps most importantly from a clinical viewpoint, the heterogeneous sensitivity of the different cell lines to the tested inhibitors strongly points out the need to stratify PDAC into different therapeutically relevant subgroups to improve cancer treatment. The therapeutic relevance of stratification is nicely demonstrated by a study in *Kras* mutant GEMMs, which showed that therapy-resistant PDAC tumors were enriched for *Kras* amplification after combined treatment with MAPK and ERK inhibitors, while those from non-small cell lung carcinoma driven by identical oncogenic mutant *KRAS* showed no such changes in *KRAS* allele frequency (Chung et al., 2017b). This shows that selective pressure leads to heterogenous outcomes depending on the tissue of origin and the underlying genetic and epigenetic diversity (Chung et al., 2017b). Treatment of advanced disease with either a MEK (GDC-0973) or PI3K inhibitor (GDC-0941) alone showed modest tumor growth inhibition and did not significantly enhance overall survival. However, combination of the two agents resulted in a significant survival advantage as compared with control tumor-bearing mice but failed to show any dramatic response compared to standard regimen (Junttila et al., 2015). This is consistent with another PDAC study done in $Kras^{G12D}$,$p53^{-/-}$ tumors, where combination treatment of MEKi (PD0325901 with

GSK1120212) or PI3Ki (BEZ235 and GDC0941) fared better than single agent treatment but overall only showed limited efficacy (Ischenko et al., 2015). In line with these findings, a combination therapy of MEKi (AZD-6244) and PI3Ki (BKM-120 or GDC-0941) delayed tumor growth and extended survival in a *Kras*^{G12D}-driven PDAC mouse model, but did not provide durable responses (Alagesan et al., 2015). Furthermore, another study in a *Kras*-driven TSC1-haploinsufficient PDAC mouse model that is strongly dependent on MTOR activity, showed that only dual inhibition of MEK and PI3K was able to reduce MTOR activity and result in increased apoptosis (Kong et al., 2016). In agreement with the data published in PDAC, the importance of patient stratification when designing combinatorial treatments is also evident in other tumor entities such as colorectal cancer, where the efficacy of the combined inhibition of the MEK and MTOR pathways depends on the mutational status of TP53 (Garcia-Garcia et al., 2015), or PTEN (Milella et al., 2017). The lack of proper stratification therefore might also partly explain, why combinatorial treatments with MEK/ERKi (Selumetinib) and PI3Ki (MK2206) performed worse than standard chemotherapy in a recent PDAC clinical trial (Chung et al., 2017a).

Considering this, more work is needed to characterize PDAC heterogeneity, especially as it relates to the complex feedback activation and signaling network engaged by targeted inhibition of MTOR. Innovative approaches such as combining single-cell immunohistochemical and phospho-proteomic analysis in conjunction with bioinformatics to monitor signaling rewiring and adaptive resistance upon MTOR inhibition (Wei et al., 2016) might provide an invaluable tool to predict personalized therapies, stratify patients and help in the search for novel combination therapies with more specific phenotype-based targets. In addition, future work might consider triple therapies for MTOR that might better interfere with the adaptive rewiring and therapy resistance as has been shown for the combined inhibition of MEK/ERK/HDAC in PDAC (Ischenko et al., 2015) or MEK/PI3K/BCL2 (Clarke et al., 2019) in colorectal cancer cells.

12 References

Adamska, A., Domenichini, A., and Falasca, M. (2017). Pancreatic Ductal Adenocarcinoma: Current and Evolving Therapies. International Journal of Molecular Sciences *18*, 1338.

Afgan, E., Baker, D., van den Beek, M., Blankenberg, D., Bouvier, D., Cech, M., Chilton, J., Clements, D., Coraor, N., Eberhard, C.*, et al.* (2016). The Galaxy platform for accessible, reproducible and collaborative biomedical analyses: 2016 update. Nucleic acids research *44*, W3-w10.

Alagesan, B., Contino, G., Guimaraes, A. R., Corcoran, R. B., Deshpande, V., Wojtkiewicz, G. R., Hezel, A. F., Wong, K.-K., Loda, M., Weissleder, R.*, et al.* (2015). Combined MEK and PI3K inhibition in a mouse model of pancreatic cancer. Clinical cancer research : an official journal of the American Association for Cancer Research *21*, 396-404.

Alessi, D. R., Deak, M., Casamayor, A., Caudwell, F. B., Morrice, N., Norman, D. G., Gaffney, P., Reese, C. B., MacDougall, C. N., Harbison, D.*, et al.* (1997). 3-Phosphoinositide-dependent protein kinase-1 (PDK1): structural and functional homology with the Drosophila DSTPK61 kinase. Current biology : CB *7*, 776-789.

Anders, S., Pyl, P. T., and Huber, W. (2015). HTSeq—a Python framework to work with high-throughput sequencing data. Bioinformatics *31*, 166-169.

Annunziata, C. M., Davis, R. E., Demchenko, Y., Bellamy, W., Gabrea, A., Zhan, F., Lenz, G., Hanamura, I., Wright, G., Xiao, W.*, et al.* (2007). Frequent engagement of the classical and alternative NF-kappaB pathways by diverse genetic abnormalities in multiple myeloma. Cancer cell *12*, 115-130.

Annunziata, C. M., Stavnes, H. T., Kleinberg, L., Berner, A., Hernandez, L. F., Birrer, M. J., Steinberg, S. M., Davidson, B., and Kohn, E. C. (2010). Nuclear factor kappaB transcription factors are coexpressed and convey a poor outcome in ovarian cancer. Cancer *116*, 3276-3284.

Ardito, C. M., Gruner, B. M., Takeuchi, K. K., Lubeseder-Martellato, C., Teichmann, N., Mazur, P. K., Delgiorno, K. E., Carpenter, E. S., Halbrook, C. J., Hall, J. C.*, et al.* (2012). EGF receptor is required for KRAS-induced pancreatic tumorigenesis. Cancer Cell *22*, 304-317.

Awasthi, N., Monahan, S., Stefaniak, A., Schwarz, M. A., and Schwarz, R. E. (2018). Inhibition of the MEK/ERK pathway augments nab-paclitaxel-based chemotherapy effects in preclinical models of pancreatic cancer. Oncotarget *9*, 5274-5286.

Babicki, S., Arndt, D., Marcu, A., Liang, Y., Grant, J. R., Maciejewski, A., and Wishart, D. S. (2016). Heatmapper: web-enabled heat mapping for all. Nucleic acids research *44*, W147-153.

Babiker, H. M., Karass, M., Recio-Boiles, A., Chandana, S. R., McBride, A., and Mahadevan, D. (2019). Everolimus for the treatment of advanced pancreatic ductal adenocarcinoma (PDAC). Expert Opinion on Investigational Drugs *28*, 583-592.

Bailey, P., Chang, D. K., Nones, K., Johns, A. L., Patch, A.-M., Gingras, M.-C., Miller, D. K., Christ, A. N., Bruxner, T. J. C., Quinn, M. C.*, et al.* (2016). Genomic analyses identify molecular subtypes of pancreatic cancer. Nature *531*, 47-52.

Baker, L. A., Tiriac, H., Clevers, H., and Tuveson, D. A. (2016). Modeling pancreatic cancer with organoids. Trends Cancer *2*, 176-190.

Balko, J. M., Giltnane, J. M., Wang, K., Schwarz, L. J., Young, C. D., Cook, R. S., Owens, P., Sanders, M. E., Kuba, M. G., Sanchez, V.*, et al.* (2014). Molecular profiling of the residual disease of triple-negative breast cancers after neoadjuvant chemotherapy identifies actionable therapeutic targets. Cancer Discov *4*, 232-245.

Bang, D., Wilson, W., Ryan, M., Yeh, J. J., and Baldwin, A. S. (2013). GSK-3alpha promotes oncogenic KRAS function in pancreatic cancer via TAK1-TAB stabilization and regulation of noncanonical NF-kappaB. Cancer Discov *3*, 690-703.

Basturk, O., Hong, S.-M., Wood, L. D., Adsay, N. V., Albores-Saavedra, J., Biankin, A. V., Brosens, L. A. A., Fukushima, N., Goggins, M., Hruban, R. H.*, et al.* (2015). A REVISED CLASSIFICATION SYSTEM AND RECOMMENDATIONS FROM THE BALTIMORE CONSENSUS MEETING FOR NEOPLASTIC PRECURSOR LESIONS IN THE PANCREAS. The American journal of surgical pathology *39*, 1730-1741.

Becker, A. E., Hernandez, Y. G., Frucht, H., and Lucas, A. L. (2014). Pancreatic ductal adenocarcinoma: risk factors, screening, and early detection. World J Gastroenterol *20*, 11182-11198.

Beger, C., Ramadani, M., Meyer, S., Leder, G., Kruger, M., Welte, K., Gansauge, F., and Beger, H. G. (2004). Down-regulation of BRCA1 in chronic pancreatitis and sporadic pancreatic adenocarcinoma. Clinical cancer research : an official journal of the American Association for Cancer Research *10*, 3780-3787.

Beirowski, B., Babetto, E., Golden, J. P., Chen, Y. J., Yang, K., Gross, R. W., Patti, G. J., and Milbrandt, J. (2014). Metabolic regulator LKB1 is crucial for Schwann cell-mediated axon maintenance. Nature neuroscience *17*, 1351-1361.

Beug, H., Muller, H., Grieser, S., Doederlein, G., and Graf, T. (1981). Hematopoietic cells transformed in vitro by REVT avian reticuloendotheliosis virus express characteristics of very immature lymphoid cells. Virology *115*, 295-309.

Bhosale, P., Cox, V., Faria, S., Javadi, S., Viswanathan, C., Koay, E., and Tamm, E. (2018). Genetics of pancreatic cancer and implications for therapy. Abdominal Radiology *43*, 404-414.

Biankin, A. V., Waddell, N., Kassahn, K. S., Gingras, M. C., Muthuswamy, L. B., Johns, A. L., Miller, D. K., Wilson, P. J., Patch, A. M., Wu, J.*, et al.* (2012). Pancreatic cancer genomes reveal aberrations in axon guidance pathway genes. Nature *491*, 399-405.

Bieging, K. T., Mello, S. S., and Attardi, L. D. (2014). Unravelling mechanisms of p53-mediated tumour suppression. Nature reviews Cancer *14*, 359-370.

Blomstrand, H., Scheibling, U., Bratthall, C., Green, H., and Elander, N. O. (2019). Real world evidence on gemcitabine and nab-paclitaxel combination chemotherapy in advanced pancreatic cancer. BMC Cancer *19*, 40.

Boj, S. F., Hwang, C. I., Baker, L. A., Chio, II, Engle, D. D., Corbo, V., Jager, M., Ponz-Sarvise, M., Tiriac, H., Spector, M. S.*, et al.* (2015). Organoid models of human and mouse ductal pancreatic cancer. Cell *160*, 324-338.

Bradford, M. M. (1976). A rapid and sensitive method for the quantitation of microgram quantities of protein utilizing the principle of protein-dye binding. Analytical biochemistry *72*, 248-254.

Brand, R. E., Lerch, M. M., Rubinstein, W. S., Neoptolemos, J. P., Whitcomb, D. C., Hruban, R. H., Brentnall, T. A., Lynch, H. T., and Canto, M. I. (2007). Advances in counselling and surveillance of patients at risk for pancreatic cancer. Gut *56*, 1460-1469.

Brown, R. E., and Law, A. (2006). Morphoproteomic demonstration of constitutive nuclear factor-kappaB activation in glioblastoma multiforme with genomic correlates and therapeutic implications. Annals of clinical and laboratory science *36*, 421-426.

Burmi, R. S., Maginn, E. N., Gabra, H., Stronach, E. A., and Wasan, H. S. (2019). Combined inhibition of the PI3K/mTOR/MEK pathway induces Bim/Mcl-1-regulated apoptosis in pancreatic cancer cells. Cancer biology & therapy *20*, 21-30.

Burnette, W. N. (1981). "Western blotting": electrophoretic transfer of proteins from sodium dodecyl sulfate--polyacrylamide gels to unmodified nitrocellulose and radiographic detection with antibody and radioiodinated protein A. Analytical biochemistry *112*, 195-203.

Burris, H. A., 3rd, Moore, M. J., Andersen, J., Green, M. R., Rothenberg, M. L., Modiano, M. R., Cripps, M. C., Portenoy, R. K., Storniolo, A. M., Tarassoff, P.*, et al.* (1997). Improvements in survival and clinical benefit with gemcitabine as first-line therapy for patients with advanced pancreas cancer: a randomized trial. Journal of clinical oncology : official journal of the American Society of Clinical Oncology *15*, 2403-2413.

Caamaño, J. H., Rizzo, C. A., Durham, S. K., Barton, D. S., Raventós-Suárez, C., Snapper, C. M., and Bravo, R. (1998). Nuclear factor (NF)-kappa B2 (p100/p52) is required for normal splenic microarchitecture and B cell-mediated immune responses. The Journal of experimental medicine *187*, 185-196.

Cameron, M. E., Yakovenko, A., and Trevino, J. G. (2018). Glucose and Lactate Transport in Pancreatic Cancer: Glycolytic Metabolism Revisited. Journal of oncology *2018*, 6214838.

Canon, J., Rex, K., Saiki, A. Y., Mohr, C., Cooke, K., Bagal, D., Gaida, K., Holt, T., Knutson, C. G., Koppada, N.*, et al.* (2019). The clinical KRAS(G12C) inhibitor AMG 510 drives anti-tumour immunity. Nature *575*, 217-223.

Cao, P., Maira, S. M., Garcia-Echeverria, C., and Hedley, D. W. (2009). Activity of a novel, dual PI3-kinase/mTor inhibitor NVP-BEZ235 against primary human pancreatic cancers grown as orthotopic xenografts. Br J Cancer *100*, 1267-1276.

Capurso, G., Boccia, S., Salvia, R., Del Chiaro, M., Frulloni, L., Arcidiacono, P. G., Zerbi, A., Manta, R., Fabbri, C., Ventrucci, M.*, et al.* (2013). Risk Factors for Intraductal Papillary Mucinous Neoplasm (IPMN) of the Pancreas: A Multicentre Case-Control Study. Am J Gastroenterol *108*, 1003-1009.

Chadwick, M. L., Lane, A., Thomas, D., Smith, A. R., White, A. R., Davidson, D., Feng, Y., Boscolo, E., Zheng, Y., Adams, D. M.*, et al.* (2018). Combined mTOR and MEK inhibition is an effective therapy in a novel mouse model for angiosarcoma. Oncotarget *9*, 24750-24765.

Chaika, N. V., Gebregiworgis, T., Lewallen, M. E., Purohit, V., Radhakrishnan, P., Liu, X., Zhang, B., Mehla, K., Brown, R. B., Caffrey, T.*, et al.* (2012). MUC1 mucin stabilizes and activates hypoxia-

inducible factor 1 alpha to regulate metabolism in pancreatic cancer. Proc Natl Acad Sci U S A *109*, 13787-13792.

Chandler, N. M., Canete, J. J., and Callery, M. P. (2004). Increased expression of NF-kappa B subunits in human pancreatic cancer cells. The Journal of surgical research *118*, 9-14.

Chen, J. (2016). The Cell-Cycle Arrest and Apoptotic Functions of p53 in Tumor Initiation and Progression. Cold Spring Harb Perspect Med *6*, a026104.

Chen, J., and Chen, Z. J. (2013). Regulation of NF-κB by Ubiquitination. Current opinion in immunology *25*, 4-12.

Cheng, H., Zou, Y., Ross, J. S., Wang, K., Liu, X., Halmos, B., Ali, S. M., Liu, H., Verma, A., Montagna, C.*, et al.* (2015). RICTOR Amplification Defines a Novel Subset of Patients with Lung Cancer Who May Benefit from Treatment with mTORC1/2 Inhibitors. Cancer Discov *5*, 1262-1270.

Cherfils, J., and Zeghouf, M. (2013). Regulation of small GTPases by GEFs, GAPs, and GDIs. Physiological reviews *93*, 269-309.

Chien, Y., Scuoppo, C., Wang, X., Fang, X., Balgley, B., Bolden, J. E., Premsrirut, P., Luo, W., Chicas, A., Lee, C. S.*, et al.* (2011). Control of the senescence-associated secretory phenotype by NF-kappaB promotes senescence and enhances chemosensitivity. Genes Dev *25*, 2125-2136.

Chllamma, M. K., Cook, N., Dhani, N. C., Giby, K., Dodd, A., Wang, L., Hedley, D. W., Moore, M. J., and Knox, J. J. (2016). FOLFIRINOX for advanced pancreatic cancer: the Princess Margaret Cancer Centre experience. British Journal of Cancer *115*, 649-654.

Choi, M. H., Mejlænder-Andersen, E., Manueldas, S., El Jellas, K., Steine, S. J., Tjensvoll, K., Sætran, H. A., Knappskog, S., Hoem, D., Nordgård, O.*, et al.* (2019). Mutation analysis by deep sequencing of pancreatic juice from patients with pancreatic ductal adenocarcinoma. BMC Cancer *19*, 11.

Chresta, C. M., Davies, B. R., Hickson, I., Harding, T., Cosulich, S., Critchlow, S. E., Vincent, J. P., Ellston, R., Jones, D., Sini, P.*, et al.* (2010). AZD8055 is a potent, selective, and orally bioavailable ATP-competitive mammalian target of rapamycin kinase inhibitor with in vitro and in vivo antitumor activity. Cancer Res *70*, 288-298.

Chung, V., McDonough, S., Philip, P. A., Cardin, D., Wang-Gillam, A., Hui, L., Tejani, M. A., Seery, T. E., Dy, I. A., Al Baghdadi, T.*, et al.* (2017a). Effect of Selumetinib and MK-2206 vs Oxaliplatin and Fluorouracil in Patients With Metastatic Pancreatic Cancer After Prior Therapy: SWOG S1115 Study Randomized Clinical Trial. JAMA Oncol *3*, 516-522.

Chung, W. J., Daemen, A., Cheng, J. H., Long, J. E., Cooper, J. E., Wang, B. E., Tran, C., Singh, M., Gnad, F., Modrusan, Z.*, et al.* (2017b). Kras mutant genetically engineered mouse models of human cancers are genomically heterogeneous. Proc Natl Acad Sci U S A *114*, E10947-E10955.

Clark, K., Peggie, M., Plater, L., Sorcek, R. J., Young, E. R., Madwed, J. B., Hough, J., McIver, E. G., and Cohen, P. (2011). Novel cross-talk within the IKK family controls innate immunity. The Biochemical journal *434*, 93-104.

Clarke, P. A., Roe, T., Swabey, K., Hobbs, S. M., McAndrew, C., Tomlin, K., Westwood, I., Burke, R., van Montfort, R., and Workman, P. (2019). Dissecting mechanisms of resistance to targeted drug combination therapy in human colorectal cancer. Oncogene *38*, 5076-5090.

Claudio, E., Brown, K., Park, S., Wang, H., and Siebenlist, U. (2002). BAFF-induced NEMO-independent processing of NF-kappa B2 in maturing B cells. Nature immunology *3*, 958-965.

Collisson, E. A., Sadanandam, A., Olson, P., Gibb, W. J., Truitt, M., Gu, S., Cooc, J., Weinkle, J., Kim, G. E., Jakkula, L*., et al.* (2011). Subtypes of pancreatic ductal adenocarcinoma and their differing responses to therapy. Nature medicine *17*, 500-503.

Colombo, F., Zambrano, S., and Agresti, A. (2018). NF-kappaB, the Importance of Being Dynamic: Role and Insights in Cancer. Biomedicines *6*.

Conroy, T., Desseigne, F., Ychou, M., Bouche, O., Guimbaud, R., Becouarn, Y., Adenis, A., Raoul, J. L., Gourgou-Bourgade, S., de la Fouchardiere, C*., et al.* (2011). FOLFIRINOX versus gemcitabine for metastatic pancreatic cancer. N Engl J Med *364*, 1817-1825.

Conroy, T., Hammel, P., Hebbar, M., Abdelghani, M. B., Wei, A. C.-c., Raoul, J.-L., Chone, L., Francois, E., Artru, P., Biagi, J. J*., et al.* (2018). Unicancer GI PRODIGE 24/CCTG PA.6 trial: A multicenter international randomized phase III trial of adjuvant mFOLFIRINOX versus gemcitabine (gem) in patients with resected pancreatic ductal adenocarcinomas. Journal of Clinical Oncology *36*, LBA4001-LBA4001.

Conway, J. R. W., Warren, S. C., Herrmann, D., Murphy, K. J., Cazet, A. S., Vennin, C., Shearer, R. F., Killen, M. J., Magenau, A., Mélénec, P*., et al.* (2018). Intravital Imaging to Monitor Therapeutic Response in Moving Hypoxic Regions Resistant to PI3K Pathway Targeting in Pancreatic Cancer. Cell reports *23*, 3312-3326.

Coope, H. J., Atkinson, P. G., Huhse, B., Belich, M., Janzen, J., Holman, M. J., Klaus, G. G., Johnston, L. H., and Ley, S. C. (2002). CD40 regulates the processing of NF-kappaB2 p100 to p52. The EMBO journal *21*, 5375-5385.

Cox, A. D., Der, C. J., and Philips, M. R. (2015). Targeting RAS Membrane Association: Back to the Future for Anti-RAS Drug Discovery? Clinical cancer research : an official journal of the American Association for Cancer Research *21*, 1819-1827.

Crnogorac-Jurcevic, T., Chelala, C., Barry, S., Harada, T., Bhakta, V., Lattimore, S., Jurcevic, S., Bronner, M., Lemoine, N. R., and Brentnall, T. A. (2013). Molecular Analysis of Precursor Lesions in Familial Pancreatic Cancer. PLoS ONE *8*, e54830.

Csibi, A., Fendt, S. M., Li, C., Poulogiannis, G., Choo, A. Y., Chapski, D. J., Jeong, S. M., Dempsey, J. M., Parkhitko, A., Morrison, T*., et al.* (2013). The mTORC1 pathway stimulates glutamine metabolism and cell proliferation by repressing SIRT4. Cell *153*, 840-854.

Daemen, A., Peterson, D., Sahu, N., McCord, R., Du, X., Liu, B., Kowanetz, K., Hong, R., Moffat, J., Gao, M*., et al.* (2015). Metabolite profiling stratifies pancreatic ductal adenocarcinomas into subtypes with distinct sensitivities to metabolic inhibitors. Proc Natl Acad Sci U S A *112*, E4410-4417.

Darwish, N. H. E., Sudha, T., Godugu, K., Bharali, D. J., Elbaz, O., El-Ghaffar, H. A. A., Azmy, E., Anber, N., and Mousa, S. A. (2019). Novel Targeted Nano-Parthenolide Molecule against NF-kB in Acute Myeloid Leukemia. Molecules *24*, 2103.

Davies, C. C., Harvey, E., McMahon, R. F., Finegan, K. G., Connor, F., Davis, R. J., Tuveson, D. A., and Tournier, C. (2014). Impaired JNK signaling cooperates with KrasG12D expression to accelerate pancreatic ductal adenocarcinoma. Cancer Res *74*, 3344-3356.

De Silva, N. S., Anderson, M. M., Carette, A., Silva, K., Heise, N., Bhagat, G., and Klein, U. (2016). Transcription factors of the alternative NF-kappaB pathway are required for germinal center B-cell development. Proc Natl Acad Sci U S A *113*, 9063-9068.

de Vries, A., Flores, E. R., Miranda, B., Hsieh, H.-M., van Oostrom, C. T. M., Sage, J., and Jacks, T. (2002). Targeted point mutations of p53 lead to dominant-negative inhibition of wild-type p53 function. Proceedings of the National Academy of Sciences of the United States of America *99*, 2948-2953.

DeGraffenried, L. A., Fulcher, L., Friedrichs, W. E., Grunwald, V., Ray, R. B., and Hidalgo, M. (2004). Reduced PTEN expression in breast cancer cells confers susceptibility to inhibitors of the PI3 kinase/Akt pathway. Annals of oncology : official journal of the European Society for Medical Oncology *15*, 1510-1516.

Dejardin, E., Droin, N. M., Delhase, M., Haas, E., Cao, Y., Makris, C., Li, Z. W., Karin, M., Ware, C. F., and Green, D. R. (2002). The lymphotoxin-beta receptor induces different patterns of gene expression via two NF-kappaB pathways. Immunity *17*, 525-535.

DeLeo, A. B., Jay, G., Appella, E., Dubois, G. C., Law, L. W., and Old, L. J. (1979). Detection of a transformation-related antigen in chemically induced sarcomas and other transformed cells of the mouse. Proc Natl Acad Sci U S A *76*, 2420-2424.

DiDonato, J. A., Mercurio, F., and Karin, M. (2012). NF-kappaB and the link between inflammation and cancer. Immunol Rev *246*, 379-400.

Diersch, S., Wenzel, P., Szameitat, M., Eser, P., Paul, M. C., Seidler, B., Eser, S., Messer, M., Reichert, M., Pagel, P.*, et al.* (2013). Efemp1 and p27(Kip1) modulate responsiveness of pancreatic cancer cells towards a dual PI3K/mTOR inhibitor in preclinical models. Oncotarget *4*, 277-288.

Doppler, H., Liou, G. Y., and Storz, P. (2013). Downregulation of TRAF2 mediates NIK-induced pancreatic cancer cell proliferation and tumorigenicity. PLoS One *8*, e53676.

Driscoll, D. R., Karim, S. A., Sano, M., Gay, D. M., Jacob, W., Yu, J., Mizukami, Y., Gopinathan, A., Jodrell, D. I., Evans, T. R.*, et al.* (2016). mTORC2 Signaling Drives the Development and Progression of Pancreatic Cancer. Cancer Res *76*, 6911-6923.

el-Deiry, W. S., Tokino, T., Velculescu, V. E., Levy, D. B., Parsons, R., Trent, J. M., Lin, D., Mercer, W. E., Kinzler, K. W., and Vogelstein, B. (1993). WAF1, a potential mediator of p53 tumor suppression. Cell *75*, 817-825.

Elghazi, L., Blandino-Rosano, M., Alejandro, E., Cras-Méneur, C., and Bernal-Mizrachi, E. (2017). Role of nutrients and mTOR signaling in the regulation of pancreatic progenitors development. Mol Metab *6*, 560-573.

Engeland, K. (2018). Cell cycle arrest through indirect transcriptional repression by p53: I have a DREAM. Cell death and differentiation *25*, 114-132.

Eser, S., Reiff, N., Messer, M., Seidler, B., Gottschalk, K., Dobler, M., Hieber, M., Arbeiter, A., Klein, S., Kong, B.*, et al.* (2013). Selective requirement of PI3K/PDK1 signaling for Kras oncogene-driven pancreatic cell plasticity and cancer. Cancer cell *23*, 406-420.

Ewald, F., Grabinski, N., Grottke, A., Windhorst, S., Norz, D., Carstensen, L., Staufer, K., Hofmann, B. T., Diehl, F., David, K.*, et al.* (2013). Combined targeting of AKT and mTOR using MK-2206 and RAD001 is synergistic in the treatment of cholangiocarcinoma. International journal of cancer *133*, 2065-2076.

Feil, R., Wagner, J., Metzger, D., and Chambon, P. (1997). Regulation of Cre recombinase activity by mutated estrogen receptor ligand-binding domains. Biochemical and biophysical research communications *237*, 752-757.

Finlay, C. A., Hinds, P. W., and Levine, A. J. (1989). The p53 proto-oncogene can act as a suppressor of transformation. Cell *57*, 1083-1093.

Fiorini, C., Cordani, M., Padroni, C., Blandino, G., Di Agostino, S., and Donadelli, M. (2015). Mutant p53 stimulates chemoresistance of pancreatic adenocarcinoma cells to gemcitabine. Biochimica et Biophysica Acta (BBA) - Molecular Cell Research *1853*, 89-100.

Fotopoulos, G., Syrigos, K., and Saif, M. W. (2016). Genetic factors affecting patient responses to pancreatic cancer treatment. Annals of gastroenterology *29*, 466-476.

Freed-Pastor, W. A., and Prives, C. (2012). Mutant p53: one name, many proteins. Genes Dev *26*, 1268-1286.

Fuhler, G. M., Tyl, M. R., Olthof, S. G., Lyndsay Drayer, A., Blom, N., and Vellenga, E. (2009). Distinct roles of the mTOR components Rictor and Raptor in MO7e megakaryocytic cells. European journal of haematology *83*, 235-245.

Fusco, A. J., Savinova, O. V., Talwar, R., Kearns, J. D., Hoffmann, A., and Ghosh, G. (2008). Stabilization of RelB requires multidomain interactions with p100/p52. J Biol Chem *283*, 12324-12332.

Gannon, M., Herrera, P. L., and Wright, C. V. (2000). Mosaic Cre-mediated recombination in pancreas using the pdx-1 enhancer/promoter. Genesis (New York, NY : 2000) *26*, 143-144.

Gao, N., Flynn, D. C., Zhang, Z., Zhong, X. S., Walker, V., Liu, K. J., Shi, X., and Jiang, B. H. (2004). G1 cell cycle progression and the expression of G1 cyclins are regulated by PI3K/AKT/mTOR/p70S6K1 signaling in human ovarian cancer cells. American journal of physiology Cell physiology *287*, C281-291.

Garcia-Garcia, C., Rivas, M. A., Ibrahim, Y. H., Calvo, M. T., Gris-Oliver, A., Rodriguez, O., Grueso, J., Anton, P., Guzman, M., Aura, C.*, et al.* (2015). MEK plus PI3K/mTORC1/2 Therapeutic Efficacy Is Impacted by TP53 Mutation in Preclinical Models of Colorectal Cancer. Clinical cancer research : an official journal of the American Association for Cancer Research *21*, 5499-5510.

Garrido-Laguna, I., Tan, A. C., Uson, M., Angenendt, M., Ma, W. W., Villaroel, M. C., Zhao, M., Rajeshkumar, N. V., Jimeno, A., Donehower, R.*, et al.* (2010). Integrated preclinical and clinical development of mTOR inhibitors in pancreatic cancer. Br J Cancer *103*, 649-655.

Genkinger, J. M., Spiegelman, D., Anderson, K. E., Bergkvist, L., Bernstein, L., van den Brandt, P. A., English, D. R., Freudenheim, J. L., Fuchs, C. S., Giles, G. G.*, et al.* (2009). Alcohol intake and pancreatic cancer risk: a pooled analysis of fourteen cohort studies. Cancer epidemiology, biomarkers & prevention : a publication of the American Association for Cancer Research, cosponsored by the American Society of Preventive Oncology *18*, 765-776.

Goecks, J., Mortimer, N. T., Mobley, J. A., Bowersock, G. J., Taylor, J., and Schlenke, T. A. (2013). Integrative Approach Reveals Composition of Endoparasitoid Wasp Venoms. PLOS ONE *8*, e64125.

Golan, T., Hammel, P., Reni, M., Van Cutsem, E., Macarulla, T., Hall, M. J., Park, J. O., Hochhauser, D., Arnold, D., Oh, D. Y.*, et al.* (2019). Maintenance Olaparib for Germline BRCA-Mutated Metastatic Pancreatic Cancer. The New England journal of medicine.

Gopinathan, A., Morton, J. P., Jodrell, D. I., and Sansom, O. J. (2015). GEMMs as preclinical models for testing pancreatic cancer therapies. Disease Models & Mechanisms *8*, 1185.

Grabiner, B. C., Nardi, V., Birsoy, K., Possemato, R., Shen, K., Sinha, S., Jordan, A., Beck, A. H., and Sabatini, D. M. (2014). A diverse array of cancer-associated MTOR mutations are hyperactivating and can predict rapamycin sensitivity. Cancer Discov *4*, 554-563.

Gray, C. M., McCorkell, K. A., Chunduru, S. K., McKinlay, M. A., and May, M. J. (2014). Negative feedback regulation of NF-kappaB-inducing kinase is proteasome-dependent but does not require cellular inhibitors of apoptosis. Biochemical and biophysical research communications *450*, 341-346.

Guertin, D. A., Stevens, D. M., Saitoh, M., Kinkel, S., Crosby, K., Sheen, J. H., Mullholland, D. J., Magnuson, M. A., Wu, H., and Sabatini, D. M. (2009). mTOR complex 2 is required for the development of prostate cancer induced by Pten loss in mice. Cancer cell *15*, 148-159.

Guo, J.-P., Coppola, D., and Cheng, J. Q. (2011). IKBKE protein activates Akt independent of phosphatidylinositol 3-kinase/PDK1/mTORC2 and the pleckstrin homology domain to sustain malignant transformation. The Journal of biological chemistry *286*, 37389-37398.

Hamidi, T., Algul, H., Cano, C. E., Sandi, M. J., Molejon, M. I., Riemann, M., Calvo, E. L., Lomberk, G., Dagorn, J. C., Weih, F.*, et al.* (2012). Nuclear protein 1 promotes pancreatic cancer development and protects cells from stress by inhibiting apoptosis. J Clin Invest *122*, 2092-2103.

Hara, K., Maruki, Y., Long, X., Yoshino, K.-i., Oshiro, N., Hidayat, S., Tokunaga, C., Avruch, J., and Yonezawa, K. (2002). Raptor, a Binding Partner of Target of Rapamycin (TOR), Mediates TOR Action. Cell *110*, 177-189.

Harper, J. W., Adami, G. R., Wei, N., Keyomarsi, K., and Elledge, S. J. (1993). The p21 Cdk-interacting protein Cip1 is a potent inhibitor of G1 cyclin-dependent kinases. Cell *75*, 805-816.

Hassan, Z., Schneeweis, C., Wirth, M., Veltkamp, C., Dantes, Z., Feuerecker, B., Ceyhan, G. O., Knauer, S. K., Weichert, W., Schmid, R. M.*, et al.* (2018). MTOR inhibitor-based combination therapies for pancreatic cancer. British Journal Of Cancer *118*, 366.

Hayden, M. S., and Ghosh, S. (2012). NF-κB, the first quarter-century: remarkable progress and outstanding questions. Genes & Development *26*, 203-234.

Herzig, S., and Shaw, R. J. (2018). AMPK: guardian of metabolism and mitochondrial homeostasis. Nature reviews Molecular cell biology *19*, 121-135.

Hezel, A. F., Kimmelman, A. C., Stanger, B. Z., Bardeesy, N., and Depinho, R. A. (2006). Genetics and biology of pancreatic ductal adenocarcinoma. Genes Dev *20*, 1218-1249.

Hingorani, S. R., Petricoin, E. F., Maitra, A., Rajapakse, V., King, C., Jacobetz, M. A., Ross, S., Conrads, T. P., Veenstra, T. D., Hitt, B. A*., et al.* (2003). Preinvasive and invasive ductal pancreatic cancer and its early detection in the mouse. Cancer cell *4*, 437-450.

Hingorani, S. R., Wang, L., Multani, A. S., Combs, C., Deramaudt, T. B., Hruban, R. H., Rustgi, A. K., Chang, S., and Tuveson, D. A. (2005). Trp53R172H and KrasG12D cooperate to promote chromosomal instability and widely metastatic pancreatic ductal adenocarcinoma in mice. Cancer cell *7*, 469-483.

Hisa, T., Suda, K., Nobukawa, B., Ohkubo, H., Shiozawa, S., Ishigame, H., Yamao, K., and Yatabe, Y. (2007). Distribution of intraductal lesions in small invasive ductal carcinoma of the pancreas. Pancreatology *7*, 341-346.

Hosein, A. N., and Beg, M. S. (2018). Pancreatic Cancer Metabolism: Molecular Mechanisms and Clinical Applications. Current oncology reports *20*, 56.

Hruban, R. H., Goggins, M., Parsons, J., and Kern, S. E. (2000). Progression model for pancreatic cancer. Clinical cancer research : an official journal of the American Association for Cancer Research *6*, 2969-2972.

Hruban, R. H., and Klimstra, D. S. (2014). Adenocarcinoma of the pancreas. Semin Diagn Pathol *31*, 443-451.

Hruban, R. H., Maitra, A., Kern, S. E., and Goggins, M. (2007). Precursors to Pancreatic Cancer. Gastroenterology clinics of North America *36*, 831-vi.

Hruban, R. H., Takaori, K., Klimstra, D. S., Adsay, N. V., Albores-Saavedra, J., Biankin, A. V., Biankin, S. A., Compton, C., Fukushima, N., Furukawa, T*., et al.* (2004). An illustrated consensus on the classification of pancreatic intraepithelial neoplasia and intraductal papillary mucinous neoplasms. The American journal of surgical pathology *28*, 977-987.

Hsieh, A. C., Liu, Y., Edlind, M. P., Ingolia, N. T., Janes, M. R., Sher, A., Shi, E. Y., Stumpf, C. R., Christensen, C., Bonham, M. J*., et al.* (2012). The translational landscape of mTOR signalling steers cancer initiation and metastasis. Nature *485*, 55-61.

Hua, H., Kong, Q., Zhang, H., Wang, J., Luo, T., and Jiang, Y. (2019). Targeting mTOR for cancer therapy. Journal of hematology & oncology *12*, 71-71.

Hua, J., Shi, S., Liang, D., Liang, C., Meng, Q., Zhang, B., Ni, Q., Xu, J., and Yu, X. (2018). Current status and dilemma of second-line treatment in advanced pancreatic cancer: is there a silver lining? OncoTargets and therapy *11*, 4591-4608.

Huang da, W., Sherman, B. T., and Lempicki, R. A. (2009). Systematic and integrative analysis of large gene lists using DAVID bioinformatics resources. Nature protocols *4*, 44-57.

Huxley, R., Ansary-Moghaddam, A., Berrington de González, A., Barzi, F., and Woodward, M. (2005). Type-II diabetes and pancreatic cancer: a meta-analysis of 36 studies. British Journal of Cancer *92*, 2076-2083.

Hwang, M., Perez, C. A., Moretti, L., and Lu, B. (2008). The mTOR signaling network: insights from its role during embryonic development. Current medicinal chemistry *15*, 1192-1208.

Iannetti, A., Ledoux, A. C., Tudhope, S. J., Sellier, H., Zhao, B., Mowla, S., Moore, A., Hummerich, H., Gewurz, B. E., Cockell, S. J.*, et al.* (2014). Regulation of p53 and Rb Links the Alternative NF-κB Pathway to EZH2 Expression and Cell Senescence. PLOS Genetics *10*, e1004642.

Ijichi, H. (2011). Genetically-engineered mouse models for pancreatic cancer: Advances and current limitations. World J Clin Oncol *2*, 195-202.

Inoki, K., Li, Y., Xu, T., and Guan, K. L. (2003). Rheb GTPase is a direct target of TSC2 GAP activity and regulates mTOR signaling. Genes Dev *17*, 1829-1834.

Iriana, S., Ahmed, S., Gong, J., Annamalai, A. A., Tuli, R., and Hendifar, A. E. (2016). Targeting mTOR in Pancreatic Ductal Adenocarcinoma. Frontiers in oncology *6*, 99-99.

Ischenko, I., Petrenko, O., and Hayman, M. J. (2015). A MEK/PI3K/HDAC inhibitor combination therapy for KRAS mutant pancreatic cancer cells. Oncotarget *6*, 15814-15827.

Jackson, E. L., Willis, N., Mercer, K., Bronson, R. T., Crowley, D., Montoya, R., Jacks, T., and Tuveson, D. A. (2001). Analysis of lung tumor initiation and progression using conditional expression of oncogenic K-ras. Genes Dev *15*, 3243-3248.

Javle, M. M., Shroff, R. T., Xiong, H., Varadhachary, G. A., Fogelman, D., Reddy, S. A., Davis, D., Zhang, Y., Wolff, R. A., and Abbruzzese, J. L. (2010). Inhibition of the mammalian target of rapamycin (mTOR) in advanced pancreatic cancer: results of two phase II studies. BMC Cancer *10*, 368.

Jhanwar-Uniyal, M., Wainwright, J. V., Mohan, A. L., Tobias, M. E., Murali, R., Gandhi, C. D., and Schmidt, M. H. (2019). Diverse signaling mechanisms of mTOR complexes: mTORC1 and mTORC2 in forming a formidable relationship. Advances in Biological Regulation *72*, 51-62.

Jiao, Y., Shi, C., Edil, B. H., de Wilde, R. F., Klimstra, D. S., Maitra, A., Schulick, R. D., Tang, L. H., Wolfgang, C. L., Choti, M. A.*, et al.* (2011). DAXX/ATRX, MEN1, and mTOR pathway genes are frequently altered in pancreatic neuroendocrine tumors. Science (New York, NY) *331*, 1199-1203.

Jonckheere, N., Vasseur, R., and Van Seuningen, I. (2017). The cornerstone K-RAS mutation in pancreatic adenocarcinoma: From cell signaling network, target genes, biological processes to therapeutic targeting. Critical reviews in oncology/hematology *111*, 7-19.

Junqueira, L. C. U., Bignolas, G., and Brentani, R. R. (1979). Picrosirius staining plus polarization microscopy, a specific method for collagen detection in tissue sections. The Histochemical Journal *11*, 447-455.

Junttila, M. R., Devasthali, V., Cheng, J. H., Castillo, J., Metcalfe, C., Clermont, A. C., Otter, D. D., Chan, E., Bou-Reslan, H., Cao, T.*, et al.* (2015). Modeling targeted inhibition of MEK and PI3 kinase in human pancreatic cancer. Molecular cancer therapeutics *14*, 40-47.

Kaltschmidt, B., Greiner, J. F. W., Kadhim, H. M., and Kaltschmidt, C. (2018). Subunit-Specific Role of NF-κB in Cancer. Biomedicines *6*, 44.

Kanda, M., Matthaei, H., Wu, J., Hong, S.-M., Yu, J., Borges, M., Hruban, R. H., Maitra, A., Kinzler, K., Vogelstein, B., and Goggins, M. (2012). Presence of Somatic Mutations in Most Early-Stage Pancreatic Intraepithelial Neoplasia. Gastroenterology *142*, 730-733.e739.

Kang, R., Hou, W., Zhang, Q., Chen, R., Lee, Y. J., Bartlett, D. L., Lotze, M. T., Tang, D., and Zeh, H. J. (2014). RAGE is essential for oncogenic KRAS-mediated hypoxic signaling in pancreatic cancer. Cell death & disease *5*, e1480.

Karandish, F., and Mallik, S. (2016). Biomarkers and Targeted Therapy in Pancreatic Cancer. Biomarkers in Cancer *8s1*, BIC.S34414.

Kastan, M. B., Onyekwere, O., Sidransky, D., Vogelstein, B., and Craig, R. W. (1991). Participation of p53 protein in the cellular response to DNA damage. Cancer Res *51*, 6304-6311.

Kastenhuber, E. R., and Lowe, S. W. (2017). Putting p53 in Context. Cell *170*, 1062-1078.

Kawaguchi, Y., Cooper, B., Gannon, M., Ray, M., MacDonald, R. J., and Wright, C. V. (2002). The role of the transcriptional regulator Ptf1a in converting intestinal to pancreatic progenitors. Nature genetics *32*, 128-134.

Keats, J. J., Fonseca, R., Chesi, M., Schop, R., Baker, A., Chng, W. J., Van Wier, S., Tiedemann, R., Shi, C. X., Sebag, M.*, et al.* (2007). Promiscuous mutations activate the noncanonical NF-kappaB pathway in multiple myeloma. Cancer cell *12*, 131-144.

Kendellen, M. F., Bradford, J. W., Lawrence, C. L., Clark, K. S., and Baldwin, A. S. (2014). Canonical and non-canonical NF-κB signaling promotes breast cancer tumor-initiating cells. Oncogene *33*, 1297-1305.

Kent, W. J., Sugnet, C. W., Furey, T. S., Roskin, K. M., Pringle, T. H., Zahler, A. M., and Haussler, D. (2002). The human genome browser at UCSC. Genome research *12*, 996-1006.

Khalili, M., Wax, B. N., Reed, W. P., Schuss, A., Drexler, S., Weston, S. R., and Katz, D. S. (2006). Acinar cell carcinoma of the pancreas. Clinical Imaging *30*, 343-346.

Kilic-Eren, M., Boylu, T., and Tabor, V. (2013). Targeting PI3K/Akt represses Hypoxia inducible factor-1alpha activation and sensitizes Rhabdomyosarcoma and Ewing's sarcoma cells for apoptosis. Cancer cell international *13*, 36.

Kim, J., and Guan, K.-L. (2019). mTOR as a central hub of nutrient signalling and cell growth. Nature Cell Biology *21*, 63-71.

Kim, M. P., and Lozano, G. (2018). Mutant p53 partners in crime. Cell death and differentiation *25*, 161-168.

Klein, A. P. (2012). Genetic susceptibility to pancreatic cancer. Molecular carcinogenesis *51*, 14-24.

Kong, B., Wu, W., Cheng, T., Schlitter, A. M., Qian, C., Bruns, P., Jian, Z., Jager, C., Regel, I., Raulefs, S.*, et al.* (2016). A subset of metastatic pancreatic ductal adenocarcinomas depends quantitatively on oncogenic Kras/Mek/Erk-induced hyperactive mTOR signalling. Gut *65*, 647-657.

Kopp, J. L., von Figura, G., Mayes, E., Liu, F. F., Dubois, C. L., Morris, J. P. t., Pan, F. C., Akiyama, H., Wright, C. V., Jensen, K.*, et al.* (2012). Identification of Sox9-dependent acinar-to-ductal reprogramming as the principal mechanism for initiation of pancreatic ductal adenocarcinoma. Cancer cell *22*, 737-750.

Kordes, S., Richel, D. J., Klümpen, H.-J., Weterman, M. J., Stevens, A. J. W. M., and Wilmink, J. W. (2013). A phase I/II, non-randomized, feasibility/safety and efficacy study of the combination of everolimus, cetuximab and capecitabine in patients with advanced pancreatic cancer. Investigational new drugs *31*, 85-91.

Krebs, A. M., Mitschke, J., Lasierra Losada, M., Schmalhofer, O., Boerries, M., Busch, H., Boettcher, M., Mougiakakos, D., Reichardt, W., Bronsert, P.*, et al.* (2017). The EMT-activator Zeb1 is a key factor for cell plasticity and promotes metastasis in pancreatic cancer. Nat Cell Biol *19*, 518-529.

Laemmli, U. K. (1970). Cleavage of structural proteins during the assembly of the head of bacteriophage T4. Nature *227*, 680-685.

Lakatos, P. L., and Lakatos, L. (2008). Risk for colorectal cancer in ulcerative colitis: changes, causes and management strategies. World J Gastroenterol *14*, 3937-3947.

Lane, D. P. (1992). Cancer. p53, guardian of the genome. Nature *358*, 15-16.

Langmead, B., and Salzberg, S. L. (2012). Fast gapped-read alignment with Bowtie 2. Nature methods *9*, 357-359.

Larsson, S. C., Orsini, N., and Wolk, A. (2007). Body mass index and pancreatic cancer risk: A meta-analysis of prospective studies. International journal of cancer *120*, 1993-1998.

Larsson, S. C., and Wolk, A. (2012). Red and processed meat consumption and risk of pancreatic cancer: meta-analysis of prospective studies. Br J Cancer *106*, 603-607.

Lawrence, C. L., and Baldwin, A. S. (2016). Non-Canonical EZH2 Transcriptionally Activates RelB in Triple Negative Breast Cancer. PLoS One *11*, e0165005.

Lee, A. Y. L., Dubois, C. L., Sarai, K., Zarei, S., Schaeffer, D. F., Sander, M., and Kopp, J. L. (2018). Cell of origin affects tumour development and phenotype in pancreatic ductal adenocarcinoma. Gut.

Lee, D. W., Ramakrishnan, D., Valenta, J., Parney, I. F., Bayless, K. J., and Sitcheran, R. (2013). The NF-kappaB RelB protein is an oncogenic driver of mesenchymal glioma. PLoS One *8*, e57489.

Lee, J. V., Carrer, A., Shah, S., Snyder, N. W., Wei, S., Venneti, S., Worth, A. J., Yuan, Z. F., Lim, H. W., Liu, S.*, et al.* (2014). Akt-dependent metabolic reprogramming regulates tumor cell histone acetylation. Cell metabolism *20*, 306-319.

Lennerz, J. K., and Stenzinger, A. (2015). Allelic Ratio of KRAS Mutations in Pancreatic Cancer. The Oncologist *20*, e8-e9.

Leonard, B., McCann, J. L., Starrett, G. J., Kosyakovsky, L., Luengas, E. M., Molan, A. M., Burns, M. B., McDougle, R. M., Parker, P. J., Brown, W. L., and Harris, R. S. (2015). The PKC/NF-kappaB signaling pathway induces APOBEC3B expression in multiple human cancers. Cancer Res *75*, 4538-4547.

Leonardi, M., Perna, E., Tronnolone, S., Colecchia, D., and Chiariello, M. (2019). Activated kinase screening identifies the IKBKE oncogene as a positive regulator of autophagy. Autophagy *15*, 312-326.

Lesina, M., Wormann, S. M., Morton, J., Diakopoulos, K. N., Korneeva, O., Wimmer, M., Einwachter, H., Sperveslage, J., Demir, I. E., Kehl, T.*, et al.* (2016). RelA regulates CXCL1/CXCR2-dependent oncogene-induced senescence in murine Kras-driven pancreatic carcinogenesis. J Clin Invest *126*, 2919-2932.

Li, C., Cui, J. F., Chen, M. B., Liu, C. Y., Liu, F., Zhang, Q. D., Zou, J., and Lu, P. H. (2015a). The preclinical evaluation of the dual mTORC1/2 inhibitor INK-128 as a potential anti-colorectal cancer agent. Cancer Biol Ther *16*, 34-42.

Li, D., Morris, J. S., Liu, J., Hassan, M. M., Day, R. S., Bondy, M. L., and Abbruzzese, J. L. (2009). Body Mass Index and Risk, Age of Onset, and Survival in Patients With Pancreatic Cancer. JAMA *301*, 2553-2562.

Li, N., Lu, X. Y., Shi, W. Y., Mao, F. J., Yang, X. Y., Luo, Y. B., and Li, W. (2019). Combined mTOR/MEK inhibition prevents proliferation and induces apoptosis in NF2-mutant tumors. European review for medical and pharmacological sciences *23*, 5874-5883.

Li, Q., Yang, G., Feng, M., Zheng, S., Cao, Z., Qiu, J., You, L., Zheng, L., Hu, Y., Zhang, T., and Zhao, Y. (2018). NF-kappaB in pancreatic cancer: Its key role in chemoresistance. Cancer letters *421*, 127-134.

Li, Y., Zhou, Q. L., Sun, W., Chandrasekharan, P., Cheng, H. S., Ying, Z., Lakshmanan, M., Raju, A., Tenen, D. G., Cheng, S. Y.*, et al.* (2015b). Non-canonical NF-kappaB signalling and ETS1/2 cooperatively drive C250T mutant TERT promoter activation. Nat Cell Biol *17*, 1327-1338.

Liang, C., Zhang, M., and Sun, S. C. (2006). beta-TrCP binding and processing of NF-kappaB2/p100 involve its phosphorylation at serines 866 and 870. Cellular signalling *18*, 1309-1317.

Liang, S.-Q., Bührer, E. D., Berezowska, S., Marti, T. M., Xu, D., Froment, L., Yang, H., Hall, S. R. R., Vassella, E., Yang, Z.*, et al.* (2019). mTOR mediates a mechanism of resistance to chemotherapy and defines a rational combination strategy to treat KRAS-mutant lung cancer. Oncogene *38*, 622-636.

Lin, G., Zeng, Z., Wang, X., Wu, Z., Wang, J., Wang, C., Sun, Q., Chen, Y., and Quan, H. (2012). Cholecystectomy and risk of pancreatic cancer: a meta-analysis of observational studies. Cancer causes & control : CCC *23*, 59-67.

Ling, J., Kang, Y., Zhao, R., Xia, Q., Lee, D. F., Chang, Z., Li, J., Peng, B., Fleming, J. B., Wang, H.*, et al.* (2012). KrasG12D-induced IKK2/beta/NF-kappaB activation by IL-1alpha and p62 feedforward loops is required for development of pancreatic ductal adenocarcinoma. Cancer cell *21*, 105-120.

Linke, M., Fritsch, S. D., Sukhbaatar, N., Hengstschlager, M., and Weichhart, T. (2017). mTORC1 and mTORC2 as regulators of cell metabolism in immunity. FEBS letters *591*, 3089-3103.

Liou, G.-Y., Döppler, H., DelGiorno, Kathleen E., Zhang, L., Leitges, M., Crawford, Howard C., Murphy, Michael P., and Storz, P. (2016). Mutant KRas-Induced Mitochondrial Oxidative Stress in Acinar Cells Upregulates EGFR Signaling to Drive Formation of Pancreatic Precancerous Lesions. Cell reports *14*, 2325-2336.

Livak, K. J., and Schmittgen, T. D. (2001). Analysis of relative gene expression data using real-time quantitative PCR and the 2(-Delta Delta C(T)) Method. Methods *25*, 402-408.

Lohr, J. G., Stojanov, P., Carter, S. L., Cruz-Gordillo, P., Lawrence, M. S., Auclair, D., Sougnez, C., Knoechel, B., Gould, J., Saksena, G.*, et al.* (2014). Widespread genetic heterogeneity in multiple myeloma: implications for targeted therapy. Cancer cell *25*, 91-101.

Lou, H.-z., Weng, X.-c., Pan, H.-m., Pan, Q., Sun, P., Liu, L.-l., and Chen, B. (2014). The novel mTORC1/2 dual inhibitor INK-128 suppresses survival and proliferation of primary and transformed human pancreatic cancer cells. Biochemical and biophysical research communications *450*, 973-978.

Love, M. I., Huber, W., and Anders, S. (2014). Moderated estimation of fold change and dispersion for RNA-seq data with DESeq2. Genome biology *15*, 550.

Lu, H., Liu, C., Velazquez, R., Wang, H., Dunkl, L. M., Kazic-Legueux, M., Haberkorn, A., Billy, E., Manchado, E., Brachmann, S. M.*, et al.* (2019). SHP2 inhibition overcomes RTK-mediated pathway re-activation in KRAS mutant tumors treated with MEK inhibitors. Molecular cancer therapeutics, molcanther.0852.2018.

Lu, S., Jang, H., Nussinov, R., and Zhang, J. (2016). The Structural Basis of Oncogenic Mutations G12, G13 and Q61 in Small GTPase K-Ras4B. Scientific Reports *6*, 21949.

Lucas, A. L., Shakya, R., Lipsyc, M. D., Mitchel, E. B., Kumar, S., Hwang, C., Deng, L., Devoe, C., Chabot, J. A., Szabolcs, M.*, et al.* (2013). High Prevalence of BRCA1 and BRCA2 Germline Mutations with Loss of Heterozygosity in a Series of Resected Pancreatic Adenocarcinoma and Other Neoplastic Lesions. Clinical Cancer Research *19*, 3396.

Maier, H. J., Wagner, M., Schips, T. G., Salem, H. H., Baumann, B., and Wirth, T. (2013). Requirement of NEMO/IKKgamma for effective expansion of KRAS-induced precancerous lesions in the pancreas. Oncogene *32*, 2690-2695.

Maisonneuve, P., Marshall, B. C., and Lowenfels, A. B. (2007). Risk of pancreatic cancer in patients with cystic fibrosis. Gut *56*, 1327.

Manerba, M., Di Ianni, L., Govoni, M., Comparone, A., and Di Stefano, G. (2018). The activation of lactate dehydrogenase induced by mTOR drives neoplastic change in breast epithelial cells. PloS one *13*, e0202588-e0202588.

Maniati, E., Bossard, M., Cook, N., Candido, J. B., Emami-Shahri, N., Nedospasov, S. A., Balkwill, F. R., Tuveson, D. A., and Hagemann, T. (2011). Crosstalk between the canonical NF-kappaB and Notch signaling pathways inhibits Ppargamma expression and promotes pancreatic cancer progression in mice. J Clin Invest *121*, 4685-4699.

Manning, B. D., and Toker, A. (2017). AKT/PKB Signaling: Navigating the Network. Cell *169*, 381-405.

Martin-Caballero, J., Flores, J. M., Garcia-Palencia, P., and Serrano, M. (2001). Tumor susceptibility of p21(Waf1/Cip1)-deficient mice. Cancer Res *61*, 6234-6238.

Masri, J., Bernath, A., Martin, J., Jo, O. D., Vartanian, R., Funk, A., and Gera, J. (2007). mTORC2 activity is elevated in gliomas and promotes growth and cell motility via overexpression of rictor. Cancer Res *67*, 11712-11720.

Maubach, G., Feige, M. H., Lim, M. C. C., and Naumann, M. (2019). NF-kappaB-inducing kinase in cancer. Biochimica et biophysica acta Reviews on cancer *1871*, 40-49.

Mayer, I. A., and Arteaga, C. L. (2016). The PI3K/AKT Pathway as a Target for Cancer Treatment. Annual Review of Medicine *67*, 11-28.

McWilliams, R. R., Wieben, E. D., Rabe, K. G., Pedersen, K. S., Wu, Y., Sicotte, H., and Petersen, G. M. (2011). Prevalence of CDKN2A mutations in pancreatic cancer patients: implications for genetic counseling. European journal of human genetics : EJHG *19*, 472-478.

Melstrom, L. G., Salabat, M. R., Ding, X.-Z., Milam, B. M., Strouch, M., Pelling, J. C., and Bentrem, D. J. (2008). Apigenin Inhibits the GLUT-1 Glucose Transporter and the Phosphoinositide 3-Kinase/Akt Pathway in Human Pancreatic Cancer Cells. Pancreas *37*, 426-431.

Metsalu, T., and Vilo, J. (2015). ClustVis: a web tool for visualizing clustering of multivariate data using Principal Component Analysis and heatmap. Nucleic acids research *43*, W566-570.

Mezencev, R., Matyunina, L. V., Wagner, G. T., and McDonald, J. F. (2016). Acquired resistance of pancreatic cancer cells to cisplatin is multifactorial with cell context-dependent involvement of resistance genes. Cancer Gene Therapy *23*, 446-453.

Milam, M. R., Celestino, J., Wu, W., Broaddus, R. R., Schmeler, K. M., Slomovitz, B. M., Soliman, P. T., Gershenson, D. M., Wang, H., Ellenson, L. H., and Lu, K. H. (2007). Reduced progression of endometrial hyperplasia with oral mTOR inhibition in the Pten heterozygote murine model. American journal of obstetrics and gynecology *196*, 247.e241-245.

Milan, S. A., and Yeo, C. J. (2012). Neuroendocrine tumors of the pancreas. Current Opinion in Oncology *24*, 46-55.

Milella, M., Falcone, I., Conciatori, F., Matteoni, S., Sacconi, A., De Luca, T., Bazzichetto, C., Corbo, V., Simbolo, M., Sperduti, I.*, et al.* (2017). PTEN status is a crucial determinant of the functional outcome of combined MEK and mTOR inhibition in cancer. Scientific Reports *7*, 43013.

Moore, M. J., Goldstein, D., Hamm, J., Figer, A., Hecht, J. R., Gallinger, S., Au, H. J., Murawa, P., Walde, D., Wolff, R. A.*, et al.* (2007). Erlotinib plus gemcitabine compared with gemcitabine alone in patients with advanced pancreatic cancer: a phase III trial of the National Cancer Institute of Canada Clinical Trials Group. J Clin Oncol *25*, 1960-1966.

Morran, D. C., Wu, J., Jamieson, N. B., Mrowinska, A., Kalna, G., Karim, S. A., Au, A. Y., Scarlett, C. J., Chang, D. K., Pajak, M. Z.*, et al.* (2014). Targeting mTOR dependency in pancreatic cancer. Gut *63*, 1481-1489.

Morrison Joly, M., Hicks, D. J., Jones, B., Sanchez, V., Estrada, M. V., Young, C., Williams, M., Rexer, B. N., Sarbassov dos, D., Muller, W. J., *et al.* (2016). Rictor/mTORC2 Drives Progression and Therapeutic Resistance of HER2-Amplified Breast Cancers. Cancer Res *76*, 4752-4764.

Morton, J. P., Timpson, P., Karim, S. A., Ridgway, R. A., Athineos, D., Doyle, B., Jamieson, N. B., Oien, K. A., Lowy, A. M., Brunton, V. G., *et al.* (2010). Mutant p53 drives metastasis and overcomes growth arrest/senescence in pancreatic cancer. Proceedings of the National Academy of Sciences *107*, 246-251.

Mosmann, T. (1983). Rapid colorimetric assay for cellular growth and survival: application to proliferation and cytotoxicity assays. Journal of immunological methods *65*, 55-63.

Mueller, S., Engleitner, T., Maresch, R., Zukowska, M., Lange, S., Kaltenbacher, T., Konukiewitz, B., Ollinger, R., Zwiebel, M., Strong, A., *et al.* (2018). Evolutionary routes and KRAS dosage define pancreatic cancer phenotypes. Nature *554*, 62-68.

Muller, Patricia A., and Vousden, Karen H. (2014). Mutant p53 in Cancer: New Functions and Therapeutic Opportunities. Cancer cell *25*, 304-317.

Mullis, K., Faloona, F., Scharf, S., Saiki, R., Horn, G., and Erlich, H. (1986). Specific enzymatic amplification of DNA in vitro: the polymerase chain reaction. Cold Spring Harb Symp Quant Biol *51 Pt 1*, 263-273.

Murakami, M., Ichisaka, T., Maeda, M., Oshiro, N., Hara, K., Edenhofer, F., Kiyama, H., Yonezawa, K., and Yamanaka, S. (2004). mTOR is essential for growth and proliferation in early mouse embryos and embryonic stem cells. Molecular and cellular biology *24*, 6710-6718.

Murthy, D., Attri, K. S., and Singh, P. K. (2018). Phosphoinositide 3-Kinase Signaling Pathway in Pancreatic Ductal Adenocarcinoma Progression, Pathogenesis, and Therapeutics. Frontiers in physiology *9*, 335-335.

Muzumdar, M. D., Tasic, B., Miyamichi, K., Li, L., and Luo, L. (2007). A global double-fluorescent Cre reporter mouse. Genesis (New York, NY : 2000) *45*, 593-605.

Nakhai, H., Sel, S., Favor, J., Mendoza-Torres, L., Paulsen, F., Duncker, G. I., and Schmid, R. M. (2007). Ptf1a is essential for the differentiation of GABAergic and glycinergic amacrine cells and horizontal cells in the mouse retina. Development (Cambridge, England) *134*, 1151-1160.

Nakshatri, H. (2019). NF-κB Signaling Pathways in Carcinogenesis. In Predictive Biomarkers in Oncology: Applications in Precision Medicine, S. Badve, and G.L. Kumar, eds. (Cham: Springer International Publishing), pp. 321-325.

Navas, C., Hernández-Porras, I., Schuhmacher, A. J., Sibilia, M., Guerra, C., and Barbacid, M. (2012). EGF receptor signaling is essential for k-ras oncogene-driven pancreatic ductal adenocarcinoma. Cancer cell *22*, 318-330.

Ni, T., Li, X.-Y., Lu, N., An, T., Liu, Z.-P., Fu, R., Lv, W.-C., Zhang, Y.-W., Xu, X.-J., Grant Rowe, R., *et al.* (2016). Snail1-dependent p53 repression regulates expansion and activity of tumour-initiating cells in breast cancer. Nature cell biology *18*, 1221-1232.

Nishina, T., Yamaguchi, N., Gohda, J., Semba, K., and Inoue, J. (2009). NIK is involved in constitutive activation of the alternative NF-kappaB pathway and proliferation of pancreatic cancer cells. Biochem Biophys Res Commun *388*, 96-101.

Novack, D. V., Yin, L., Hagen-Stapleton, A., Schreiber, R. D., Goeddel, D. V., Ross, F. P., and Teitelbaum, S. L. (2003). The IkappaB function of NF-kappaB2 p100 controls stimulated osteoclastogenesis. J Exp Med *198*, 771-781.

O'Reilly, K. E., Rojo, F., She, Q. B., Solit, D., Mills, G. B., Smith, D., Lane, H., Hofmann, F., Hicklin, D. J., Ludwig, D. L.*, et al.* (2006). mTOR inhibition induces upstream receptor tyrosine kinase signaling and activates Akt. Cancer Res *66*, 1500-1508.

Olive, K. P., Tuveson, D. A., Ruhe, Z. C., Yin, B., Willis, N. A., Bronson, R. T., Crowley, D., and Jacks, T. (2004). Mutant p53 gain of function in two mouse models of Li-Fraumeni syndrome. Cell *119*, 847-860.

Orth, M., Metzger, P., Gerum, S., Mayerle, J., Schneider, G., Belka, C., Schnurr, M., and Lauber, K. (2019). Pancreatic ductal adenocarcinoma: biological hallmarks, current status, and future perspectives of combined modality treatment approaches. Radiation Oncology *14*, 141.

Ossewaarde, J. M., de Vries, A., Bestebroer, T., and Angulo, A. F. (1996). Application of a Mycoplasma group-specific PCR for monitoring decontamination of Mycoplasma-infected Chlamydia sp. strains. Applied and environmental microbiology *62*, 328-331.

Paquette, M., El-Houjeiri, L., and Pause, A. (2018). mTOR Pathways in Cancer and Autophagy. Cancers *10*, 18.

Paxian, S., Liptay, S., Adler, G., Hameister, H., and Schmid, R. M. (1999). Genomic organization and chromosomal mapping of mouse nuclear factor kappa B 2 (NFKB2). Immunogenetics *49*, 743-750.

Paxian, S., Merkle, H., Riemann, M., Wilda, M., Adler, G., Hameister, H., Liptay, S., Pfeffer, K., and Schmid, R. M. (2002). Abnormal organogenesis of Peyer's patches in mice deficient for NF-kappaB1, NF-kappaB2, and Bcl-3. Gastroenterology *122*, 1853-1868.

Payne, S. N., Maher, M. E., Tran, N. H., Van De Hey, D. R., Foley, T. M., Yueh, A. E., Leystra, A. A., Pasch, C. A., Jeffrey, J. J., Clipson, L.*, et al.* (2015). PIK3CA mutations can initiate pancreatic tumorigenesis and are targetable with PI3K inhibitors. Oncogenesis *4*, e169.

Perri, F., Pisconti, S., and Della Vittoria Scarpati, G. (2016). P53 mutations and cancer: a tight linkage. Annals of translational medicine *4*, 522-522.

Phyu, S. M., and Smith, T. A. D. (2019). Combination treatment of cancer cells with pan-Akt and pan-mTOR inhibitors: effects on cell cycle distribution, p-Akt expression level and radiolabelled-choline incorporation. Investigational new drugs *37*, 424-430.

Pike, K. G., Malagu, K., Hummersone, M. G., Menear, K. A., Duggan, H. M., Gomez, S., Martin, N. M., Ruston, L., Pass, S. L., and Pass, M. (2013). Optimization of potent and selective dual mTORC1 and mTORC2 inhibitors: the discovery of AZD8055 and AZD2014. Bioorg Med Chem Lett *23*, 1212-1216.

Pinho, A. V., Mawson, A., Gill, A., Arshi, M., Warmerdam, M., Giry-Laterriere, M., Eling, N., Lie, T., Kuster, E., Camargo, S.*, et al.* (2016). Sirtuin 1 stimulates the proliferation and the expression of glycolysis genes in pancreatic neoplastic lesions. Oncotarget *7*, 74768-74778.

Pires, B. R. B., Silva, R. C. M. C., Ferreira, G. M., and Abdelhay, E. (2018). NF-kappaB: Two Sides of the Same Coin. Genes *9*, 24.

Platt, F. M., Hurst, C. D., Taylor, C. F., Gregory, W. M., Harnden, P., and Knowles, M. A. (2009). Spectrum of phosphatidylinositol 3-kinase pathway gene alterations in bladder cancer. Clinical cancer research : an official journal of the American Association for Cancer Research *15*, 6008-6017.

Polireddy, K., Singh, K., Pruski, M., Jones, N. C., Manisundaram, N. V., Ponnela, P., Ouellette, M., Van Buren, G., Younes, M., Bynon, J. S.*, et al.* (2019). Mutant p53R175H promotes cancer initiation in the pancreas by stabilizing HSP70. Cancer letters *453*, 122-130.

Polley, S., Passos, D. O., Huang, D. B., Mulero, M. C., Mazumder, A., Biswas, T., Verma, I. M., Lyumkis, D., and Ghosh, G. (2016). Structural Basis for the Activation of IKK1/alpha. Cell reports *17*, 1907-1914.

Pópulo, H., Lopes, J. M., and Soares, P. (2012). The mTOR Signalling Pathway in Human Cancer. International Journal of Molecular Sciences *13*, 1886-1918.

Prabhu, L., Mundade, R., Korc, M., Loehrer, P. J., and Lu, T. (2014). Critical role of NF-κB in pancreatic cancer. Oncotarget *5*, 10969-10975.

Pramanik, K. C., Makena, M. R., Bhowmick, K., and Pandey, M. K. (2018). Advancement of NF-κB Signaling Pathway: A Novel Target in Pancreatic Cancer. International journal of molecular sciences *19*, 3890.

Pylayeva-Gupta, Y., Das, S., Handler, J. S., Hajdu, C. H., Coffre, M., Koralov, S. B., and Bar-Sagi, D. (2016). IL35-Producing B Cells Promote the Development of Pancreatic Neoplasia. Cancer Discov *6*, 247-255.

Quante, A. S., Ming, C., Rottmann, M., Engel, J., Boeck, S., Heinemann, V., Westphalen, C. B., and Strauch, K. (2016). Projections of cancer incidence and cancer-related deaths in Germany by 2020 and 2030. Cancer Medicine *5*, 2649-2656.

Rahib, L., Smith, B. D., Aizenberg, R., Rosenzweig, A. B., Fleshman, J. M., and Matrisian, L. M. (2014). Projecting cancer incidence and deaths to 2030: the unexpected burden of thyroid, liver, and pancreas cancers in the United States. Cancer Res *74*, 2913-2921.

Raimondi, S., Lowenfels, A. B., Morselli-Labate, A. M., Maisonneuve, P., and Pezzilli, R. (2010). Pancreatic cancer in chronic pancreatitis; aetiology, incidence, and early detection. Best practice & research Clinical gastroenterology *24*, 349-358.

Rajurkar, M., Dang, K., Fernandez-Barrena, M. G., Liu, X., Fernandez-Zapico, M. E., Lewis, B. C., and Mao, J. (2017). IKBKE Is Required during KRAS-Induced Pancreatic Tumorigenesis. Cancer research *77*, 320-329.

Raphael, B. J., Hruban, R. H., Aguirre, A. J., Moffitt, R. A., Yeh, J. J., Stewart, C., Robertson, A. G., Cherniack, A. D., Gupta, M., Getz, G.*, et al.* (2017). Integrated Genomic Characterization of Pancreatic Ductal Adenocarcinoma. Cancer cell *32*, 185-203.e113.

Reid, M. A., Lowman, X. H., Pan, M., Tran, T. Q., Warmoes, M. O., Ishak Gabra, M. B., Yang, Y., Locasale, J. W., and Kong, M. (2016). IKKbeta promotes metabolic adaptation to glutamine deprivation via phosphorylation and inhibition of PFKFB3. Genes Dev *30*, 1837-1851.

Riedlinger, T., Haas, J., Busch, J., van de Sluis, B., Kracht, M., and Schmitz, M. L. (2018). The Direct and Indirect Roles of NF-kappaB in Cancer: Lessons from Oncogenic Fusion Proteins and Knock-in Mice. Biomedicines *6*.

Rocha, S., Martin, A. M., Meek, D. W., and Perkins, N. D. (2003). p53 represses cyclin D1 transcription through down regulation of Bcl-3 and inducing increased association of the p52 NF-kappaB subunit with histone deacetylase 1. Molecular and cellular biology *23*, 4713-4727.

Rodrik-Outmezguine, V. S., Chandarlapaty, S., Pagano, N. C., Poulikakos, P. I., Scaltriti, M., Moskatel, E., Baselga, J., Guichard, S., and Rosen, N. (2011). mTOR kinase inhibition causes feedback-dependent biphasic regulation of AKT signaling. Cancer Discov *1*, 248-259.

Rojo, F., González-Pérez, A., Furriol, J., Nicolau, M. J., Ferrer, J., Burgués, O., Sabbaghi, M., González-Navarrete, I., Cristobal, I., Serrano, L.*, et al.* (2016). Non-canonical NF-κB pathway activation predicts outcome in borderline oestrogen receptor positive breast carcinoma. British Journal Of Cancer *115*, 322.

Roy, P., Sarkar, U. A., and Basak, S. (2018). The NF-kappaB Activating Pathways in Multiple Myeloma. Biomedicines *6*.

Rozengurt, E., Sinnett-Smith, J., and Kisfalvi, K. (2010). Crosstalk between insulin/insulin-like growth factor-1 receptors and G protein-coupled receptor signaling systems: a novel target for the antidiabetic drug metformin in pancreatic cancer. Clinical cancer research : an official journal of the American Association for Cancer Research *16*, 2505-2511.

Rozengurt, E., Soares, H. P., and Sinnet-Smith, J. (2014). Suppression of feedback loops mediated by PI3K/mTOR induces multiple overactivation of compensatory pathways: an unintended consequence leading to drug resistance. Molecular cancer therapeutics *13*, 2477-2488.

Saitoh, T., Nakayama, M., Nakano, H., Yagita, H., Yamamoto, N., and Yamaoka, S. (2003). TWEAK induces NF-kappaB2 p100 processing and long lasting NF-kappaB activation. J Biol Chem *278*, 36005-36012.

Sausen, M., Phallen, J., Adleff, V., Jones, S., Leary, R. J., Barrett, M. T., Anagnostou, V., Parpart-Li, S., Murphy, D., Kay Li, Q.*, et al.* (2015). Clinical implications of genomic alterations in the tumour and circulation of pancreatic cancer patients. Nature Communications *6*, 7686.

Saxon, J. A., Yu, H., Polosukhin, V. V., Stathopoulos, G. T., Gleaves, L. A., McLoed, A. G., Massion, P. P., Yull, F. E., Zhao, Z., and Blackwell, T. S. (2018). p52 expression enhances lung cancer progression. Sci Rep *8*, 6078.

Saxton, R. A., and Sabatini, D. M. (2017). mTOR Signaling in Growth, Metabolism, and Disease. Cell *168*, 960-976.

Schild, C., Wirth, M., Reichert, M., Schmid, R. M., Saur, D., and Schneider, G. (2009). PI3K signaling maintains c-myc expression to regulate transcription of E2F1 in pancreatic cancer cells. Molecular carcinogenesis *48*, 1149-1158.

Schlieman, M. G., Fahy, B. N., Ramsamooj, R., Beckett, L., and Bold, R. J. (2003). Incidence, mechanism and prognostic value of activated AKT in pancreas cancer. Br J Cancer *89*, 2110-2115.

Schmidt, K. M., Hellerbrand, C., Ruemmele, P., Michalski, C. W., Kong, B., Kroemer, A., Hackl, C., Schlitt, H. J., Geissler, E. K., and Lang, S. A. (2017). Inhibition of mTORC2 component RICTOR impairs tumor growth in pancreatic cancer models. Oncotarget *8*, 24491-24505.

Schneider, G., and Kramer, O. H. (2011). NFkappaB/p53 crosstalk-a promising new therapeutic target. Biochimica et biophysica acta *1815*, 90-103.

Schneider, G., Saur, D., Siveke, J. T., Fritsch, R., Greten, F. R., and Schmid, R. M. (2006). IKKα controls p52/RelB at the skp2 gene promoter to regulate G1- to S-phase progression. The EMBO journal *25*, 3801-3812.

Schofield, H. K., Zeller, J., Espinoza, C., Halbrook, C. J., Del Vecchio, A., Magnuson, B., Fabo, T., Daylan, A. E. C., Kovalenko, I., Lee, H.-J*., et al.* (2018). Mutant p53R270H drives altered metabolism and increased invasion in pancreatic ductal adenocarcinoma. JCI insight *3*, e97422.

Schonhuber, N., Seidler, B., Schuck, K., Veltkamp, C., Schachtler, C., Zukowska, M., Eser, S., Feyerabend, T. B., Paul, M. C., Eser, P*., et al.* (2014). A next-generation dual-recombinase system for time- and host-specific targeting of pancreatic cancer. Nature medicine *20*, 1340-1347.

Schönhuber, N., Seidler, B., Schuck, K., Veltkamp, C., Schachtler, C., Zukowska, M., Eser, S., Feyerabend, T. B., Paul, M. C., Eser, P*., et al.* (2014). A next-generation dual-recombinase system for time- and host-specific targeting of pancreatic cancer. Nat Med.

Schumm, K., Rocha, S., Caamano, J., and Perkins, N. D. (2006). Regulation of p53 tumour suppressor target gene expression by the p52 NF-kappaB subunit. The EMBO journal *25*, 4820-4832.

Scott, A. J., Lieu, C. H., and Messersmith, W. A. (2016). Therapeutic Approaches to RAS Mutation. Cancer journal (Sudbury, Mass) *22*, 165-174.

Serrano, M., Lin, A. W., McCurrach, M. E., Beach, D., and Lowe, S. W. (1997). Oncogenic ras Provokes Premature Cell Senescence Associated with Accumulation of p53 and p16INK4a. Cell *88*, 593-602.

Shukla, S. K., Gunda, V., Abrego, J., Haridas, D., Mishra, A., Souchek, J., Chaika, N. V., Yu, F., Sasson, A. R., Lazenby, A. J*., et al.* (2015). MUC16-mediated activation of mTOR and c-Myc reprograms pancreatic cancer metabolism. Oncotarget *6*, 19118-19131.

Shukuya, T., Yamada, T., Koenig, M. J., Xu, J., Okimoto, T., Li, F., Amann, J. M., and Carbone, D. P. (2019). The Effect of LKB1 Activity on the Sensitivity to PI3K/mTOR Inhibition in Non–Small Cell Lung Cancer. Journal of Thoracic Oncology *14*, 1061-1076.

Sidaway, P. (2017). Pancreatic cancer: TCGA data reveal a highly heterogeneous disease. Nat Rev Clin Oncol *14*, 648.

Siegel, R. L., Miller, K. D., and Jemal, A. (2017). Cancer statistics, 2017. CA: A Cancer Journal for Clinicians *67*, 7-30.

Siegel, R. L., Miller, K. D., and Jemal, A. (2018). Cancer statistics, 2018. CA Cancer J Clin *68*, 7-30.

Siegel, R. L., Miller, K. D., and Jemal, A. (2019). Cancer statistics, 2019. CA Cancer J Clin *69*, 7-34.

Sipos, B., Frank, S., Gress, T., Hahn, S., and Klöppel, G. (2009). Pancreatic Intraepithelial Neoplasia Revisited and Updated. Pancreatology *9*, 45-54.

Sjodahl, G., Lauss, M., Gudjonsson, S., Liedberg, F., Hallden, C., Chebil, G., Mansson, W., Hoglund, M., and Lindgren, D. (2011). A systematic study of gene mutations in urothelial carcinoma; inactivating mutations in TSC2 and PIK3R1. PLoS One *6*, e18583.

Soares, H. P., Ming, M., Mellon, M., Young, S. H., Han, L., Sinnet-Smith, J., and Rozengurt, E. (2015). Dual PI3K/mTOR Inhibitors Induce Rapid Overactivation of the MEK/ERK Pathway in Human Pancreatic Cancer Cells through Suppression of mTORC2. Molecular cancer therapeutics *14*, 1014-1023.

Son, J., Lyssiotis, C. A., Ying, H., Wang, X., Hua, S., Ligorio, M., Perera, R. M., Ferrone, C. R., Mullarky, E., Shyh-Chang, N*., et al.* (2013). Glutamine supports pancreatic cancer growth through a KRAS-regulated metabolic pathway. Nature *496*, 101-105.

Stevens, R. J., Roddam, A. W., and Beral, V. (2007). Pancreatic cancer in type 1 and young-onset diabetes: systematic review and meta-analysis. British Journal of Cancer *96*, 507-509.

Storz, P. (2013). Targeting the alternative NF-κB pathway in pancreatic cancer: a new direction for therapy? Expert Rev Anticancer Ther *13*, 501-504.

Storz, P. (2017). Acinar cell plasticity and development of pancreatic ductal adenocarcinoma. Nat Rev Gastroenterol Hepatol *14*, 296-304.

Subramanian, A., Tamayo, P., Mootha, V. K., Mukherjee, S., Ebert, B. L., Gillette, M. A., Paulovich, A., Pomeroy, S. L., Golub, T. R., Lander, E. S., and Mesirov, J. P. (2005). Gene set enrichment analysis: a knowledge-based approach for interpreting genome-wide expression profiles. Proc Natl Acad Sci U S A *102*, 15545-15550.

Sun, Q., Zhang, B., Hu, Q., Qin, Y., Xu, W., Liu, W., Yu, X., and Xu, J. (2018). The impact of cancer-associated fibroblasts on major hallmarks of pancreatic cancer. Theranostics *8*, 5072-5087.

Sun, S. Y. (2013). mTOR kinase inhibitors as potential cancer therapeutic drugs. Cancer letters *340*, 1-8.

Taniguchi, K., and Karin, M. (2018). NF-kappaB, inflammation, immunity and cancer: coming of age. Nature reviews Immunology *18*, 309-324.

Tanti, J. F., and Jager, J. (2009). Cellular mechanisms of insulin resistance: role of stress-regulated serine kinases and insulin receptor substrates (IRS) serine phosphorylation. Current opinion in pharmacology *9*, 753-762.

Tarasov, V., Jung, P., Verdoodt, B., Lodygin, D., Epanchintsev, A., Menssen, A., Meister, G., and Hermeking, H. (2007). Differential regulation of microRNAs by p53 revealed by massively parallel sequencing: miR-34a is a p53 target that induces apoptosis and G1-arrest. Cell Cycle *6*, 1586-1593.

Tchkonia, T., Zhu, Y., van Deursen, J., Campisi, J., and Kirkland, J. L. (2013). Cellular senescence and the senescent secretory phenotype: therapeutic opportunities. J Clin Invest *123*, 966-972.

Tee, A. R. (2018). The Target of Rapamycin and Mechanisms of Cell Growth. International journal of molecular sciences *19*, 880.

Tee, A. R., Manning, B. D., Roux, P. P., Cantley, L. C., and Blenis, J. (2003). Tuberous sclerosis complex gene products, Tuberin and Hamartin, control mTOR signaling by acting as a GTPase-activating protein complex toward Rheb. Current biology : CB *13*, 1259-1268.

Tergaonkar, V., Pando, M., Vafa, O., Wahl, G., and Verma, I. (2002). p53 stabilization is decreased upon NFkappaB activation: a role for NFkappaB in acquisition of resistance to chemotherapy. Cancer cell *1*, 493-503.

Terzić, J., Grivennikov, S., Karin, E., and Karin, M. (2010). Inflammation and Colon Cancer. Gastroenterology *138*, 2101-2114.e2105.

Tian, T., Li, X., and Zhang, J. (2019). mTOR Signaling in Cancer and mTOR Inhibitors in Solid Tumor Targeting Therapy. International Journal of Molecular Sciences *20*, 755.

Toufektchan, E., and Toledo, F. (2018). The Guardian of the Genome Revisited: p53 Downregulates Genes Required for Telomere Maintenance, DNA Repair, and Centromere Structure. Cancers *10*, 135.

Towbin, H., Staehelin, T., and Gordon, J. (1979). Electrophoretic transfer of proteins from polyacrylamide gels to nitrocellulose sheets: procedure and some applications. Proc Natl Acad Sci U S A *76*, 4350-4354.

Trikudanathan, G., Philip, A., Dasanu, C. A., and Baker, W. L. (2011). Association between Helicobacter pylori infection and pancreatic cancer. A cumulative meta-analysis. JOP : Journal of the pancreas *12*, 26-31.

Tsai, F. D., Lopes, M. S., Zhou, M., Court, H., Ponce, O., Fiordalisi, J. J., Gierut, J. J., Cox, A. D., Haigis, K. M., and Philips, M. R. (2015). K-Ras4A splice variant is widely expressed in cancer and uses a hybrid membrane-targeting motif. Proc Natl Acad Sci U S A *112*, 779-784.

Utomo, W. K., Narayanan, V., Biermann, K., van Eijck, C. H. J., Bruno, M. J., Peppelenbosch, M. P., and Braat, H. (2014). mTOR is a promising therapeutical target in a subpopulation of pancreatic adenocarcinoma. Cancer letters *346*, 309-317.

Vazquez, A., Kamphorst, J. J., Markert, E. K., Schug, Z. T., Tardito, S., and Gottlieb, E. (2016). Cancer metabolism at a glance. Journal of Cell Science *129*, 3367.

Veite-Schmahl, M. J., Rivers, A. C., Regan, D. P., and Kennedy, M. A. (2017). The Mouse Model of Pancreatic Cancer Atlas (MMPCA) for classification of pancreatic cancer lesions: A large histological investigation of the Ptf1aCre/+;LSL-KrasG12D/+ transgenic mouse model of pancreatic cancer. PLoS One *12*, e0187552.

Vijayakumaran, R., Tan, K. H., Miranda, P. J., Haupt, S., and Haupt, Y. (2015). Regulation of Mutant p53 Protein Expression. Frontiers in oncology *5*, 284-284.

Vincent, A., Herman, J., Schulick, R., Hruban, R. H., and Goggins, M. (2011). Pancreatic cancer. Lancet (London, England) *378*, 607-620.

Von Hoff, D. D., Ervin, T., Arena, F. P., Chiorean, E. G., Infante, J., Moore, M., Seay, T., Tjulandin, S. A., Ma, W. W., Saleh, M. N., *et al.* (2013). Increased survival in pancreatic cancer with nab-paclitaxel plus gemcitabine. The New England journal of medicine *369*, 1691-1703.

Waddell, N., Pajic, M., Patch, A.-M., Chang, D. K., Kassahn, K. S., Bailey, P., Johns, A. L., Miller, D., Nones, K., Quek, K., *et al.* (2015). Whole genomes redefine the mutational landscape of pancreatic cancer. Nature *518*, 495-501.

Wang, J., Jacob, N. K., Ladner, K. J., Beg, A., Perko, J. D., Tanner, S. M., Liyanarachchi, S., Fishel, R., and Guttridge, D. C. (2009). RelA/p65 functions to maintain cellular senescence by regulating genomic stability and DNA repair. EMBO reports *10*, 1272-1278.

Warburg, O. (1956). On the origin of cancer cells. Science (New York, NY) *123*, 309-314.

Waters, A. M., and Der, C. J. (2018). KRAS: The Critical Driver and Therapeutic Target for Pancreatic Cancer. Cold Spring Harbor perspectives in medicine *8*, a031435.

Wei, F., Zhang, Y., Geng, L., Zhang, P., Wang, G., and Liu, Y. (2015). mTOR inhibition induces EGFR feedback activation in association with its resistance to human pancreatic cancer. Int J Mol Sci *16*, 3267-3282.

Wei, W., Shin, Y. S., Xue, M., Matsutani, T., Masui, K., Yang, H., Ikegami, S., Gu, Y., Herrmann, K., Johnson, D., *et al.* (2016). Single-Cell Phosphoproteomics Resolves Adaptive Signaling Dynamics and Informs Targeted Combination Therapy in Glioblastoma. Cancer cell *29*, 563-573.

Weichert, W., Boehm, M., Gekeler, V., Bahra, M., Langrehr, J., Neuhaus, P., Denkert, C., Imre, G., Weller, C., Hofmann, H. P., *et al.* (2007). High expression of RelA/p65 is associated with activation of nuclear factor-kappaB-dependent signaling in pancreatic cancer and marks a patient population with poor prognosis. Br J Cancer *97*, 523-530.

Wharry, C. E., Haines, K. M., Carroll, R. G., and May, M. J. (2009). Constitutive noncanonical NFκB signaling in pancreatic cancer cells. Cancer Biology & Therapy *8*, 1567-1576.

Wilson, T. R., Fridlyand, J., Yan, Y., Penuel, E., Burton, L., Chan, E., Peng, J., Lin, E., Wang, Y., Sosman, J., *et al.* (2012). Widespread potential for growth-factor-driven resistance to anticancer kinase inhibitors. Nature *487*, 505-509.

Witkiewicz, A. K., McMillan, E. A., Balaji, U., Baek, G., Lin, W. C., Mansour, J., Mollaee, M., Wagner, K. U., Koduru, P., Yopp, A., *et al.* (2015). Whole-exome sequencing of pancreatic cancer defines genetic diversity and therapeutic targets. Nat Commun *6*, 6744.

Wu, C. Y., Carpenter, E. S., Takeuchi, K. K., Halbrook, C. J., Peverley, L. V., Bien, H., Hall, J. C., DelGiorno, K. E., Pal, D., Song, Y., *et al.* (2014). PI3K regulation of RAC1 is required for KRAS-induced pancreatic tumorigenesis in mice. Gastroenterology *147*, 1405-1416.e1407.

Xia, L., Tan, S., Zhou, Y., Lin, J., Wang, H., Oyang, L., Tian, Y., Liu, L., Su, M., Wang, H., *et al.* (2018). Role of the NFκB-signaling pathway in cancer. OncoTargets and therapy *11*, 2063-2073.

Xia, Y., Shen, S., and Verma, I. M. (2014). NF-kappaB, an active player in human cancers. Cancer Immunol Res *2*, 823-830.

Xiao, G., Fong, A., and Sun, S. C. (2004). Induction of p100 processing by NF-kappaB-inducing kinase involves docking IkappaB kinase alpha (IKKalpha) to p100 and IKKalpha-mediated phosphorylation. J Biol Chem *279*, 30099-30105.

Yadav, D., and Lowenfels, A. B. (2013). The epidemiology of pancreatitis and pancreatic cancer. Gastroenterology *144*, 1252-1261.

Yamaguchi, J., Yokoyama, Y., Kokuryo, T., Ebata, T., and Nagino, M. (2018). Cells of origin of pancreatic neoplasms. Surgery Today *48*, 9-17.

Yamei Shen, C. X., Xuechun Li, Li Ba, Junjie Gu, Zhao Sun, Qin Han, and Robert Chunhua Zhao (2019). Effects of Gastric Cancer Cell-Derived Exosomes on the Immune Regulation of Mesenchymal Stem Cells by the NF-kB Signaling Pathway. Stem Cells and Development *Volume: 28*.

Yang Yang, J. W., Jinke Wang (2016). A database and functional annotation of NF-κB target genes. Int J Clin Exp Med *9*, 7986-7995.

Ying, H., Elpek, K. G., Vinjamoori, A., Zimmerman, S. M., Chu, G. C., Yan, H., Fletcher-Sananikone, E., Zhang, H., Liu, Y., Wang, W.*, et al.* (2011). PTEN is a major tumor suppressor in pancreatic ductal adenocarcinoma and regulates an NF-kappaB-cytokine network. Cancer Discov *1*, 158-169.

Ying, H., Kimmelman, A. C., Lyssiotis, C. A., Hua, S., Chu, G. C., Fletcher-Sananikone, E., Locasale, J. W., Son, J., Zhang, H., Coloff, J. L.*, et al.* (2012). Oncogenic Kras Maintains Pancreatic Tumors through Regulation of Anabolic Glucose Metabolism. Cell *149*, 656-670.

You, L., Ren, X., Du, Y., Zhao, W., Cui, M., Chen, G., and Zhao, Y. (2016). c-Fos/ERK promotes the progression from pancreatic intraepithelial neoplasia to pancreatic ductal adenocarcinoma. Oncology reports *36*, 3413-3420.

Yu, C., Chen, S., Guo, Y., and Sun, C. (2018). Oncogenic TRIM31 confers gemcitabine resistance in pancreatic cancer via activating the NF-kappaB signaling pathway. Theranostics *8*, 3224-3236.

Zeng, J.-d., Wu, W. K. K., Wang, H.-y., and Li, X.-x. (2019). Serine and one-carbon metabolism, a bridge that links mTOR signaling and DNA methylation in cancer. Pharmacological Research, 104352.

Zhan, Q. (2005). Gadd45a, a p53- and BRCA1-regulated stress protein, in cellular response to DNA damage. Mutation research *569*, 133-143.

Zhang, J., Xu, K., Liu, P., Geng, Y., Wang, B., Gan, W., Guo, J., Wu, F., Chin, Y. R., Berrios, C.*, et al.* (2016). Inhibition of Rb Phosphorylation Leads to mTORC2-Mediated Activation of Akt. Molecular cell *62*, 929-942.

Zhang, Y., Crawford, H. C., and Pasca di Magliano, M. (2018). Epithelial-Stromal Interactions in Pancreatic Cancer. Annu Rev Physiol.

Zhang, Y., Kwok-Shing Ng, P., Kucherlapati, M., Chen, F., Liu, Y., Tsang, Y. H., de Velasco, G., Jeong, K. J., Akbani, R., Hadjipanayis, A.*, et al.* (2017). A Pan-Cancer Proteogenomic Atlas of PI3K/AKT/mTOR Pathway Alterations. Cancer cell *31*, 820-832.e823.

Zhou, J., Toh, S. H., Chan, Z. L., Quah, J. Y., Chooi, J. Y., Tan, T. Z., Chong, P. S. Y., Zeng, Q., and Chng, W. J. (2018). A loss-of-function genetic screening reveals synergistic targeting of AKT/mTOR and

WTN/beta-catenin pathways for treatment of AML with high PRL-3 phosphatase. J Hematol Oncol *11*, 36.

Zhu, X. D., and Sadowski, P. D. (1995). Cleavage-dependent ligation by the FLP recombinase. Characterization of a mutant FLP protein with an alteration in a catalytic amino acid. J Biol Chem *270*, 23044-23054.

Zhu, Z., Aref, A. R., Cohoon, T. J., Barbie, T. U., Imamura, Y., Yang, S., Moody, S. E., Shen, R. R., Schinzel, A. C., Thai, T. C*., et al.* (2014). Inhibition of KRAS-driven tumorigenicity by interruption of an autocrine cytokine circuit. Cancer Discov *4*, 452-465.

Zhuang, G., Yu, K., Jiang, Z., Chung, A., Yao, J., Ha, C., Toy, K., Soriano, R., Haley, B., Blackwood, E*., et al.* (2013). Phosphoproteomic analysis implicates the mTORC2-FoxO1 axis in VEGF signaling and feedback activation of receptor tyrosine kinases. Science signaling *6*, ra25.

13 Acknowledgement

First of all, I want to thank Prof. Roland M. Schmid for giving me the opportunity to do my PhD research in his department, the II. Medizinische Klinik at Klinikum rechts der Isar.

Above all, I thank PD Dr. Günter Schneider for giving me the opportunity to perform my PhD research in his group. By proposing such an exciting, interesting, and promising project to me and by his support of me and my project, he contributed to the successful outcome of my dissertation.

I am very grateful to Prof. Angelika Schnieke for being my second advisor. Furthermore, I thank Prof. Dieter Saur for being my mentor during my PhD research. Also, I want to thank both of them for their outstanding scientific input and fruitful discussions.

I am thankful to all members of the Saur, Schneider, Rad and Reichert groups for the great working atmosphere in the lab, their constant help and support throughout the years.

I am heartedly thankfull to all of my funding sources like DAAD Germany, HEC Pakistan and Laura Bassi from TUM for their support during all my PHD study.

I am thankfull to Dr. Matthias Wirth, for performing bioinformatical analysis of RNA sequencing data.

For critical reading, giving suggestions, editing and corrections of my thesis manuscript, I want to thank Christian Schneeweis, Dr. Christian Veltkamp and Dr. Andrea Colcucio.

Finally, I want to thank all my friends and my brothers for their support. Especially I want to thank my Mother for holding my hand and giving me courage. Without her, my brothers and my friends, my dissertation would not have been possible.

Above all, I am adoringly thankful to almighty Allah for His being with me.